SPACE RESEARCH COORDINATION CENTER

ROCKET DETERMINATION OF THE DAYTIME SODIUM DISTRIBUTION IN THE UPPER ATMOSPHE

BY

ROBERT R. MEIER

DEPARTMENT OF PHYSICS

SRCC REPORT NO. 34

UNIVERSITY OF PITTSBURGH

PITTSBURGH, PENNSYLVANIA

7 SEPTEMBER 1966

The Space Research Coordination Center, established in May, 1963, has the following functions: (1) it administers predoctoral and postdoctoral fellowships in space-related science and engineering programs; (2) it makes available, on application and after review, allocations to assist new faculty members in the Division of the Natural Sciences or the School of Engineering to initiate research programs or to permit established faculty members to do preliminary work on research ideas of a novel character; (3) in the Division of the Natural Sciences it makes an annual allocation of funds to the interdisciplinary Laboratory for Atmospheric and Space Sciences; (4) in the School of Engineering it makes a similar allocation of funds to the Department of Metallurgical and Materials Engineering; and (5) in concert with the University's Knowledge Availability Systems Center, it seeks to assist in the orderly transfer of new space-generated knowledge in industrial application. The Center also issues periodic reports of space-oriented research and a comprehensive annual report.

The Center is supported by an Institutional Grant (NsG-416) from the National Aeronautics and Space Administration, strongly supplemented by grants from The A. W. Mellon Educational and Charitable Trust, the Maurice Falk Medical Fund, the Richard King Mellon Foundation and the Sarah Mellon Scaife Foundation. Much of the work described in SRCC reports is financed by other grants, made to individual faculty members.

ROCKET DETERMINATION OF THE DAYTIME SODIUM DISTRIBUTION IN THE UPPER ATMOSPHERE

By

Robert R. Meier

B. S. Duquesne University, 1962

Submitted to the Graduate Faculty in the Division of the Natural Sciences in partial fulfillment of the requirements for the degree of Doctor of Philosophy

University of Pittsburgh

1966

ROCKET DETERMINATION OF THE DAYTIME SODIUM DISTRIBUTION IN THE UPPER ATMOSPHERE

Robert R. Meier, Ph.D.
University of Pittsburgh, 1966

A rocket photometer was successfully flown on September 26, 1964, with the purpose of measuring the altitude profile of sodium in the daytime. The sodium was discovered to be concentrated in a very narrow layer of only 5 km. full width at half maximum density centered at 92.4 km. The peak density was 2.8×10^4 atoms/cm^3.

Since this distribution is inconsistent with a photochemical-diffusion theory based on the assumption of a non-local source of sodium, a new model is proposed in which charged, sodium-containing aerosol particles are concentrated into a very narrow layer by means of a wind shear mechanism. Sodium is then liberated through the action of solar radiation. The atoms diffuse away from the source until they are either oxidized by ozone or ionized. This removal must take place in a time which is of the order of the diffusion time in order to produce a narrow sodium distribution. It is quantitavely shown that the proposed model fits the experimental results under somewhat simplified conditions. AUTHOR

PREFACE

The author is deeply indebted to his advisor, Professor Thomas M. Donahue, for his guidance and encouragement throughout the course of this work. The many discussions with faculty members and fellow graduate students are gratefully acknowledged. In particular, the author would like to express his gratitude to Drs. J. E. Blamont and D. M. Hunten, who graciously made available their instruments for the groundbased support of this flight, and to Mr. Douglas Strickland, who programmed the radiative transfer solution on the I.B.M. 7090 computer. The author would also like to thank his wife, Eileen for her assistance in the preparation of this manuscript.

TABLE OF CONTENTS

1.0 INTRODUCTION

The sodium resonance doublet at 5890-5896 Å. is a well known feature of the airglow. The emission has been observed during the day, twilight, and night. Extensive reviews of the sodium airglow are given by Chamberlain[1], by Hunten[2], and by Donahue[3].

The twilight emission is due to resonance scattering of solar photons by free sodium atoms. Information about the twilight distribution of sodium in the atmosphere can be obtained by measuring the decrease in intensity as the shadow of the earth passes through the emitting layer. The derivative of the intensity with respect to shadow height gives the vertical distribution of the sodium. In practice the shadow is not sharp so that the derivative is only a first approximation to the distribution. To calculate the extent of the shadow broadening, the effects of tropospheric extinction and refraction, ozone absorption, and other factors must be taken into account[4]. The results of observations involving this type of analysis give a layer which has a density peak near 90 km. with an average width of about 9 km.[5]. Since the sunlight passes through the day layer before exciting the twilight sodium, the effect of attenuation by self absorption must be taken into account. This involves a knowledge of the daytime abundance.

During the day, the resonance scattering process also takes place. The first calculations of the dayglow intensity were performed by Donahue[6]. Subsequent elaborations on the theory were

made by Brandt and Chamberlain[7], and by Blamont and Donahue[5,8]. Since 1960, observations of the sodium dayglow have been carried out systematically at Haute Provence and also at Tromsø[5,9]. These observations show that there is a large diurnal variation in the sodium abundance. The day to twilight abundance ratio has a maximum of 5 in summer and a minimum of 2 in winter. The average abundance is 14×10^9 atoms/cm^2 with little seasonal variation.

The purpose of the rocket experiment described in this paper was to measure the sodium density distribution during the day by actually flying through the layer. The flight was successful not only in traversing the layer but also in scanning it many times from above, thus giving good altitude profiles of the distribution.

A magnetic scanning Zeeman photometer, which can observe the sodium emission in spite of a large Rayleigh scattered background at the same wavelengths, measured the dayglow on the day of the flight. Thus a comparison of the intensity observed from the ground was made with that observed during the flight. In addition, the twilight abundance was measured so that the existance of a diurnal effect could be verified.

The rocket experiment showed that the sodium was concentrated in a very narrow region, having a full width at half maximum density of only 5 km. The distribution was peaked at about 92.4 km. with a density of 2.8×10^4 atoms/cm^3. The abundance was 14×10^9 atoms/cm^2, in excellent agreement with the Zeeman observations. The twilight measurement gave an abundance of 4.7×10^9

atoms/cm^2, thus producing a day to twilight ratio of about 3. The twilight layer had an altitude of 89.2 km. and a full width of 8.8 km.

Blamont and Donahue[5] have discussed the possibility of an enhanced sodium layer in terms of a photochemical source. They concluded that the enhanced sodium distribution during the day should be at a lower altitude than the twilight layer and somewhat wider. This conclusion was not supported by the results of the rocket flight. Indeed it appears that the sodium has a local origin rather than a source involving photochemistry and diffusion alone.

In order to produce the observed sodium distribution, it is proposed that a reservoir in the form of a very thin layer of meteoric dust particles exists near 92 km. Sodium atoms (as well as other meteoric atoms) are liberated from this layer through the action of solar radiation. As the sodium diffuses away, it is either oxidized by ozone or ionized in a time which is of the order of the diffusion time, thus producing a thin layer of free atoms. In order to create a narrow dust distribution, it is suggested that the particles may be charged, so that the action of the neutral wind pulls them across the earth's magnetic field lines and introduces a vertical drift in their motion. Strong shears in the wind can readily concentrate the charged particles, thus producing an extremely narrow dust layer in spite of diffusion.

Quantitative results show that under simplified conditions, this source can produce the observed sodium layer.

2.0 EXPERIMENT

2.1 Instrumentation

The flight instrument was similar in principle to the Zeeman photometer described by Blamont and Donahue[8]. Magnetic scanning was not incorporated in the rocket experiment so that discrimination between the sodium emission and the Rayleigh scattered background at the same wavelength was impossible. However, the instrument was so selective in wavelength that the Rayleigh scattered component became negligibly small above 30 km. thus making the scanning feature unnecessary.

A sketch showing the optical system is seen in Figure 1. The instrument consisted of two separate optical channels whose objective lenses looked through two holes in the skin of a cylindrical extension of an Aerobee sounding rocket. Light was focused by the lenses through interference filters into pyrex cells. The optical channels were identical except for the cells. In one channel, the cell contained sodium while in the other, the cell was empty. The sodium cell was enclosed in an oven. When the oven was cold the sodium condensed in the tail of the cell making the two channels nearly identical. When light entered either of the channels, it was focused to the back of the cell so that ideally, no signal should have reached the exit lens and, subsequently, the photomultiplier tube. However due to effects such as scattering from the baffles and from imperfections in the glass cell, a certain amount of stray light found its way to the phototube. As might be expected, the stray light was dif-

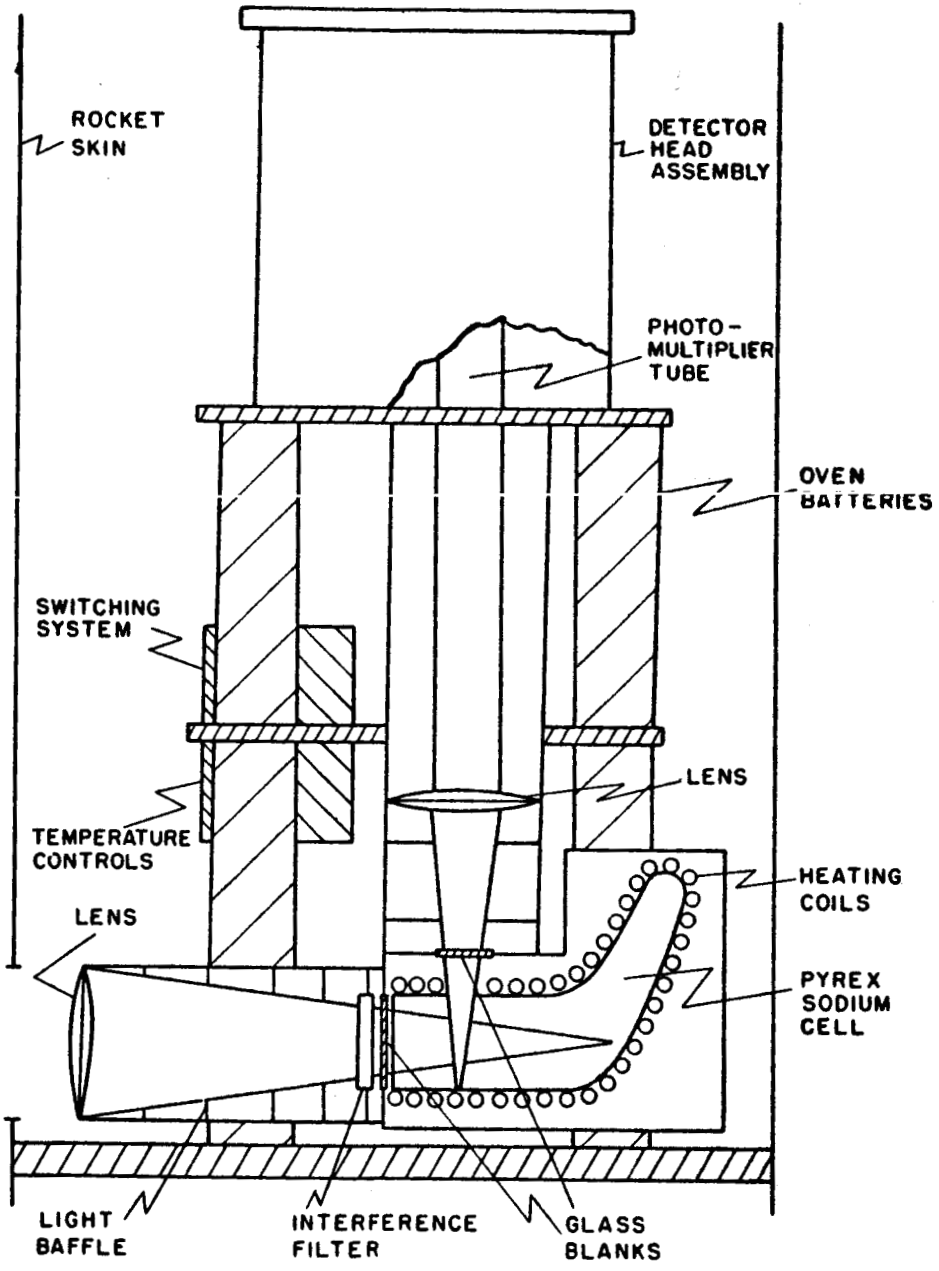

Figure 1. Sketch of experiment showing optical system.

ferent in each of the channels. To compensate for these differences, the sensitivities of the two channels were adjusted to near equality when the sodium cell was cold.

When the oven was heated, sodium vapor formed. The vapor was capable of strongly scattering radiation only at the resonant frequencies of sodium. Because the resonance scattering was virtually isotropic, a large component of the radiation was scattered in the direction of the phototube. The result was a large increase in signal due to the radiation at the sodium wavelengths while the rest of the radiation within the passband of the interference filter was essentially unaffected. Of course, the output of the second channel (hereafter referred to as the white light channel because its purpose was to measure the Rayleigh scattered continuum) was also unaltered. Then subtraction of the two signals gave the intensities at 5890 A. and 5896 A. only. Figure 2 shows a typical response curve of the instrument to a white light source.

A special heating cycle was required in order to prevent condensation of sodium vapor on the head of the cell. The oven was constructed so that the head and the tail could be heated independently, thus enabling a temperature gradient to be maintained across the cell. The heating procedure was first to heat the head of the cell to approximately 160° C. Then the tail was heated to about 145°. To cool the oven, the head was maintained at 160° as the tail cooled. Use of this cycle with the tail section of the cell always cooler insured against condensation on the head.

The temperature of each section of the oven was regulated

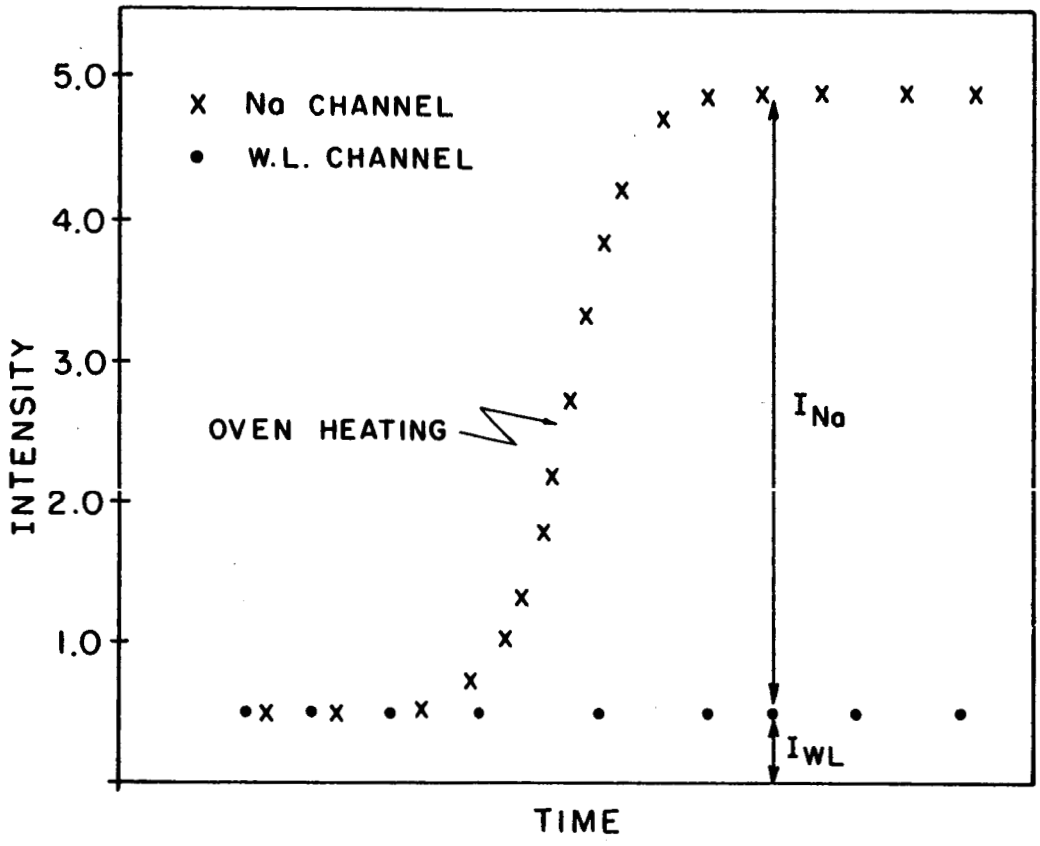

Figure 2. White light response of flight photometer.

by a thermistor controlled heating system. The thermistor current was amplified and used to control a relay, which in turn connected batteries to the heater coils. The efficiency of the system was maximized so that the temperature was regulated to better than 1%. This was sufficient to maintain a constant density of sodium vapor in the cell, thus preventing fluctuations in the signal due to temperature variations. In addition, a third thermistor was utilized as a monitor to detect changes in the tail temperature.

The objective lenses were 50 mm. in diameter with a focal length of 254 mm. The exit lenses had a diameter of 76 mm. and a focal length of 100 mm. The interference filters had the following specifications: a peak transmission of about 65% centered at 5890 A. (+6A., - 0 A.) with a full width of 40 A. at half maximum transmission. The photomultiplier tubes were ASCOP 541A's.

Glass blanks were inserted at the light input and output of the oven so that the optical parts would be protected from the heat. Because of the high temperature, the interference filter in the sodium channel was supported by a well insulated mount. The oven was mounted on teflon supports to prevent thermal contact with the other parts of the instrument.

Batteries to power the oven heater coils in flight were mounted inside the supporting posts on the experiment. The detecting system power was supplied from batteries located elsewhere in the rocket.

A block diagram of the electronics is shown in Figure 3. The signals from the two photomultiplier tubes were amplified by

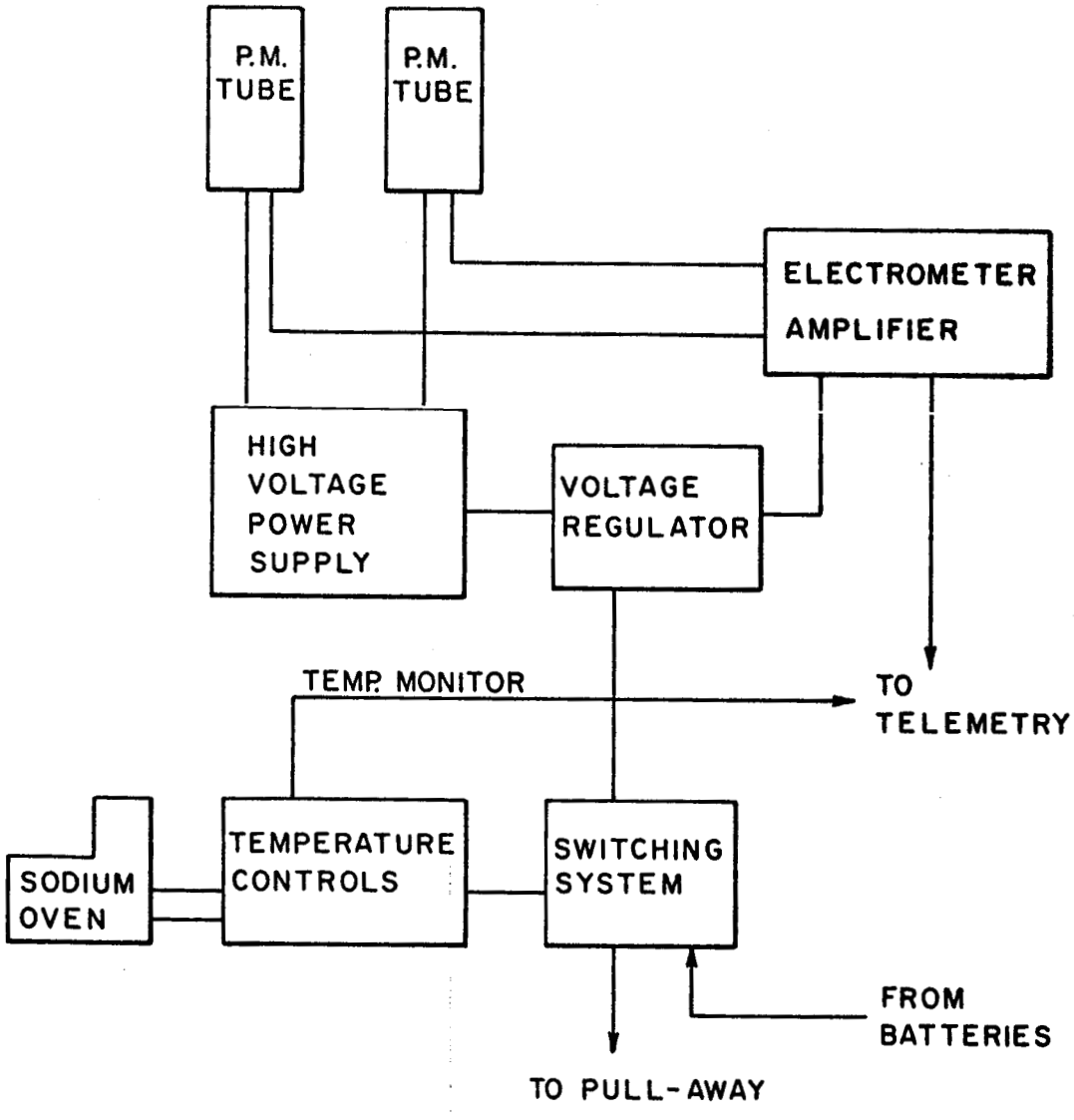

Figure 3. Block diagram of photometer electronics.

electrometers having a linear response of 1 volt/10^{-9} amp and a 0-5 volt output. These signals were then sent to the telemetry section of the rocket. The time constant of the amplifiers was about 3 msec., so that rocket rotation, which approached 3.5 rev/sec. during the first part of the flight, was easily followed by both channels of the photometer. The high voltage was monitored in order that changes in signal due to power supply fluctuations could be detected. The outputs of both the high voltage monitor and the temperature monitor were commutated at a few times per second on the telemetry system.

A remotely operated control box was connected to the experiment through the pull-away cable of the rocket. This permitted control of the amplifiers as well as the heating cycle before launch.

2.2 Calibration

The rocket photometer was operated simultaneously with a Zeeman photometer both before and on the day of the flight. A comparison of the results from the two instruments gave an absolute calibration of the flight photometer because the Zeeman photometer was already calibrated according to a method developed by Blamont and Donahue[5].

On September 11, 1964, the two instruments were operated together from about 18^h00 (EDST) to 19^h00 at Wallops Island. The Zeeman device was pointed in the direction of the pole while the flight photometer was at a 75° zenith angle. Before comparing the outputs of the two instruments, a correction had to be made for

the different angles of observation.

To determine the change in intensity as a function of direction of observation, a series of measurements were performed with the Zeeman photometer on September 14th. The instrument measured intensities at the pole and at zenith angles of 53.5° and 75° several different times during the day. The results are shown in Figure 4. I'_{Na} is the total intensity at the sodium wavelengths and I_R is the Rayleigh scattered component. The data were corrected for small variations in intensity due to the change in zenith angle of the sun. The changes were less than 25% from 50° solar elevation to 35° (the interval over which the measurements were taken).

In Figure 5 the sodium emission rate is shown as a function of observational angle. The data were not corrected in this case because the intensity did not change significantly over this range of solar elevation angle. Use of these curves permitted a comparison of the Zeeman output (I'_{Na}) and the intensity recorded by the flight instrument. In Figure 6 the results of the comparison are shown. The calibration factor was found to be about 180 kilorayleighs/ volt for a Zeeman calibration of 5.0 kR/recorder unit. There was a discrepancy between the two curves for times earlier than $18^{h}30$. This difference is probably due to the fact that the amplifiers in the flight photometer suffered from zero drift. During the calibration, the flight instrument was mounted in the rocket extension. This caused considerable difficulty in measuring the drift since the light inputs were not easy to seal. Therefore only three "zero readings" were made during the calibration run.

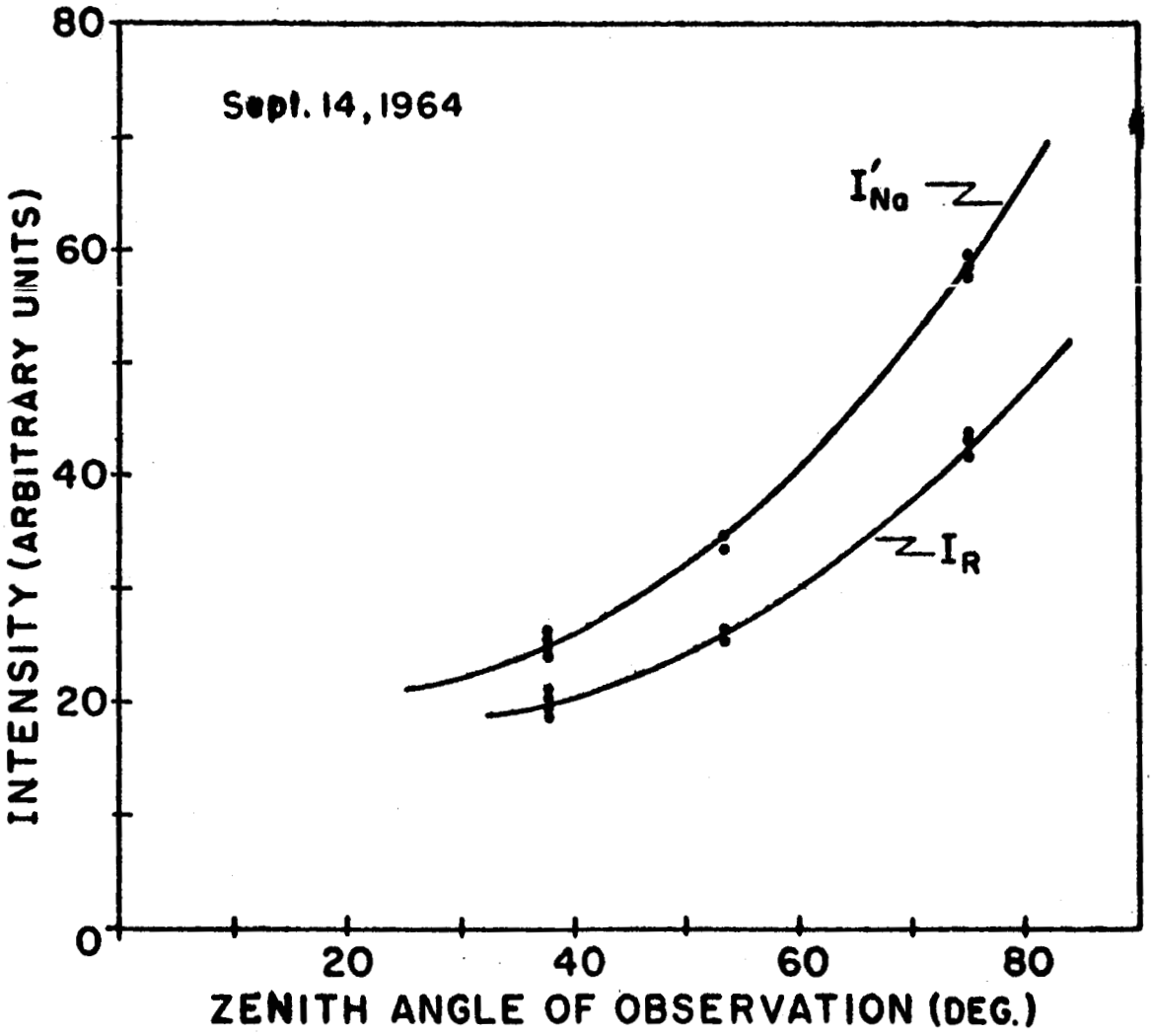

Figure 4. Variation of Zeeman output with angle of observation.

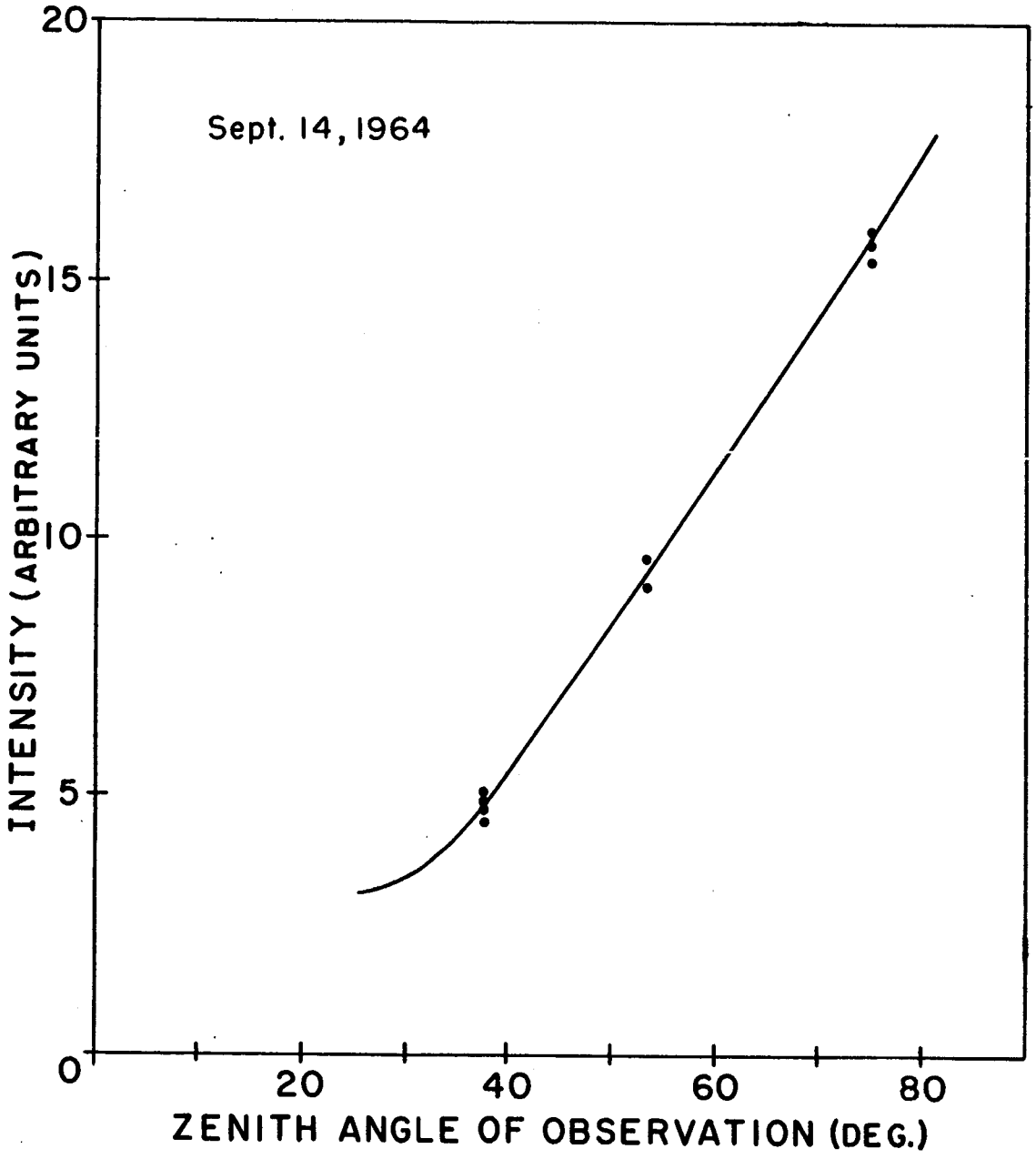

Figure 5. Variation of sodium emission (measured by the Zeeman photometer) as a function of angle of observation.

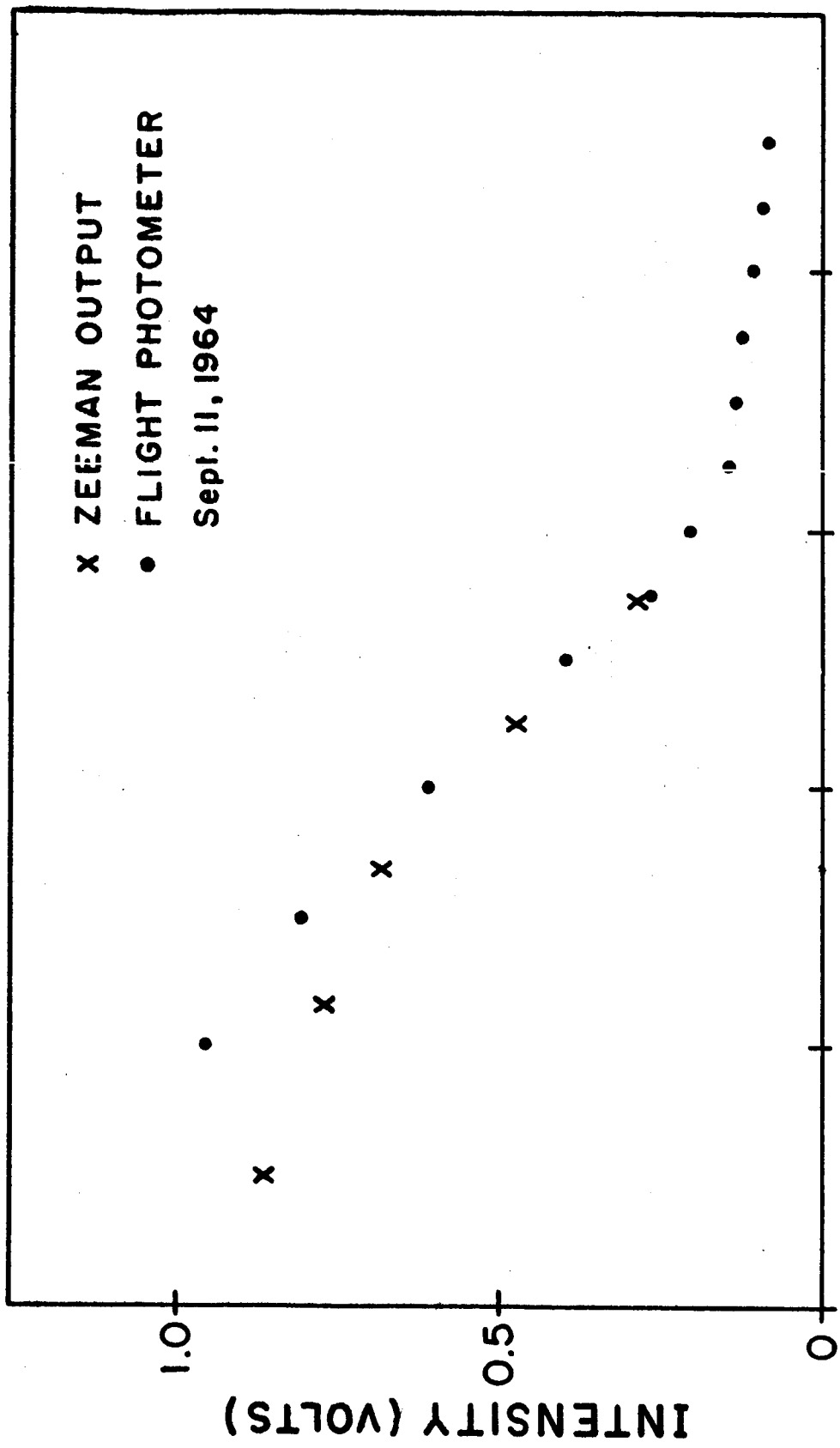

Figure 6. Comparison of Zeeman and flight photometers. The Zeeman output is multiplied by 5.55×10^{-3} volts/kR.

Unfortunately the drift was not measured in the region of the discrepancy between the two signals so that the intensity from the flight photometer could have been in error. The drift was found to be negligible from 19^h10 to 19^h30. This placed confidence in the comparison made at later times.

A different twilight photometer was provided by D. M. Hunten and was operated during several twilights by Kitt Peak personnel. An absolute calibration light source was on site so that the Hunten photometer was calibrated absolutely. The Zeeman photometer and the Hunten device were operated simultaneously on seven twilights to compare their calibrations. A typical comparison is shown in Figure 7.

There was a problem connected with the white light compensation of the Hunten photometer. The instrument was slightly over-compensated so that when the Rayleigh scattering was large as in early twilight, the sodium signal was smaller than it would have been for a correct compensation. This effect can be seen in Figure 7 in the plateau region of the curves. To correct for over compensation, a fraction of the white light intensity was added to the sodium intensity so that a plateau was obtained. Application of this technique yielded intensities for the Hunten photometer which were, on the average, 15% higher than those of the Zeeman photometer.

The calibration curve for the Hunten photometer is given in Figure 8. A "least-squares" analysis was performed on the data from the absolute calibration source. The result of the analysis yielded a calibration of 0.0500 kR/mm. To match the Zeeman in-

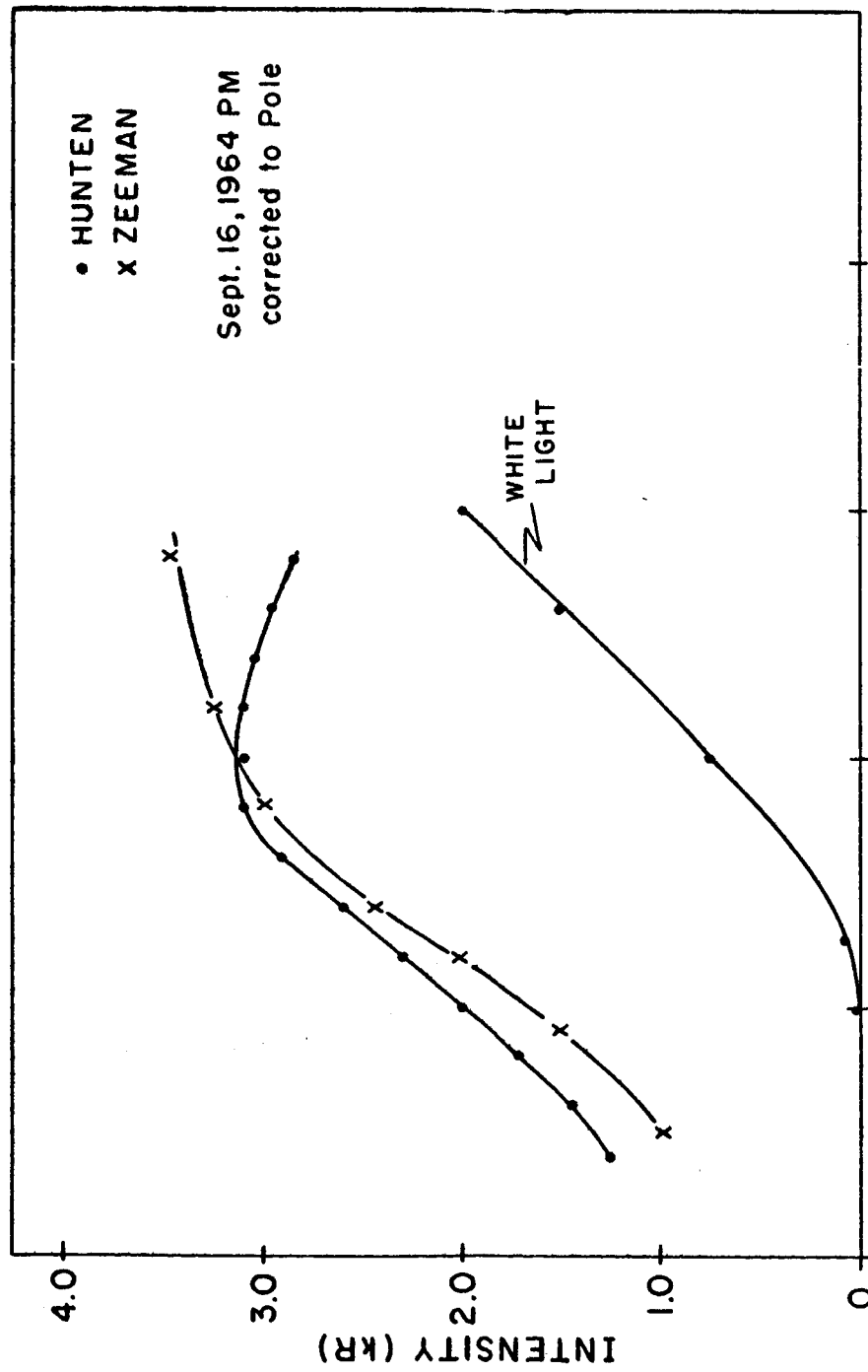

Figure 7. Comparison of Zeeman and Hunten photometers.

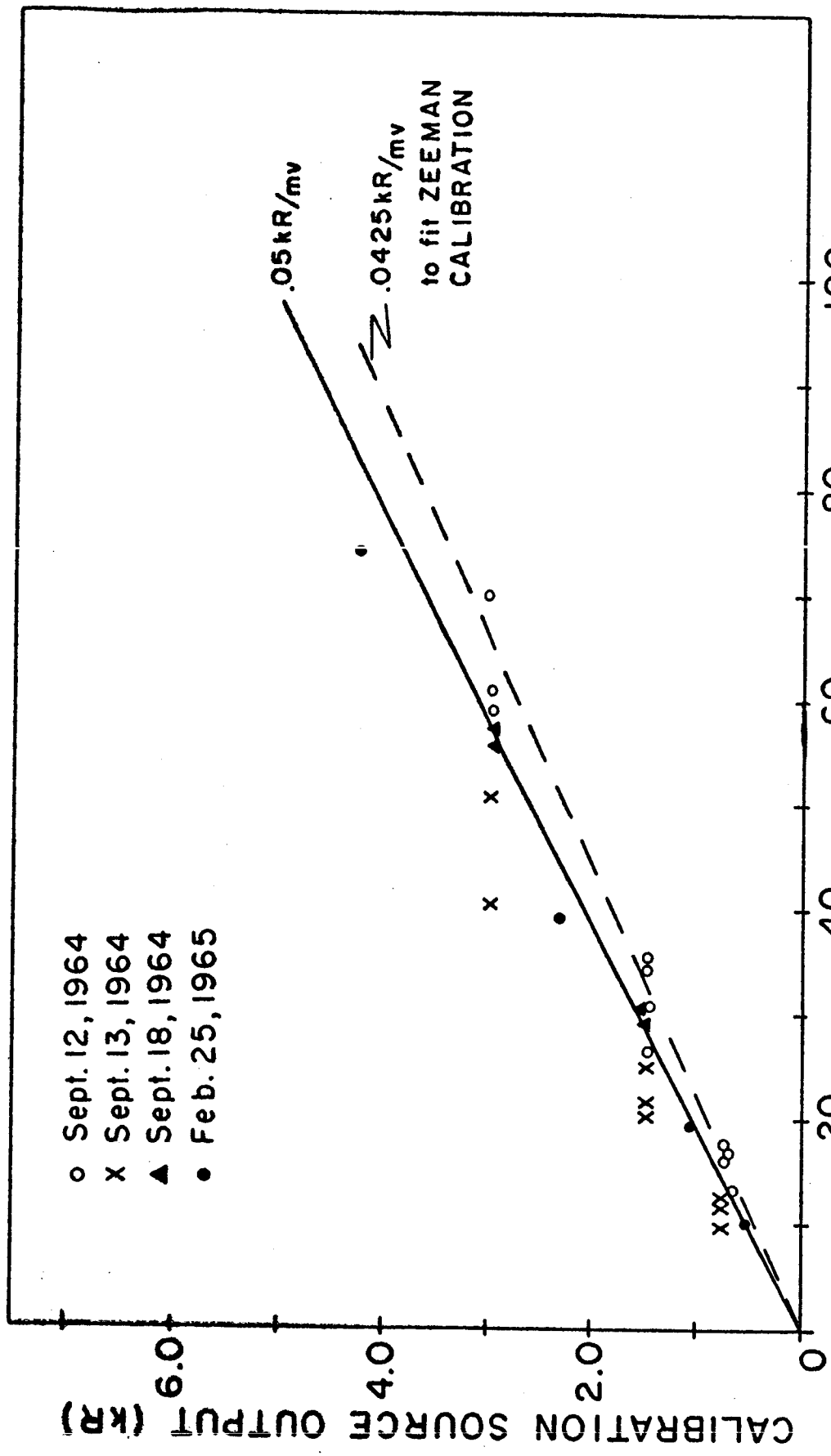

Figure 8. Calibration curve for Hunten photometer. Dashed curve is calibration necessary to fit Zeeman data.

tensities, a calibration of 0.0425 kR/mm was required. It appears that further experimental comparisons are necessary before this discrepancy can be removed. The estimated error in using a calibration of 180 kR/volt for the flight instrument was +45%, -35%.

On the day of the flight, the Zeeman photometer was pointed at a 75° zenith angle in the direction which was to be scanned by the flight photometer. After launch the rocket instrument recorded intensities at an 83° zenith angle. To compare the signals from the two photometers, an extrapolation of the curves in Figures 4 and 5 was performed. The signal on the sodium channel of the rocket experiment was about 1.1 volt immediately after launch. Unfortunately, the amplifier saturated at a rocket altitude of about 0.4 km. and stayed in this condition until about 7 km. However the white light signal remained on scale. An extrapolation of the sodium signal from 7 km. to the ground was performed using the white light data and the extrapolated Zeeman white light discrimination. The resulting signal from the sodium channel (after stray light subtraction) was very close to 1.1 volts. This is to be compared with a Zeeman intensity (I'_{Na}) of 200 kR. The agreement with the previous calibration of 180 kR/volt was excellent. These results will be discussed later when the data from the flight is examined.

It is to be noted that in the reduction of the Zeeman data the effect of polarization of the Rayleigh scattered background intensity was taken into account. This effect had previously introduced a systematic error in the magnetic scanning procedure. A discussion of this phenomenon is given by Gadsden,

Blamont, and Donahue[9].

2.3 Rocket Performance

The rocket, Aerobee 4.13, was launched at 08^h04 E.D.S.T. on September 26, 1964, from Wallops Island, Virginia (latitude $37^\circ 50'$N, longitude $75^\circ 20'$W). The launch coordinates were 122° azimuth (from North) and 85° elevation. The vehicle reached an apogee of 120.4 km. and impacted at a range of 77 km. Radar was used to obtain velocity and position data while magnetometers and sun sensors were employed to determine the orientation of the rocket.

The flight history is depicted in Figure 9. The rocket had an attitude control system (ACS) which was to put it through a series of maneuvers (not required for the sodium experiment). Unfortunately, the ACS malfunctioned at somewhat inopportune times, and thus caused difficulties in interpretation of the attitude data.

The rocket de-spin mechanism was activated at about 78 km. Due to loss of spin stabilization, the precession angle of the vehicle then became somewhat larger. At the same time, the lateral magnetometer started to carry R. F. pickup, thus making its output in many cases, questionable. The longitudinal magnetometer suffered a loss in sensitivity at launch, rendering it useless. Fortunately, there were three lateral ADCOLE-type sun sensors and one longitudinal sun sensor on board.

As the rocket passed through the sodium layer, it was not spinning although its zenith angle was changing slightly. At about 96 km., the ACS caused the rocket to increase its zenith

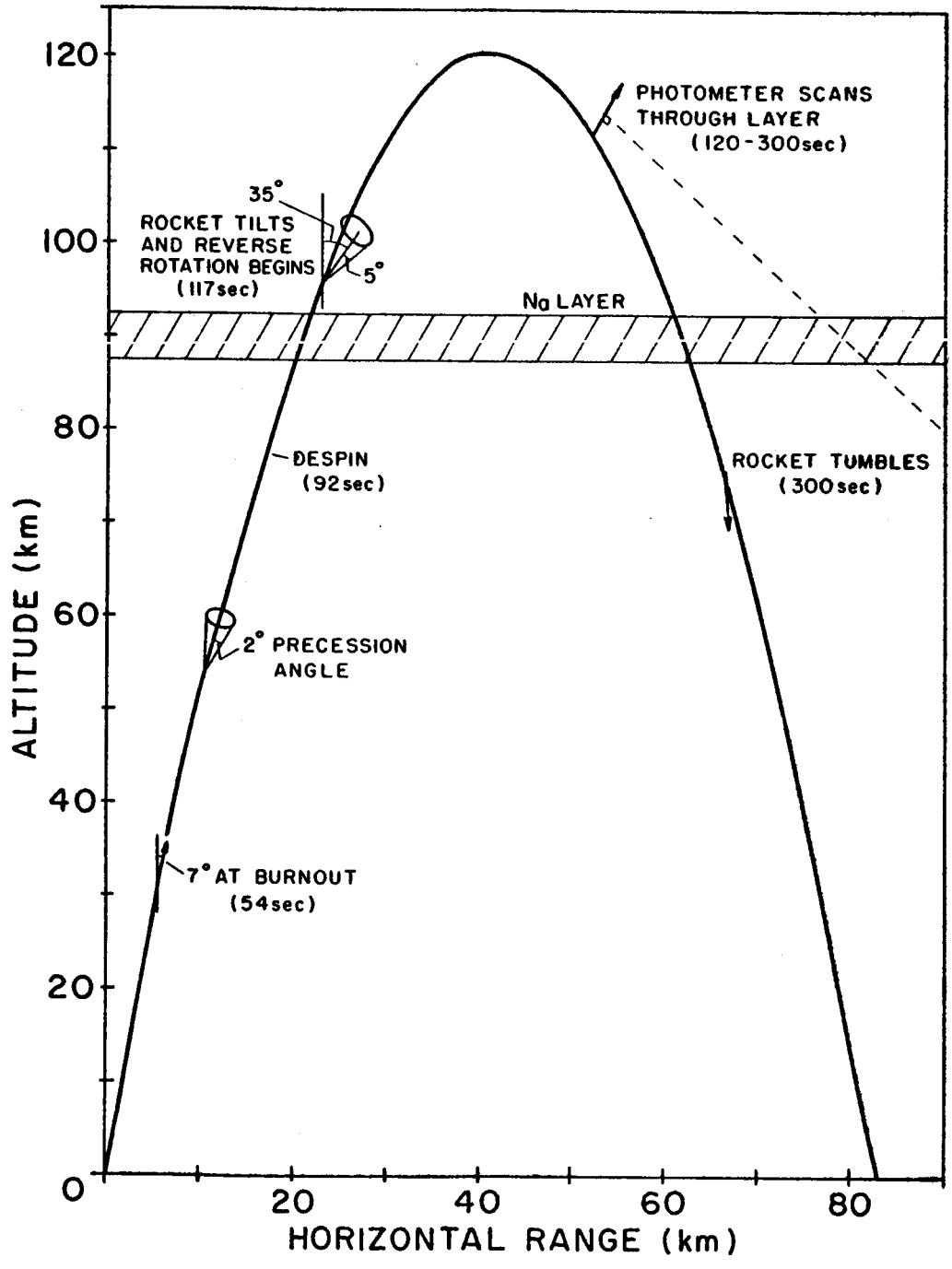

Figure 9. History of rocket flight.

angle to about 35° and to begin spinning in the opposite direction. This motion, coupled with a precession cone of near 5° half angle, continued through apogee until about 75 km. on descent where the vehicle turned over.

The methods of attitude determination are discussed in the next section and in Appendix A.

2.4 Data

Data were obtained from launch until the rocket tumbled. The rocket experiment scanned the sodium distribution from several different orientations during the flight so that excellent profiles of the layer were obtained.

The instrument was turned on before launch (the detector head was sealed). This was possible because of the small response of the photometer to Rayleigh scattering (except at the sodium wavelengths). Since the amplifiers suffered from zero drift, the zero level of the sodium channel (which must be kept positive because of telemetry) was + 2.5 volts at launch so that only a little more than half of its dynamic range was usable. It was extremely fortunate that a greater magnitude was not required during the regions of interest in the flight. The amplifiers did saturate when the photometer looked in the direction of the earth because of the large amount of Rayleigh scattering and albedo, but this was of no consequence. The sodium channel amplifier had negligible drift during the flight, although the white light signal increased slowly. This effect was taken into account in the white light data reduction. The uncertainty in the

data reduction was fairly small (about 5%).

As the rocket left the launching tower, both channels recorded signals. The sodium channel quickly saturated and was in this condition until the rocket reached an altitude of 7 km. The white light channel registered a signal first from the sky; then as the vehicle rolled, the photometer swept down across the horizon, the ocean, the horizon, and the sky once again. At a rocket zenith angle of 83°, the intensity seen by the photometer as it swept across the earth was very large and both amplifiers were overloaded. When the instrument looked at the sky again, the signal came back on scale. A sample oscillograph record of this scanning procedure is shown in Figure 10. The altitude was about 20 km. The upper trace in Figure 10 is the sodium signal, while the lower is the white light signal.

The white light channel saw virtually nothing above 30 km.when it looked up so that the sodium channel signal was entirely due to emission from atmospheric sodium. The two signals are plotted up to 95 km. in Figure 11. I^*_{Na} is the signal from the sodium channel while I_{wl} is the white light intensity (I_{wl} must be multiplied by 0.95 to adjust its sensitivity to I^*_{Na}).

Throughout the flight, the Zeeman photometer was pointed at a zenith angle of 75° in the direction which was scanned by the rocket experiment. The Zeeman signals were extrapolated to an observational angle of 83° for comparison with the data from the flight photometer. After this correction, the sodium emission recorded by the Zeeman photometer was about 60 kR. Notice that in Figure 11 the intensity seen by the flight instrument was

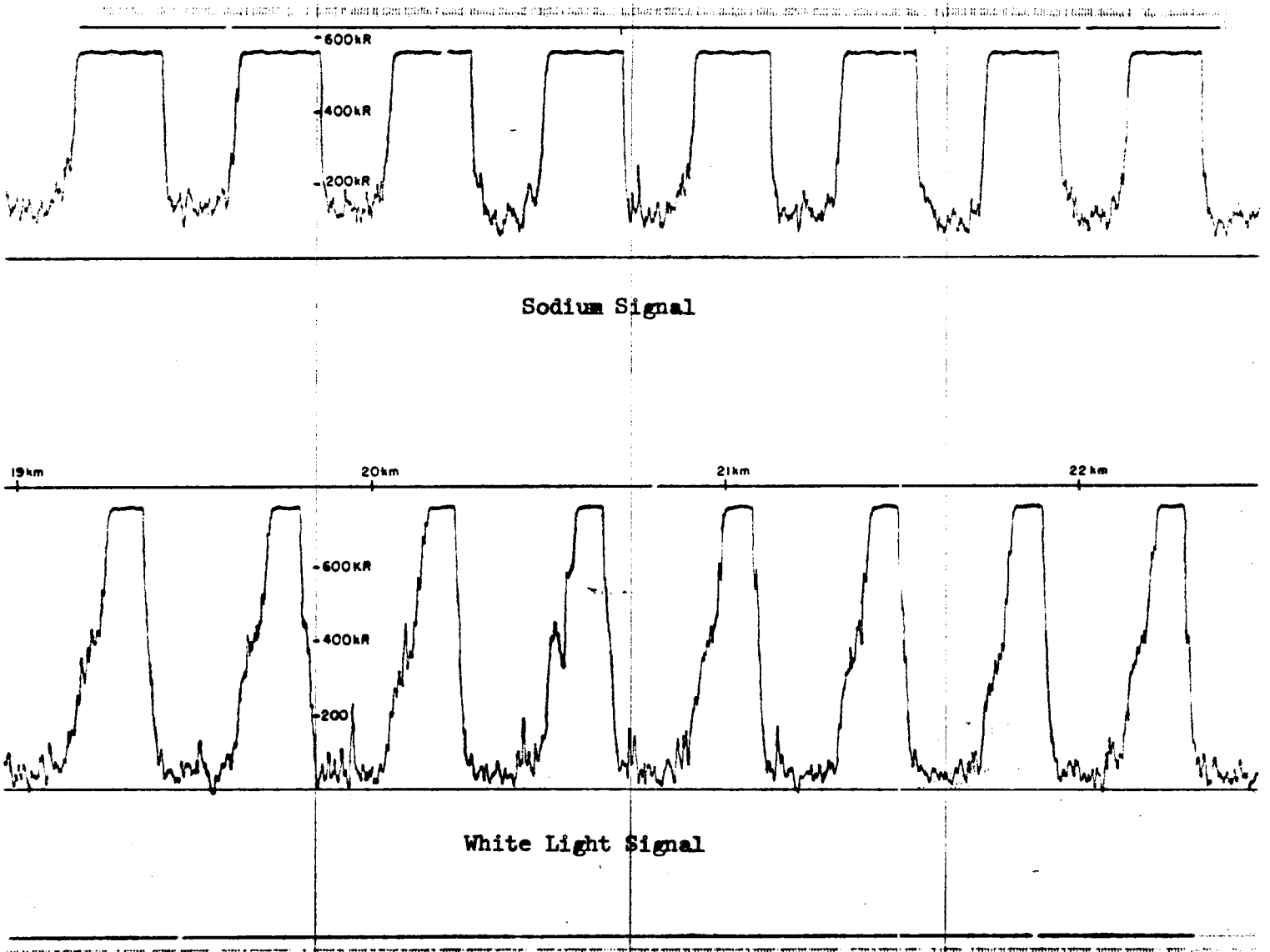

Figure 10. Oscillograph record of data during ascent. The abscissa is rocket altitude.

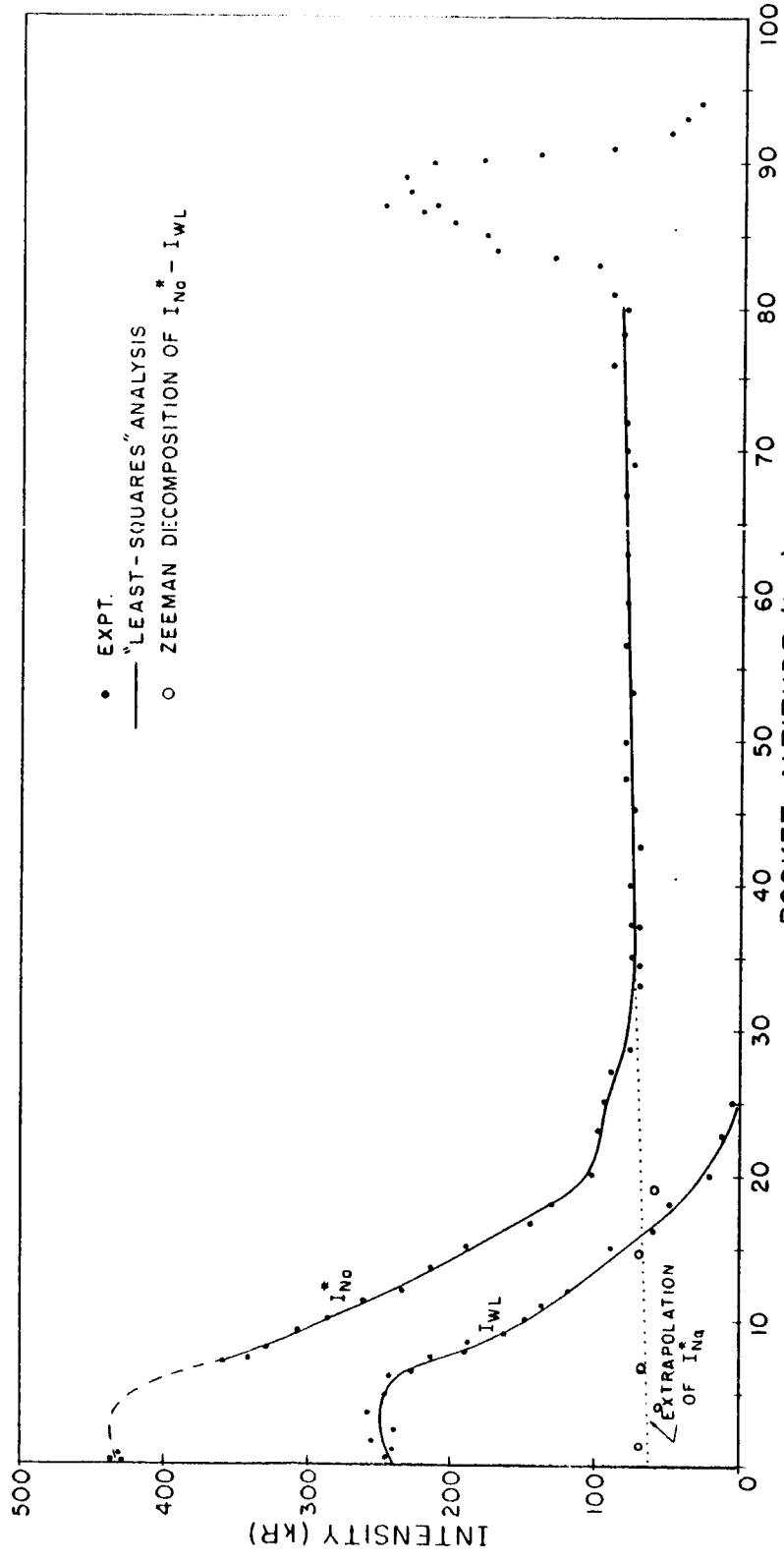

Figure 11. Sodium and white light signals during ascent. The white light signal must be multiplied by 0.95 to equalize the responses of the two channels.

about 74 kR. at 35 km. Then it slowly increased to about 83 kR. at 77 km. A "least-squares" analysis was done on the data in this region. The solid lines represent the results of this analysis. If the curve is linearly extrapolated downward to the ground, the resultant intensity is very near 60 kR. Also, the extrapolated curve (given by the dotted line in Figure 11) s traddles the circles which represent the Zeeman decomposition of I^*_{Na}. There is now very little doubt that the Zeeman photometer was actually measuring the sodium dayglow.

The dashed part of the curve given for I^*_{Na} from 0 to 7 km. was obtained by use of the Zeeman decomposition and the white light data for that region. This extrapolation was in excellent agreement with the signal from the sodium channel before saturation.

After "burn-out" the rocket began precessing with a half angle of about 2^o. Since the photometer was looking at an essentially "broad" source from below the layer, the effects of precession were not important at low altitude. As the layer was approached, however, the direction of observation became quite critical. The change in zenith angle of the rocket as it traversed the layer was small. However, it was not negligible, for it produced the very sharp change in intensity at 90 km. This important region will be discussed later when the radiative transfer methods are used to interpret the results.

As was previously mentioned, near 96 km. the rocket was tilted to a zenith angle of about 35^o and began to spin in the opposite direction. The spin rate increased to a maximum of

0.2 per sec. before the rocket turned over at 75 km. on descent. At this angle of observation, the scanning of the photometer was extremely effective in determining the spatial distribution of the sodium.

The scanning procedure for the region of the flight when the rocket was above the sodium layer is shown in Figure 12 along with a corresponding intensity plot. At "a", the photometer began to sweep through the layer; at "b" the largest amount of sodium emission was observed. Rayleigh scattering from the lower atmosphere became important at "c". The photometer then scanned across the surface of the earth and up through the layer again. An oscillograph record of a complete scan is shown in Figure 13. Again the upper trace is the signal from the sodium channel, and the lower trace is the white light signal. There were several interesting features evident in the white light trace. The intensity increased to a maximum as the photometer scanned across the horizon. The signal then decreased slightly, until the reflection of the sun in the ocean was encountered. The large increase in the signal at this point can be seen in Figure 13. The photometer then scanned across the horizon and through the layer again.

Due to the limited dynamic range in the sodium channel, Rayleigh scattering and albedo quickly saturated its amplifier as the photometer scanned the lower atmosphere. However, the sodium emission signal was well within the maximum capacity of the amplifier.

There were a total of eight complete scans from 97 km. on

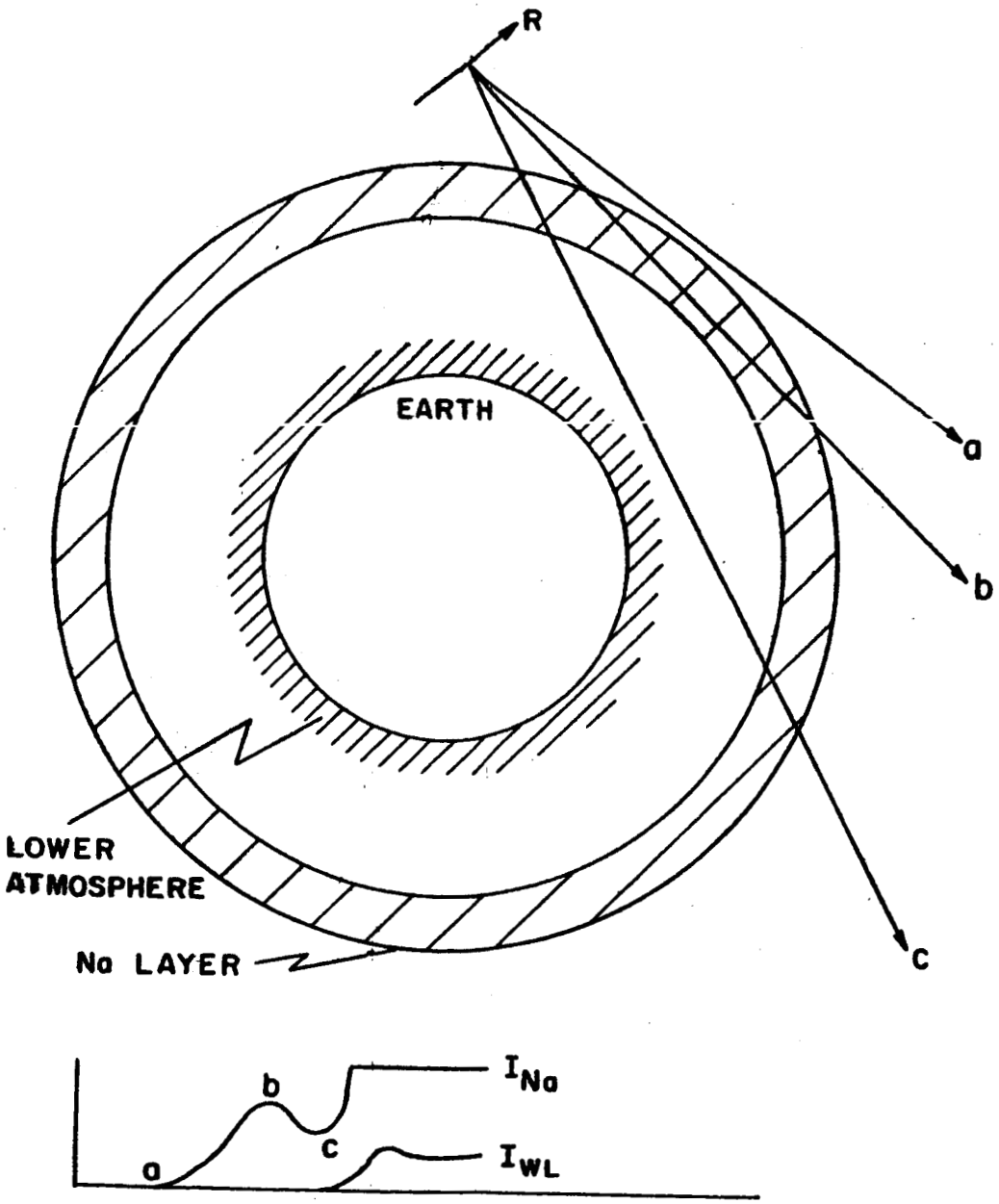

Figure 12. Diagram of scanning mode. Directions a, b, c correspond to the intensities at a, b, c.

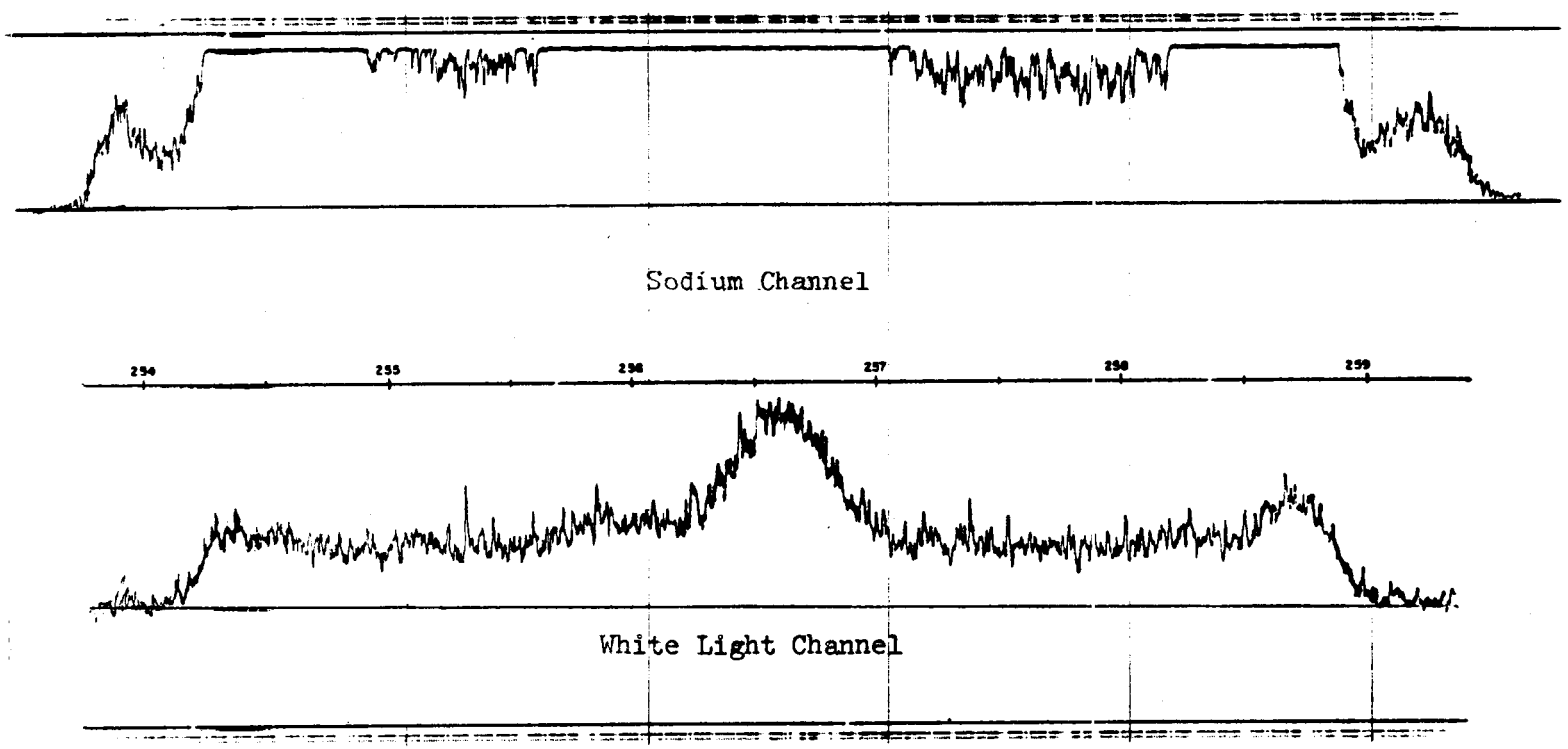

Figure 13. Oscillograph trace of Scan 6. The abscissa is elapsed time from launch.

ascent until the rocket tumbled. However poor attitude information prevented utilization of the first, last, and half of the seventh, so that eleven individual layer sweeps provided useful data.

To determine the direction of observation for the region of the flight when the rocket was above the layer, the magnetometer and sun sensor data were used. The azimuth and zenith angles of the rocket were found in this way, but the R. F. pickup on the lateral magnetometer prevented an accurate determination of the spin angle. However, a method was developed in which the data from the white light channel were utilized to find the value of the rocket spin. The method is described in Appendix A. This technique averaged over the precession of the rocket so that there was an inherent error present. Fortunately calculations proved this inaccuracy to be smaller than that encountered by the noisy magnetometer.

The data from the eleven sweeps are given in Figures 17 through 27.

2.5 Radiative Transfer Interpretation

In the steady state the density of excited atoms is given by

$$n(\underline{r}) = n_o(\underline{r}) + \int n(\underline{r}') G(\underline{r},\underline{r}')\, d\underline{r}', \qquad (1)$$

where $n_o(r)$ is the density of atoms directly excited by the solar radiation, and $G(\underline{r},\underline{r}')\, d\underline{r}d\underline{r}'$ is the probability that a photon will be emitted from a volume element $d\underline{r}'$ at $\underline{r}'$ and subsequently

be absorbed in $d\underline{r}$ at $\underline{r}$. It is possible to change variable from altitude z to optical thickness τ defined as

$$\tau(z) = \sigma_0 \int_{\infty}^{z} \rho(z')\, dz' \tag{2}$$

where σ_0 is the absorption cross section at the center of the line and $\rho(z)$ is the unexcited atom density. This is due to the fact that ρ is a function of z only. Then $n(\underline{r})$ becomes

$$n(\tau) = n_0(\tau) + \int n(\tau')\, H(\tau,\tau')\, d\tau' \tag{3}$$

where H is the probability that a photon is emitted from $d\tau'$ at τ' and later absorbed in $d\tau$ at τ.

The intensity of photons arriving at any distance τ is given by

$$4\pi I(\tau) = \gamma \int n(\tau')\, T(\tau,\tau')\, d\tau'. \tag{4}$$

In (4) γ is the radiative transition probability per unit time and $T(\tau,\tau')$ is the Holstein probability function defined as the probability that a photon will be emitted at τ' and travel a distance $|\tau-\tau'|$ without being absorbed.

Biberman[10] showed that the expression for the excited atom density $n(\tau)$ can be written in the following manner if $E(\tau)$ is defined as the probability that a photon will be emitted in a certain volume element and arrive at the boundaries without being absorbed:

$$n(\tau) = \frac{n_0(\tau)}{E(\tau)} + \frac{1}{E(\tau)} \int \left[n(\tau') - n(\tau)\right] H(\tau,\tau')\, d\tau'. \tag{5}$$

E (τ) is given by

$$E(\tau) = 1 - \int H(\tau,\tau')\, d\tau' . \qquad (6)$$

As a first approximation of the excited atom density, the first term on the right of (5) may be used. When $n_o(\tau)/E(\tau)$ does not vary rapidly as a function of τ, the approximation is very close to the true solution. Since the vertical optical thickness was found to be 0.06 for the sodium layer, this approximation was used to determine the excited atom density. The error introduced in the solution was at most only 10% near the boundries of the layer.

If πF_o is the incident solar flux, θ is its angle of incidence and K (ν) is the absorption coefficient, then the rate of absorption of direct solar radiation (continuum), γn_o, is given by

$$\pi F_o \int K(\nu) \exp(-\tau \sec\theta\, K(\nu))\, d\nu . \qquad (7)$$

This is easily seen to be

$$\pi^{\frac{1}{2}} F_o \Delta\nu \; T(\tau \sec\theta) \qquad (8)$$

where $\Delta\nu$ is the absorption line width (Doppler in the present case of sodium). Thus the excited atom density is given by

$$n(\tau) = \frac{\pi^{\frac{1}{2}} F_o \Delta\nu_D}{\gamma} \; \frac{T(\tau \sec\theta)}{E(\tau)} . \qquad (9)$$

The next step is to postulate a density distribution and relate it through the angle of observation to the optical thickness.

The sharply varying intensity observed from the upper part of the sodium distribution by the rocket experiment suggested an exponentially shaped density function. The instrument, of course, averaged the intensity over its solid angle so that the difference between, say, a Gaussian and an exponential layer could not be discerned. Therefore, for the sake of flexibility a model was chosen according to the following definition:

$$\rho(z) = \rho(z_0) \times \begin{cases} e^{-\frac{z-z_0}{H_1}} & \text{FOR } z \geq z_0 \\ e^{+\frac{z-z_0}{H_2}} & \text{FOR } z \leq z_0 \end{cases} \tag{10}$$

where z_0 is the altitude of maximum density, and H_1 and H_2 are the respective scale heights of the top and bottom of the layer respectively.

To relate the altitude distribution of sodium to the optical thickness along the line of sight, the ascending and scanning regions of the flight were considered individually. First was the case in which the photometer looked through the layer only once (ascent). The optical thickness along the line of sight can be written as

$$\tau = \sigma \int \rho(s)\, ds \tag{11}$$

where S is the path length in this direction.

From Figure 14, which shows the two modes of scanning, the following equation is evident,

$$\underline{P} + \underline{S} = \underline{R} \tag{12}$$

or

$$P^2 = R^2 + S^2 + 2RS\cos\theta \qquad (13)$$

The above quantities are defined as in the figure. Since $P = R_o+z$ and $R = R_o+h$ where z is the altitude above the earth for a particular S (and θ), and h is the altitude of the rocket, the following equation results

$$Z = \sqrt{(R_o+h)^2 + S^2 + 2(R_o+h)S\cos\theta} - R_o \qquad (14)$$

This expression is substituted into (10) to get $\rho(S)$. The density is then integrated from S=0 to $S(z_o)$ using the lower expression in (10). At $S(z_o)$ the second form of $\rho(z)$ is used for integration out to S. The maximum value of S was chosen to be S (125 km.). The excited atom density is then calculated using the standard forms for T ($\tau \sec\theta$) and E (τ). Next the intensity is determined for this particular value of θ . To include the effects of the finite instrumental solid angle, the intensity is found for various points in the interval $\theta \pm \delta$, where δ is the half angle of the input aperature. These intensities are then averaged over the field of view to give the intensity recorded by the photometer.

During the later region, the problem was somewhat more complicated because the photometer scanned through the layer twice. Essentially the same method as in the ascending case, was used to determine I (τ) although considerable care was exercised to include contributions to the intensity from two different parts of the layer.

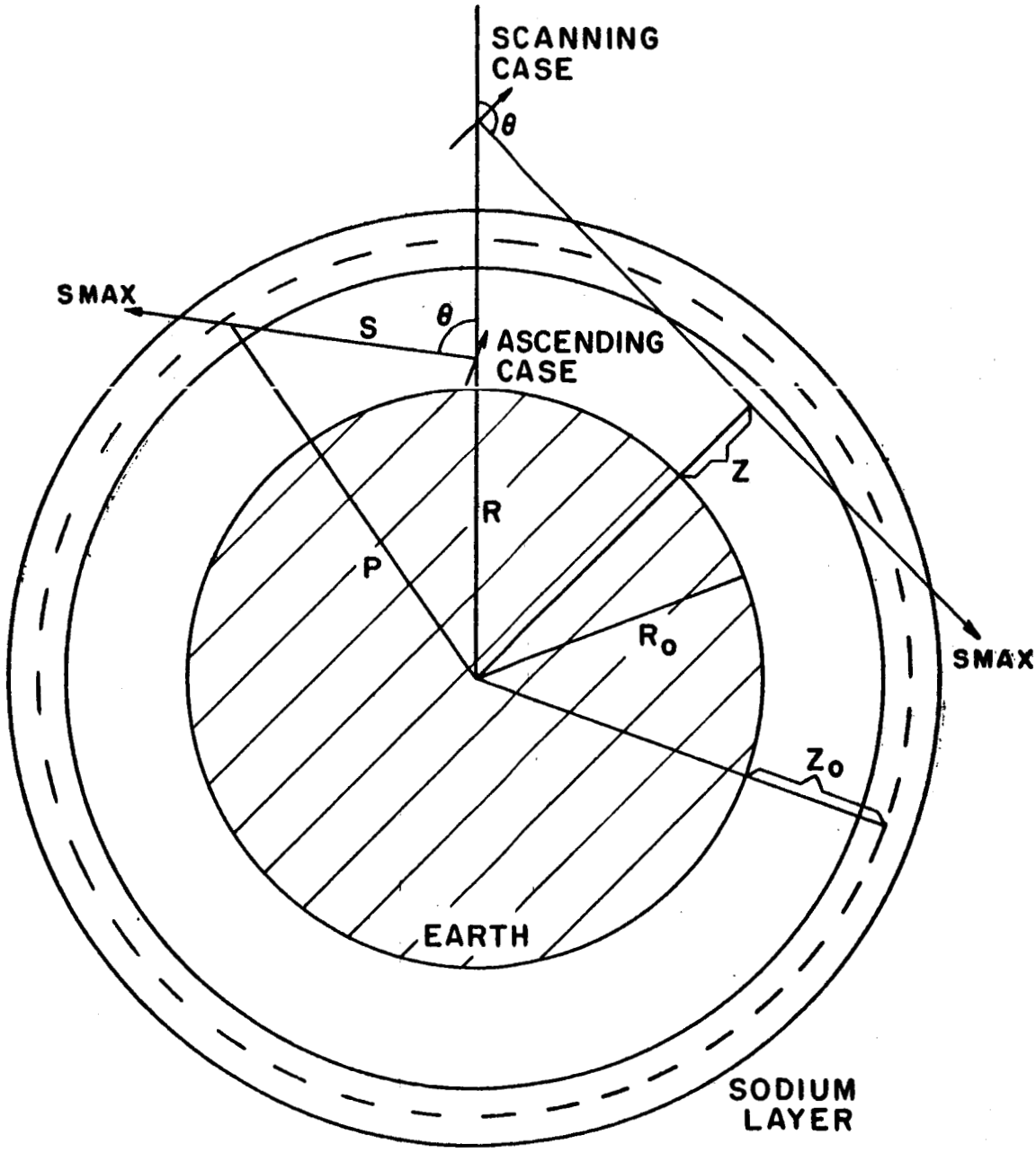

Figure 14. Geometry of ascending and scanning regions of the flight.

It is noted that in this solution it has been assumed that the elevation of the sun was constant over the entire scanning region. This was found to be a good approximation for a 14^{o} solar elevation.

This radiative transfer solution was programmed on the I.B.M. 7090 computer. The program was made quite flexible so that the intensity could be calculated for any rocket altitude and angle of observation. The solid angle effect was included in the program to give a calculation of the actual intensity recorded by the photometer. The contributions from Rayleigh scattering and albedo were not included.

The result of trying different values of z_o, $\rho(Z_o)$, H_1 and H_2 to match the ascending and scanning data yielded the following density distribution: an average peak altitude of 92.4 km. with a density of 2.8×10^{4} atoms/cm^3 and a half width of 2.5 km. The scale height was chosen to be equal on both halves of the layer. Although the experiment could only give a measure of the upper half of the distribution, the lower half could not have been too much larger; otherwise, a larger optical thickness would have been necessary to match the peak intensity. The model would than have been inconsistent with the data from other parts of the flight.

The scale height analysis involved an error of about +0.5 km. and -0.2 km. This caused an uncertainty in the density of about 20% when matching the theoretical curves to the experiment. The deviation in altitude of maximum density will be considered in conjunction with each phase of the flight.

Figure 15 gives the theoretical analysis of the ascending part of the flight up to an altitude of 75 km. where the angular coordinates of the rocket became important. Included is the experimental measurement of the intensity at the sodium wavelengths. That is, the difference between the two curves in Figure 11. The fit is quite good although in many cases because of amplifier noise, the error in reading a particular data point was as much as $\pm$ 10 kR. It is noteworthy that at ground level the theoretical calculation gave 58 kR, compared to the Zeeman photometer reading of 60 kR.

There were a few peculiar points in the experimental data for the altitude interval of 20 to 30 km. as seen in Figure 15. Near 20 km. the intensity seemed to match the curve at lower altitudes. Then from 23 km. to 26 km. there was a region of slightly higher intensity. It is tempting to suggest that ozone absorption caused the variation. As the rocket passed through the ozone layer, the absorption would decrease, causing a change in slope of the curve. It was significant that this decrease was very near the altitude at which ozone is normally distributed. However, since the change was within the mean deviation of the data, it was not certain that these points were real intensities.

When the rocket stopped spinning at about 80 km., the ACS had pointed the sodium experiment away from the earth. The zenith angle of observation was near 90°. There was a large spread in the data in this region as can be seen in Figure 16. The spread undoubtedly was real because it exceeded observational error. These fluctuations may have been due to inhomogeneities

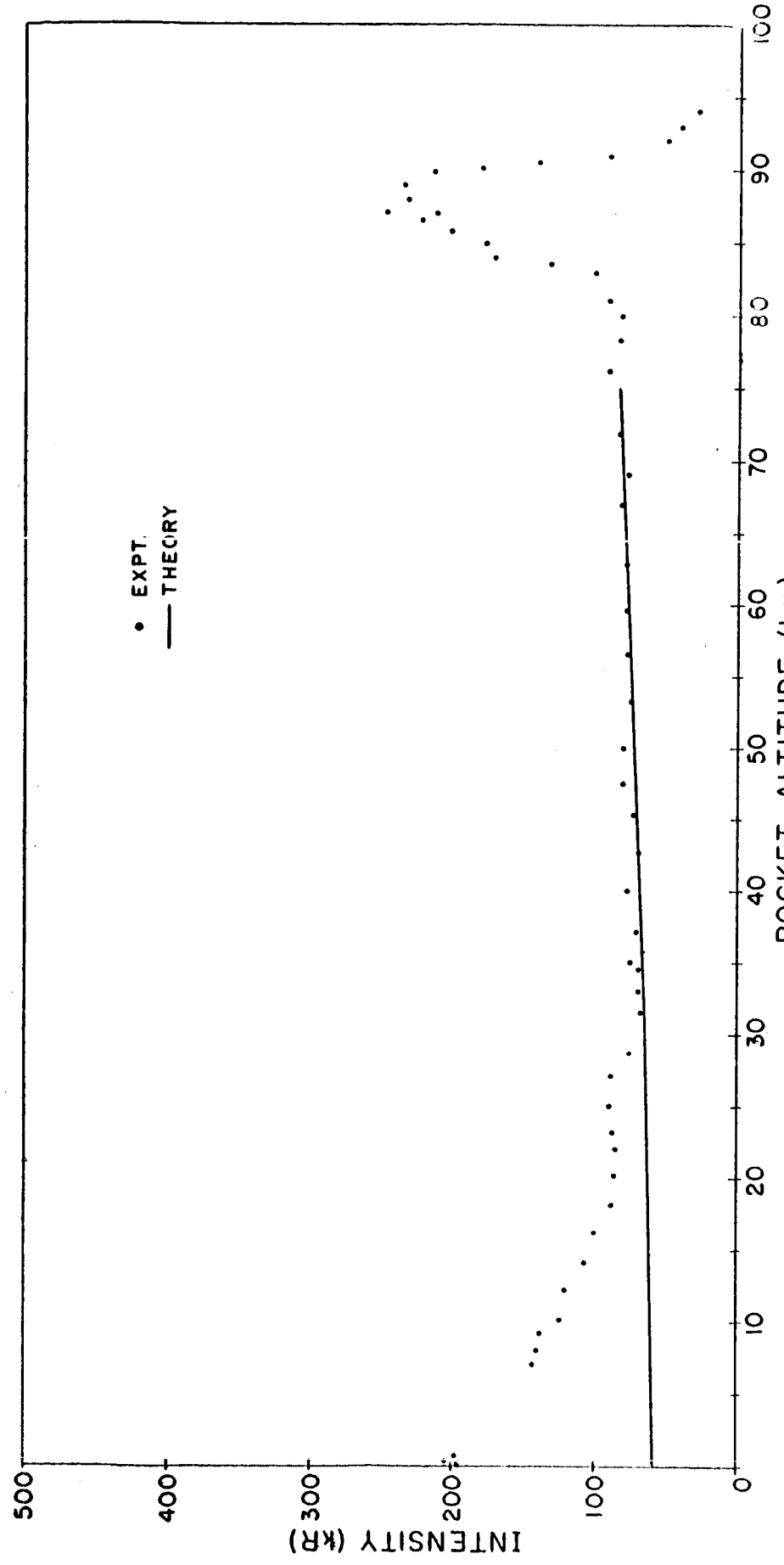

Figure 15. Experimental and theoretical intensities at the sodium wavelengths during ascent.

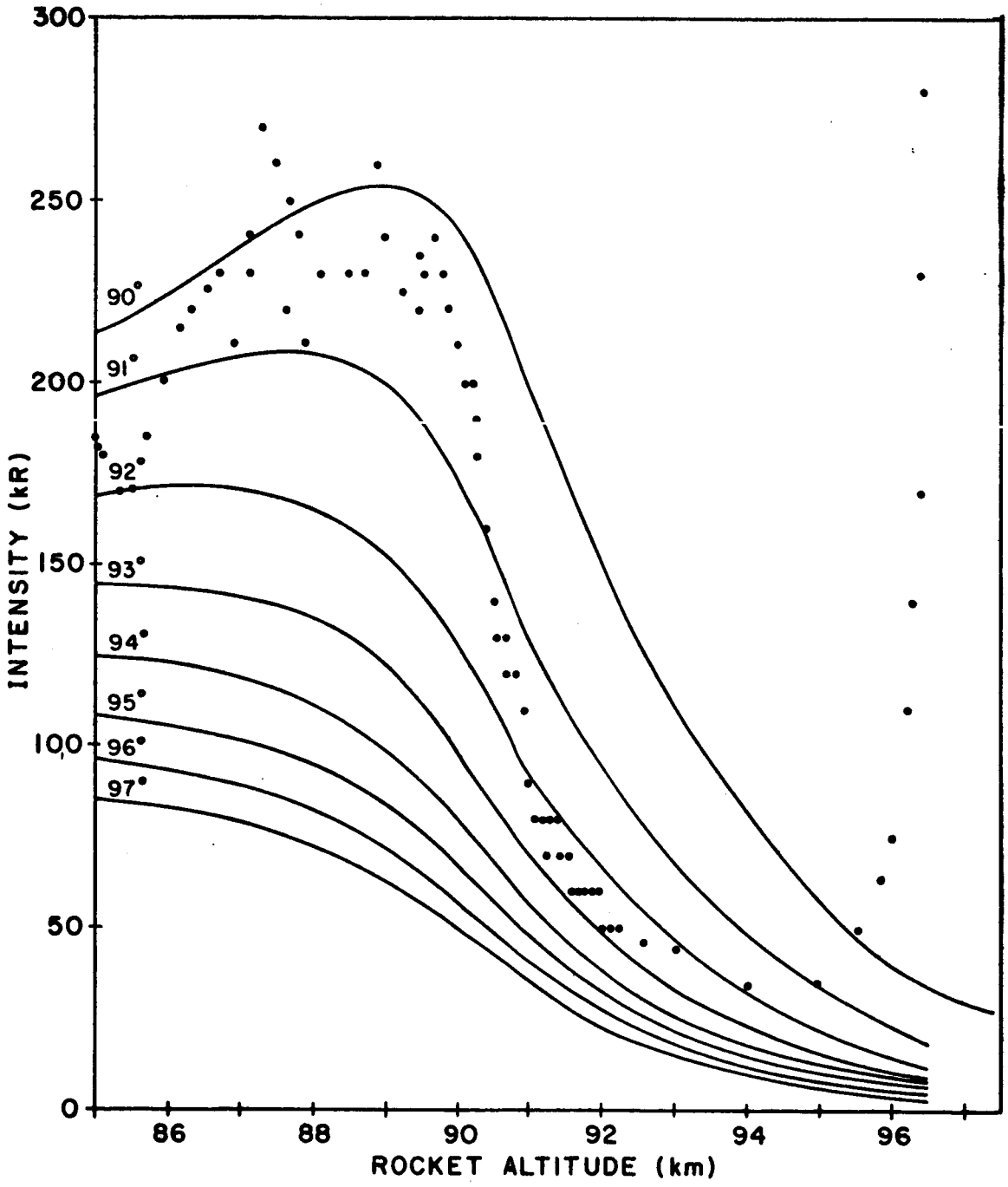

Figure 16. Experimental (dots) and theoretical (solid lines) intensities for the case when the rocket traversed the layer. The large increase at 96 km. was due to rocket motion.

in the layer, In any case, the most startling feature was the very sharp decrease between 90 and 91 km. This is to be compared with the theoretical curves which also are plotted in Figure 16 for various angles of observation. Examination of the attitude data indicated that the change in zenith angle of the rocket was about 3° from 90 to 91 km. The spin angle of the rocket was questionable because the lateral magnetometer output was very poor at this time. Therefore by using the maximum and minimum possible values for the rocket spin angle, limits could be set on the variation of the angle of observation. A comparison of these limits with the data and the theoretical curves in Figure 16 showed that the maximum possible altitude of the sodium layer (with a 2.5 km. scale height) was 90.4 km., and the minimum was 88.8 km. The most likely height determined from the attitude data was 89.8 km. It is noteworthy that the model used for the theoretical curves could not have had a scale height much more than 2.5 km.; otherwise, the required change in the direction of observation would have been incompatible with the attitude data.

The layer actually could have had a scale height of less than 2.5 km. and still have been compatible with the attitude information. However agreement with the scanning data taken later in the flight would then have been impossible.

It is conceivable that a singularity in the sodium distribution might have been responsible for the steep intensity gradient at 90 km. Since the attitude data indicated that a change in observational angle occurred at that time, an inhomogeneity in the layer did not seem to be a likely explanation.

However the attitude information was not accurate enough to entirely eliminate this possibility.

At about 95 km. the ACS began to spin the rocket in the opposite direction and tilt it over to a zenith angle of about 35°. This motion caused the large increase in intensity at 96 km. in Figure 16. Unfortunately due to the spin, precession, and poor magnetometer data, no further attitude information was obtained until the vehicle reached an altitude of about 119 km.

Figures 17 through 27 show the theoretical curves which gave the best fit to the experimental points (indicated by the dots). The intensity is plotted as a function of impact parameter Z (defined by equation (14)). The characteristics of these models are listed in Table I. The scans are given as 2a, 2b, 3a, etc., where 2a indicates the region of the second scan when the photometer first looked through the layer. The second observation of the layer in scan 2 is called 2b.

In the table, h is the rocket altitude, z_o is the height of maximum sodium density, $\rho(z_o)$ is the density there and Δz_o is the maximum error in z_o. z_o was found to be the most likely altitude from the attitude analysis and Δz_o was the largest possible error which resulted (including precession, observational difficulties, etc.). It is interesting that this error could not affect the shape of the intensity curves because the rocket precession was small in the time interval of a scan.

In Figures 28 and 29 the theoretical curves have been drawn through oscillograph records of the data to give an idea of the actual fit. For most cases, careful examination of the

Table I. Parameters used to determine the theoretical models for each scan. All scans used $H_1 = H_2 = 2.5$ km.

Scan	Rocket Altitude (km.)	z_o (km.)	$\rho(z_o)$ (at/cm^3)	Δz_o (km.)
2a	120.0	86.2	3.1×10^4	$\pm$ 7.0
2b	120.3	91.8	2.5×10^4	7.8
3a	119.4	97.9	2.5×10^4	7.5
3b	117.6	93.1	2.5×10^4	5.0
4a	114.7	91.0	2.9×10^4	4.0
4b	111.9	91.3	2.9×10^4	3.2
5a	108.3	87.8	2.5×10^4	4.0
5b	105.1	95.1	3.5×10^4	2.5
6a	101.1	94.4	2.5×10^4	1.9
6b	97.8	93.5	3.9×10^4	1.6
7a	94.1	94.8	3.1×10^4	2.1
	Averages	92.4	2.8×10^4	

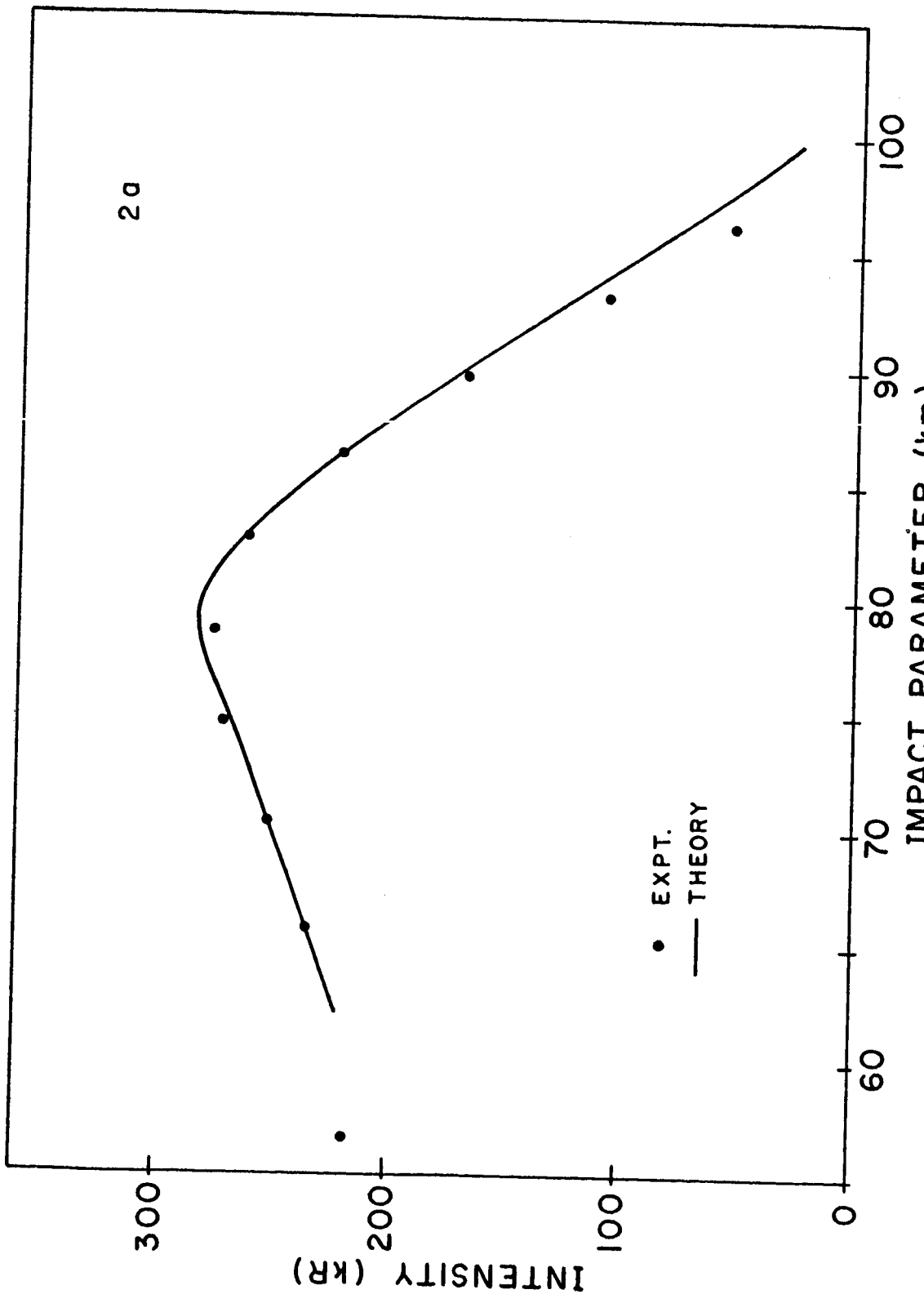
2a
INTENSITY (kR)
300
200
100
0
60
70
80
90
100
IMPACT PARAMETER (km)
EXPT.
THEORY

Figure 17.

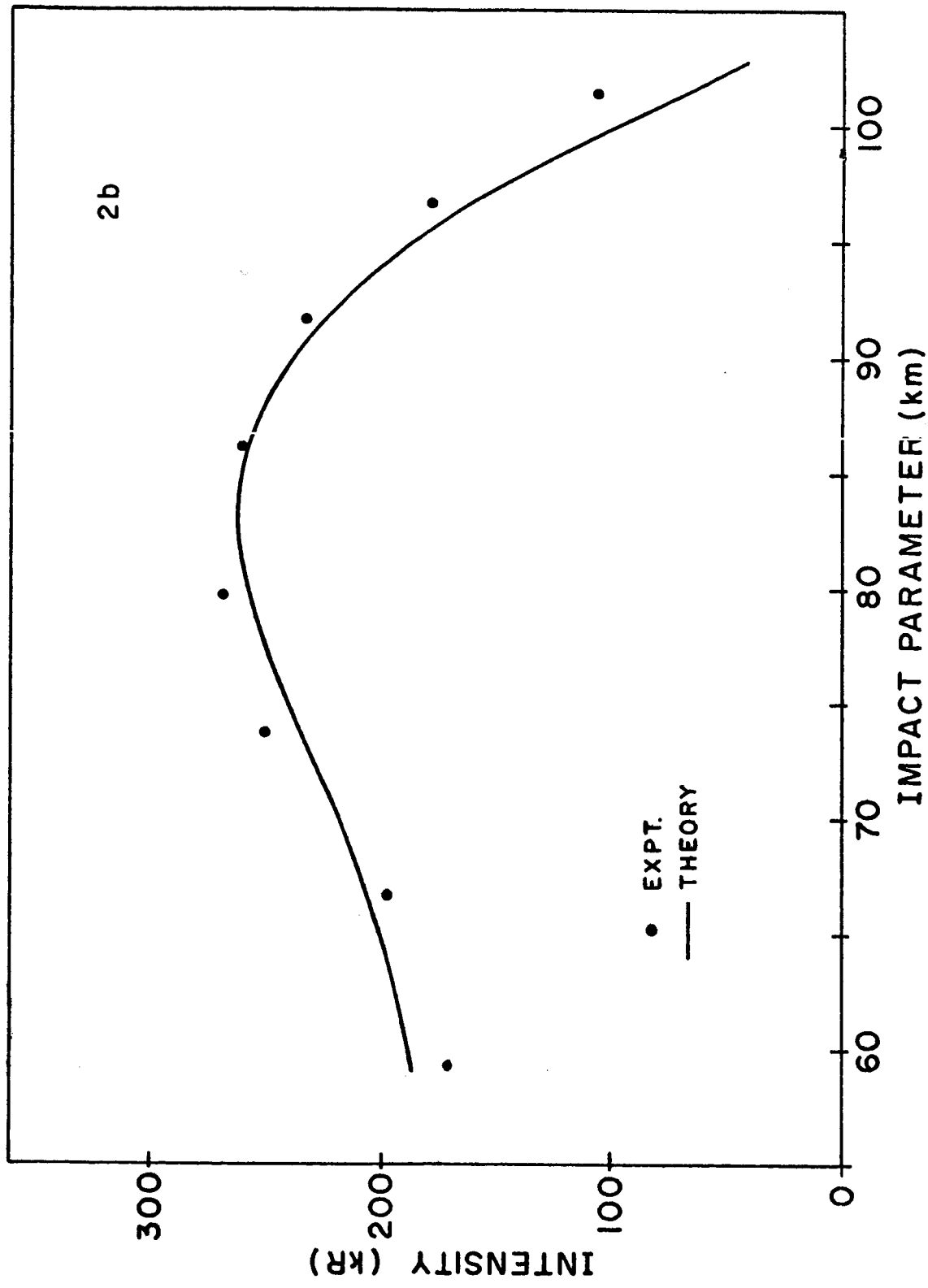
2b
INTENSITY (kR)
300
200
100
0
60
70
80
90
100
IMPACT PARAMETER (km)
EXPT.
THEORY

Figure 18.

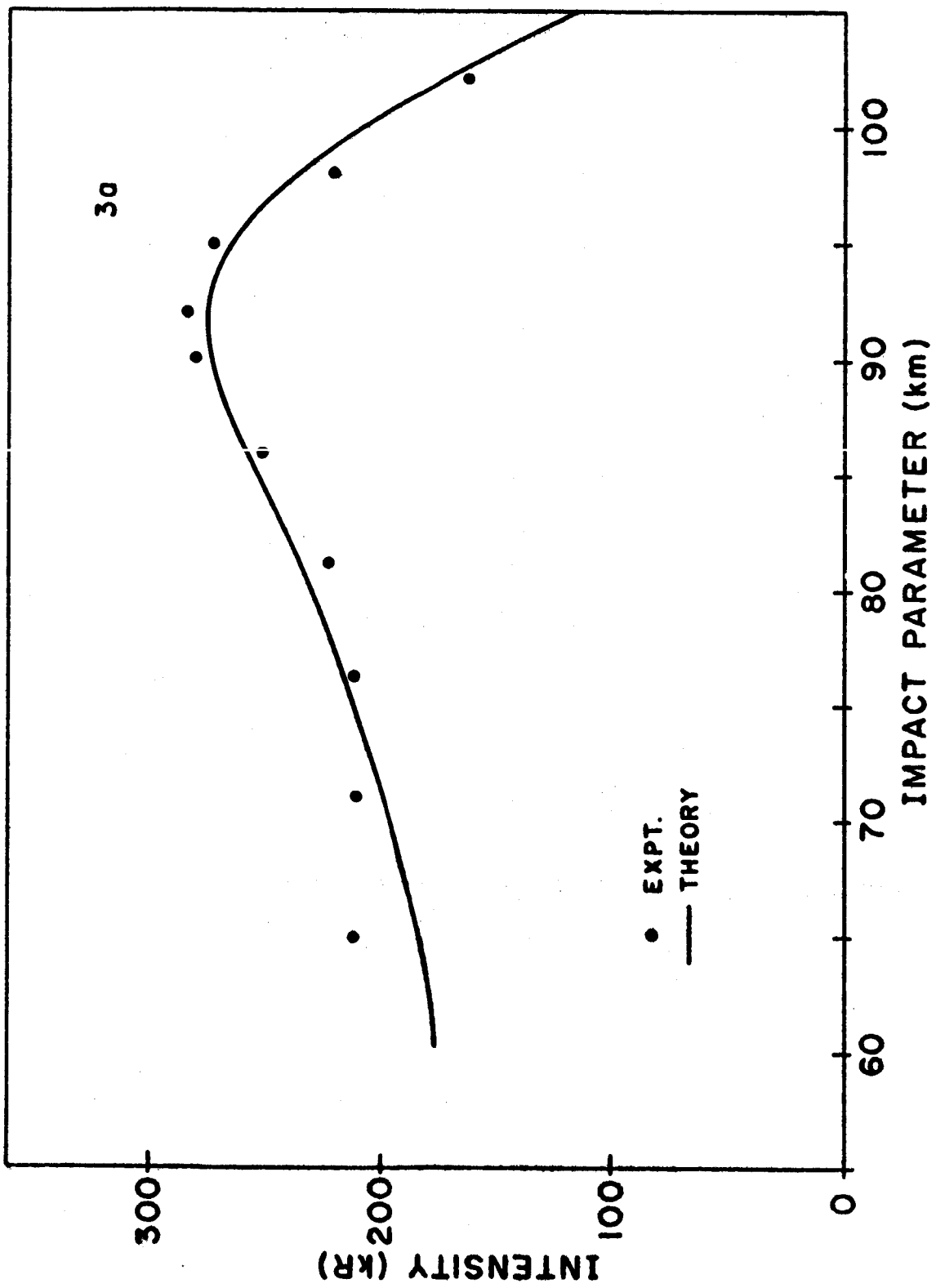
3a
INTENSITY (kR)
300
200
100
0
60
70
80
90
100
IMPACT PARAMETER (km)
EXPT.
THEORY

Figure 19.

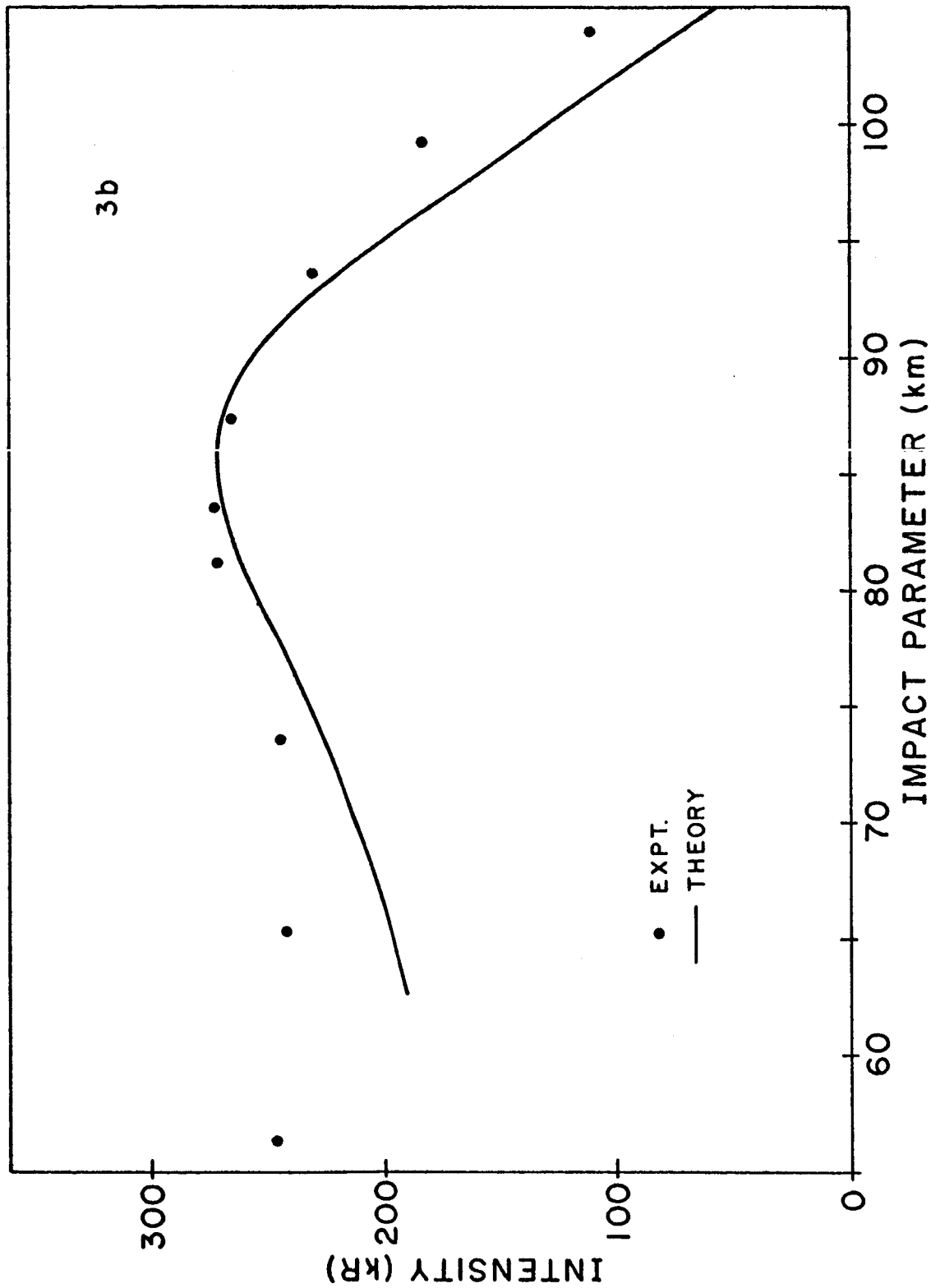
3b
INTENSITY (kR)
300
200
100
0
60
70
80
90
100
IMPACT PARAMETER (km)
EXPT.
THEORY

Figure 20

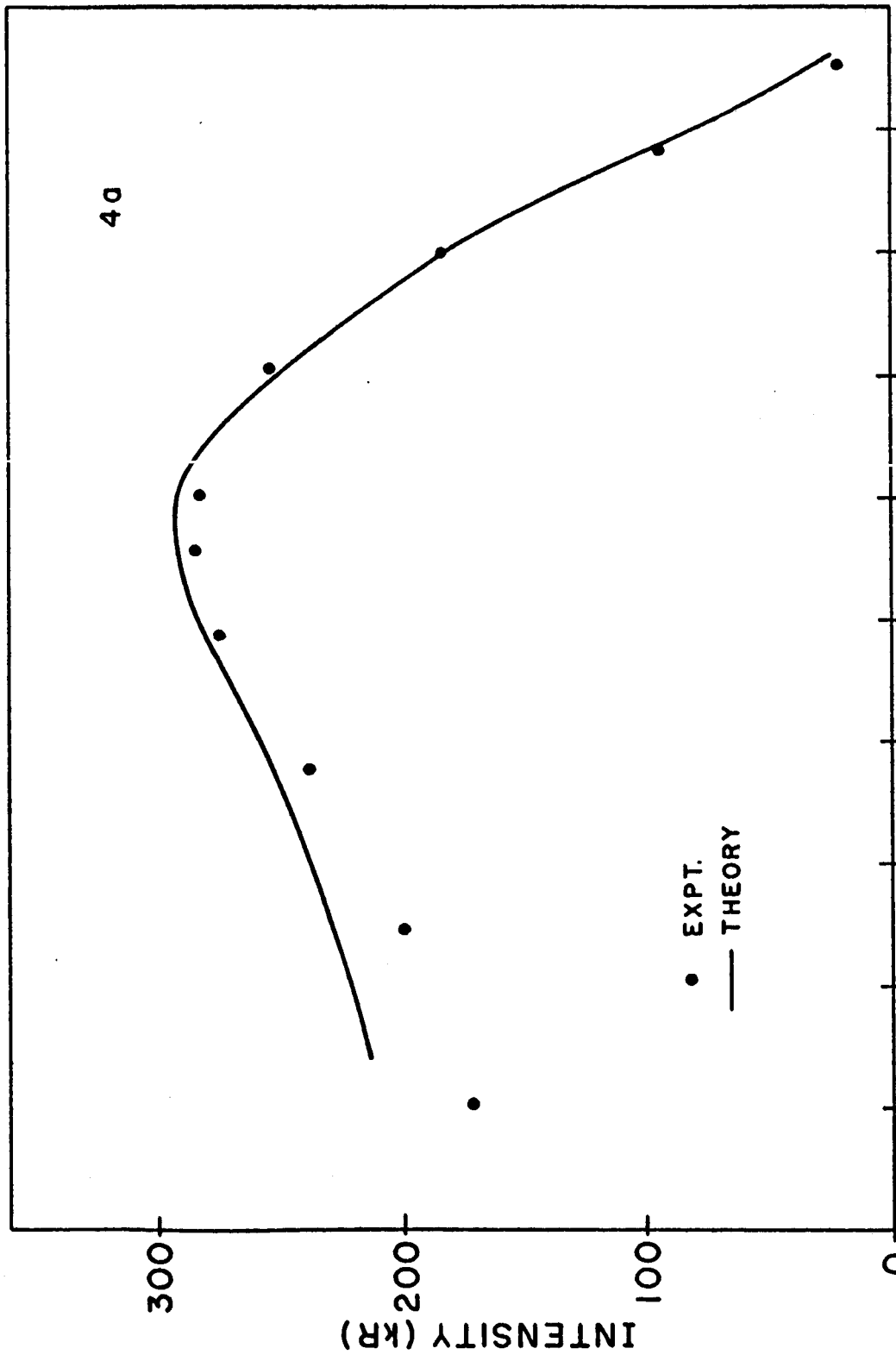
4a
EXPT.
THEORY
INTENSITY (kR)
IMPACT PARAMETER (km)
0
100
200
300
60
70
80
90
100

Figure 21.

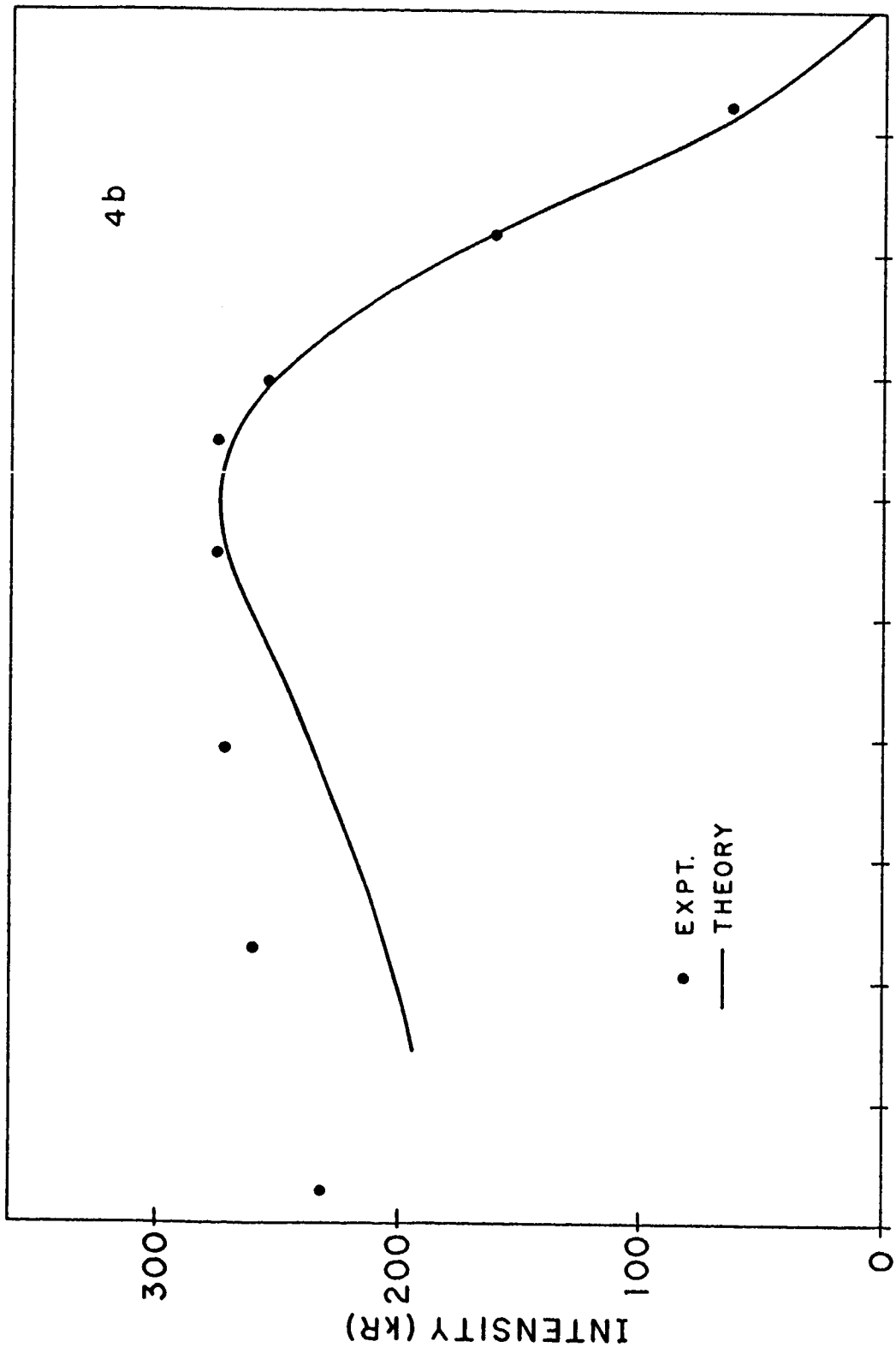
4b
INTENSITY (kR)
0
100
200
300
60
70
80
90
100
IMPACT PARAMETER (km)
EXPT.
THEORY

Figure 22.

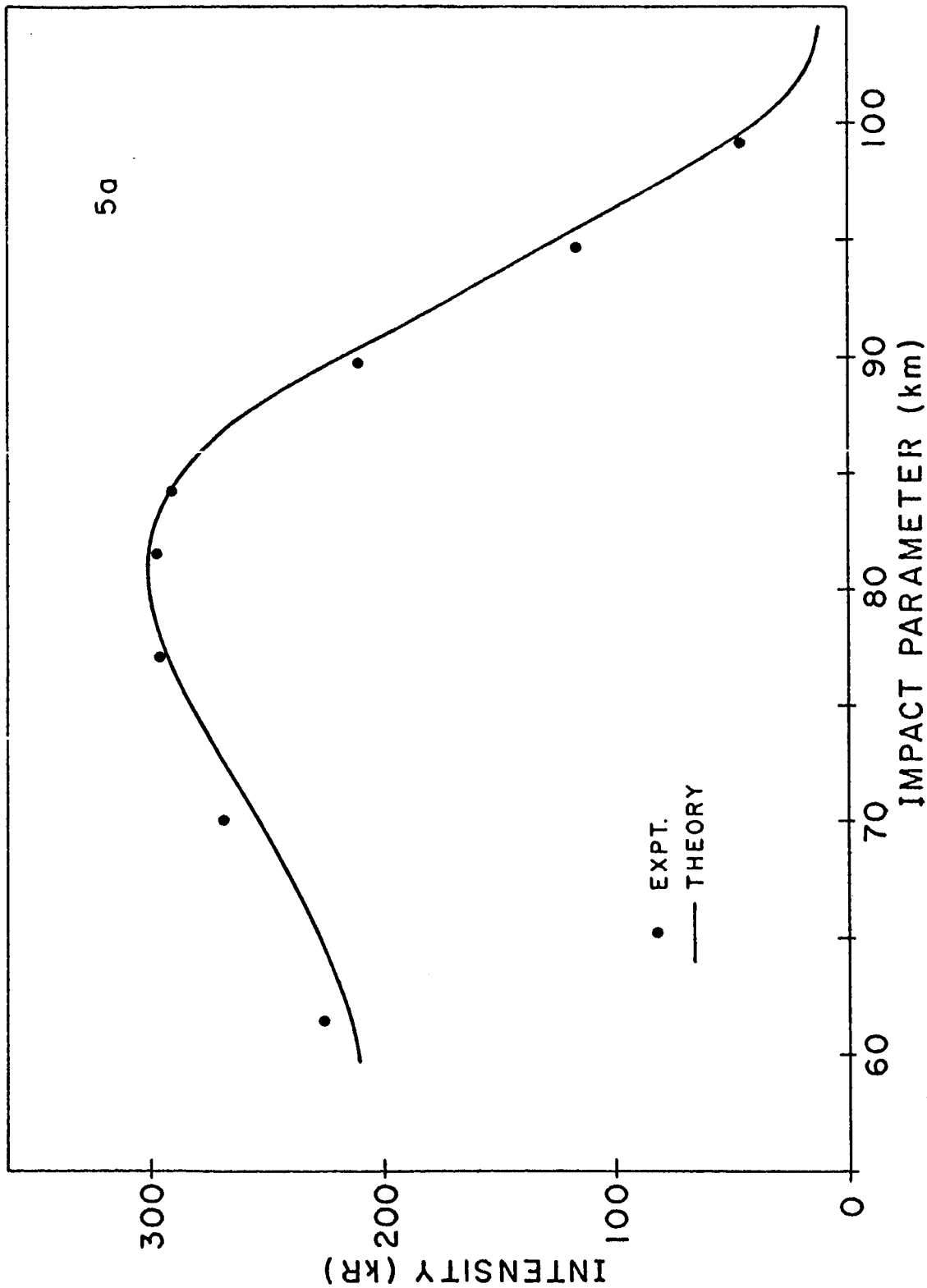
5a
INTENSITY (kR)
0
100
200
300
60
70
80
90
100
IMPACT PARAMETER (km)
EXPT.
THEORY

Figure 23.

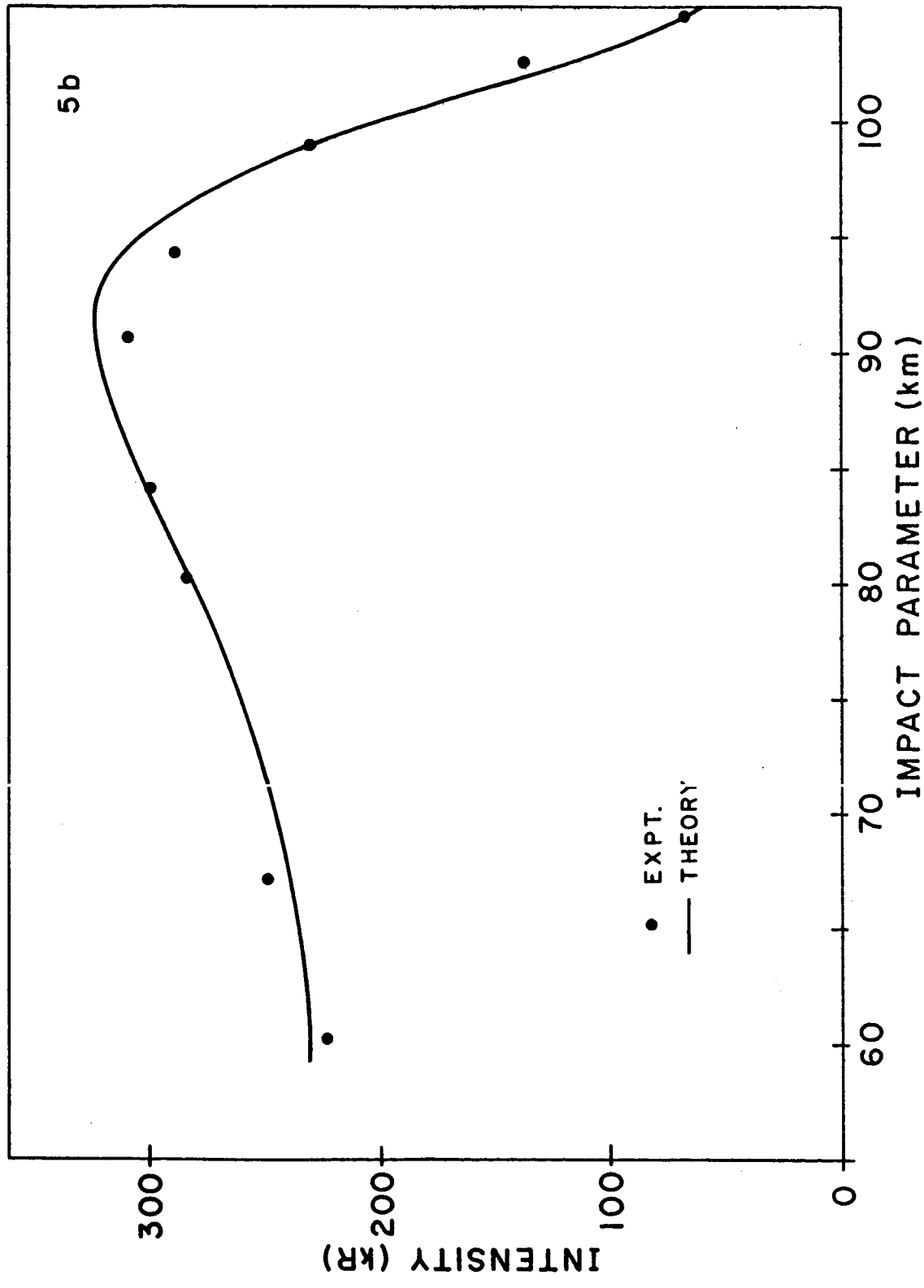
5b
INTENSITY (kR)
300
200
100
0
60
70
80
90
100
IMPACT PARAMETER (km)
EXPT.
THEORY

Figure 24.

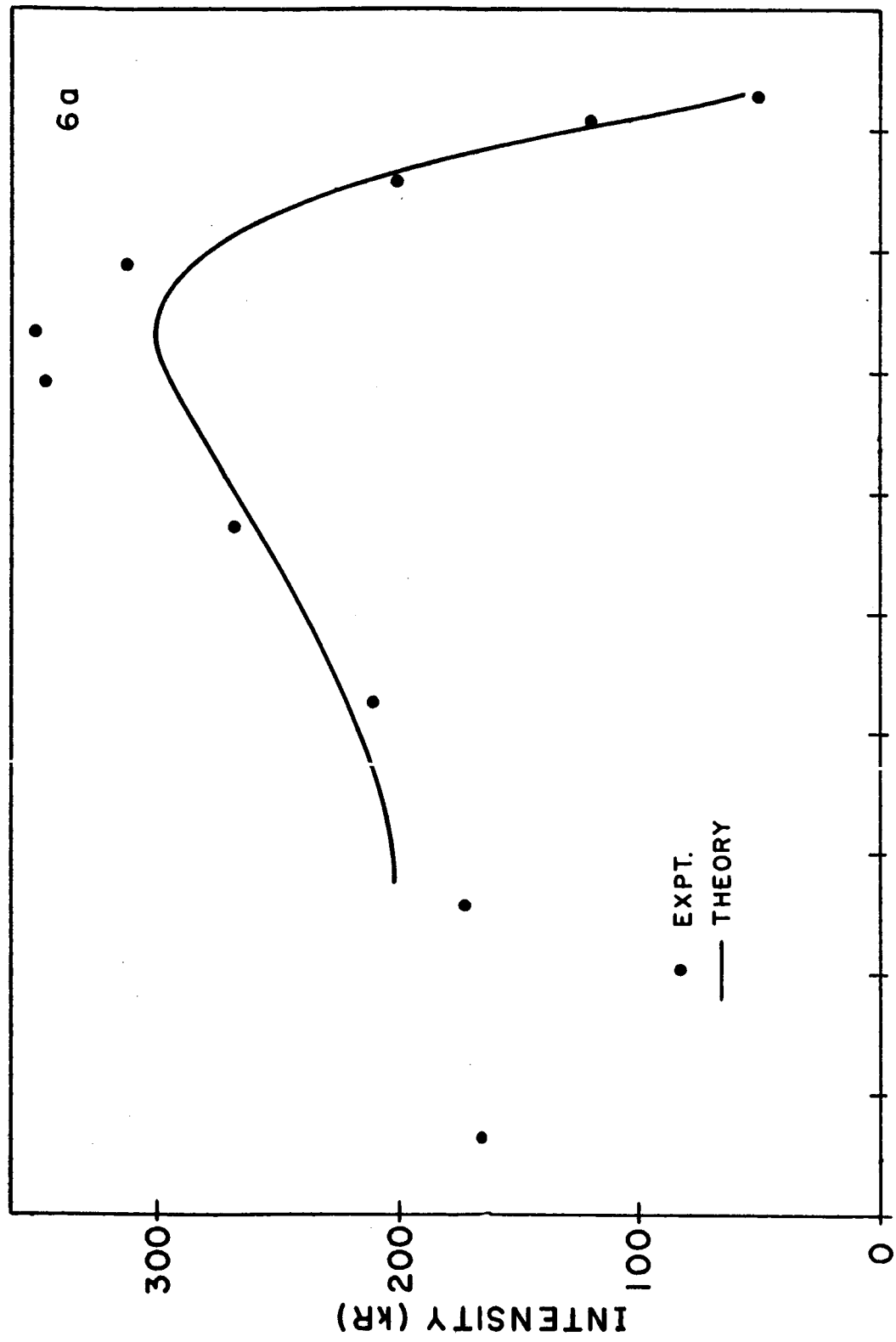
6a
INTENSITY (kR)
0
100
200
300
60
70
80
90
100
IMPACT PARAMETER (km)
EXPT.
THEORY

Figure 25.

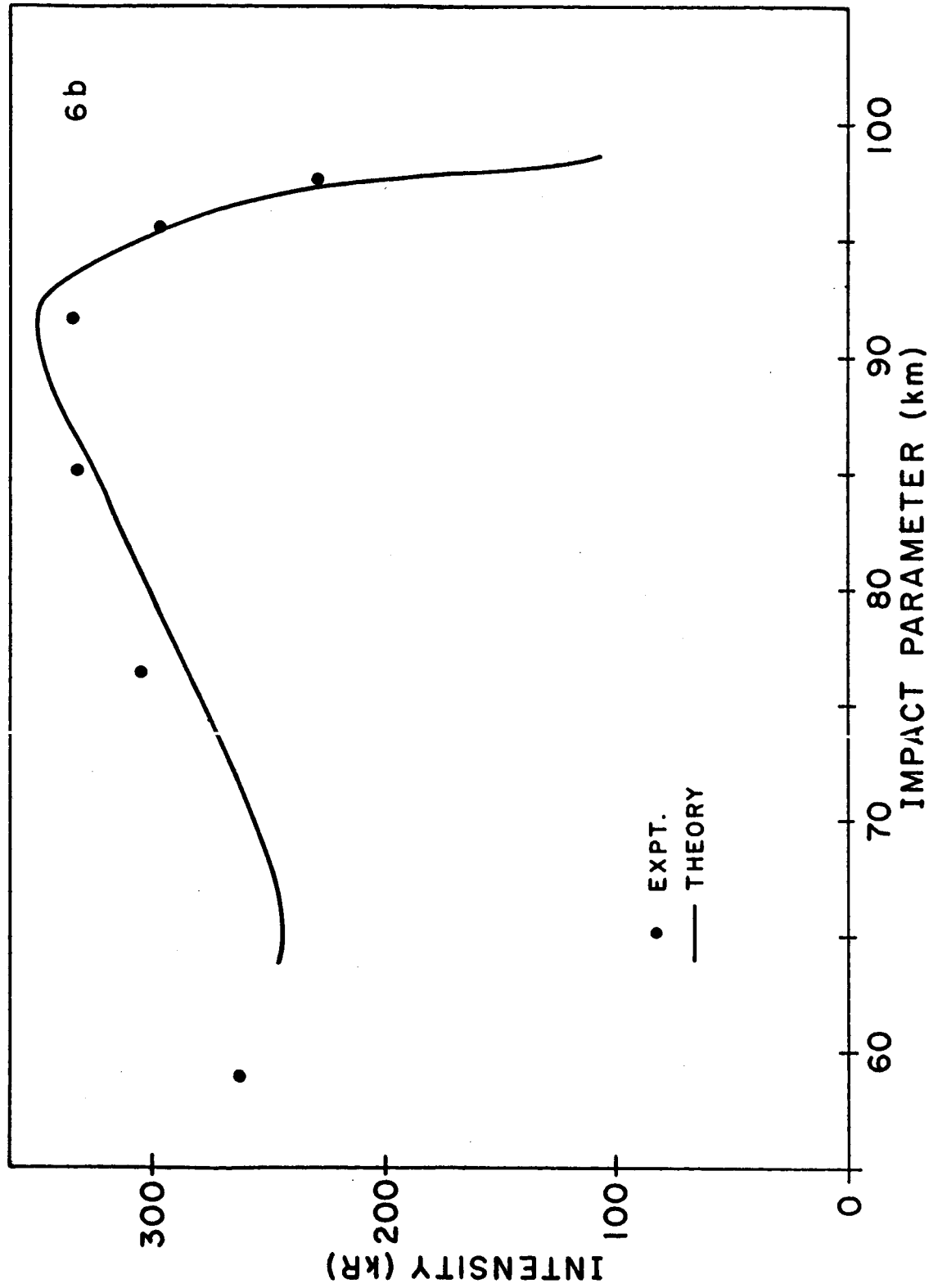
6b
INTENSITY (kR)
300
200
100
0
60
70
80
90
100
IMPACT PARAMETER (km)
EXPT.
THEORY

Figure 26.

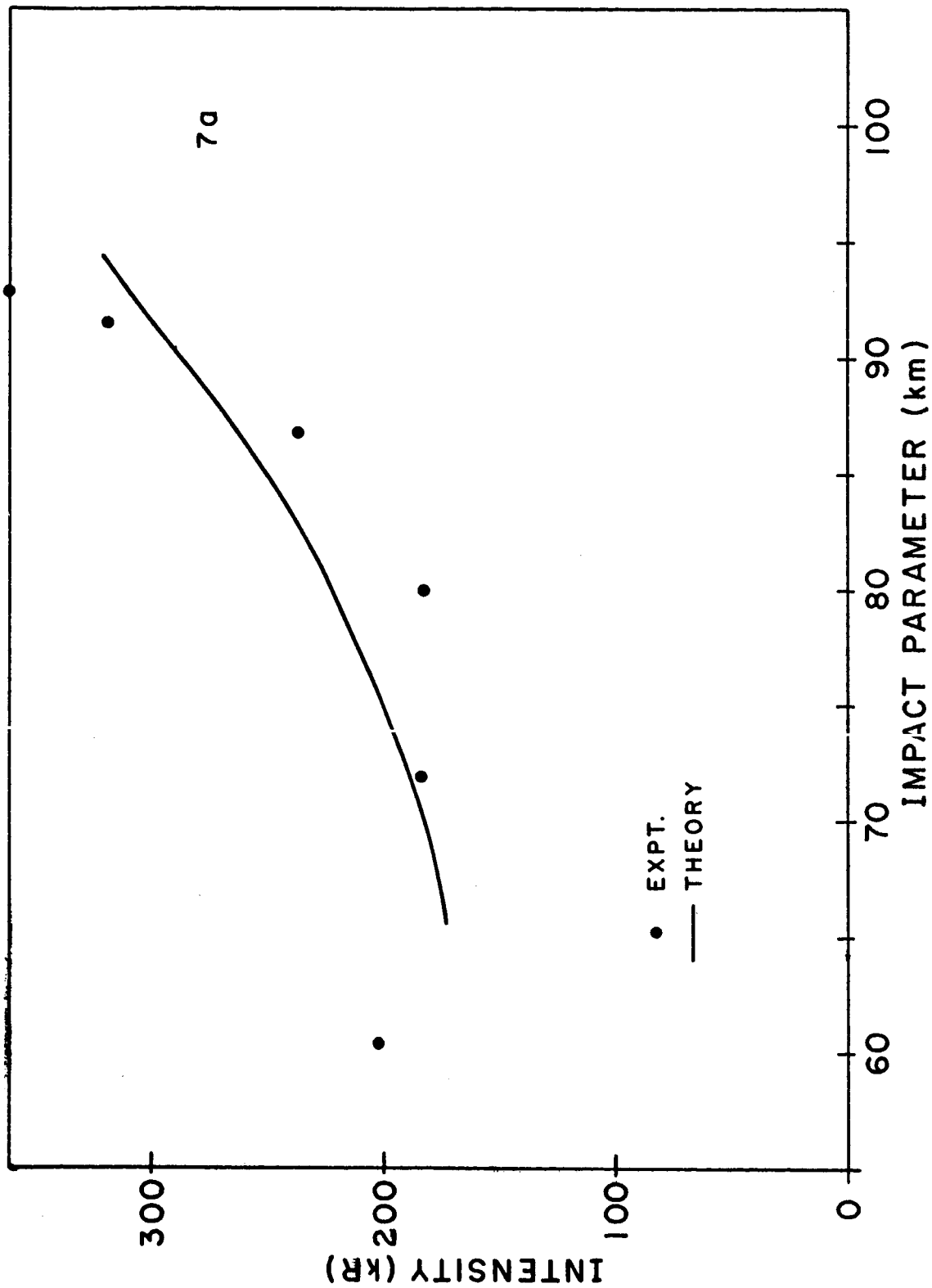
7a
INTENSITY (kR)
300
200
100
0
60
70
80
90
100
IMPACT PARAMETER (km)
EXPT.
THEORY

Figure 27.

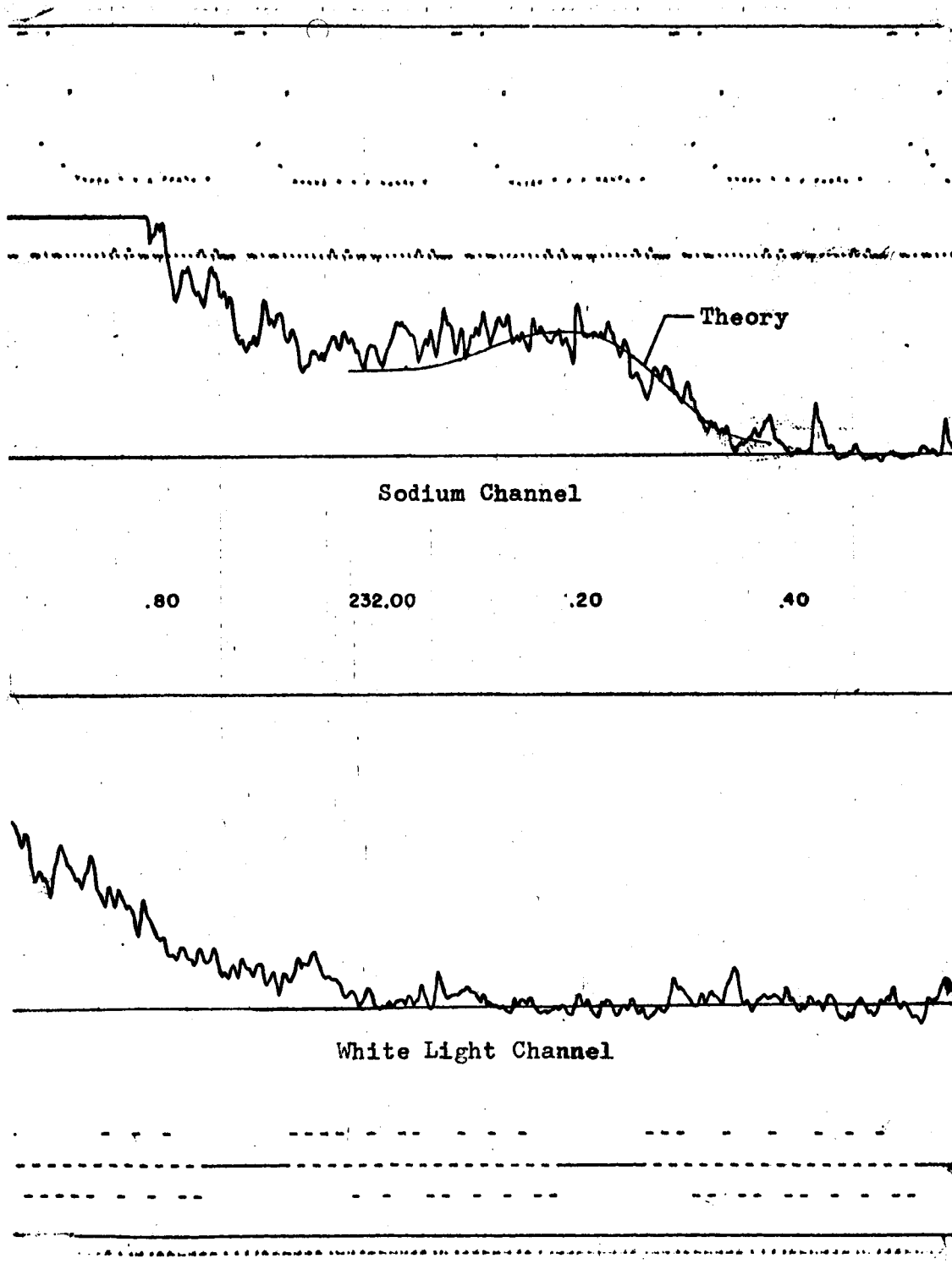

Figure 28. Oscillograph trace of Scan 4b showing theoretical curve. The abscissa is elapsed time from launch.

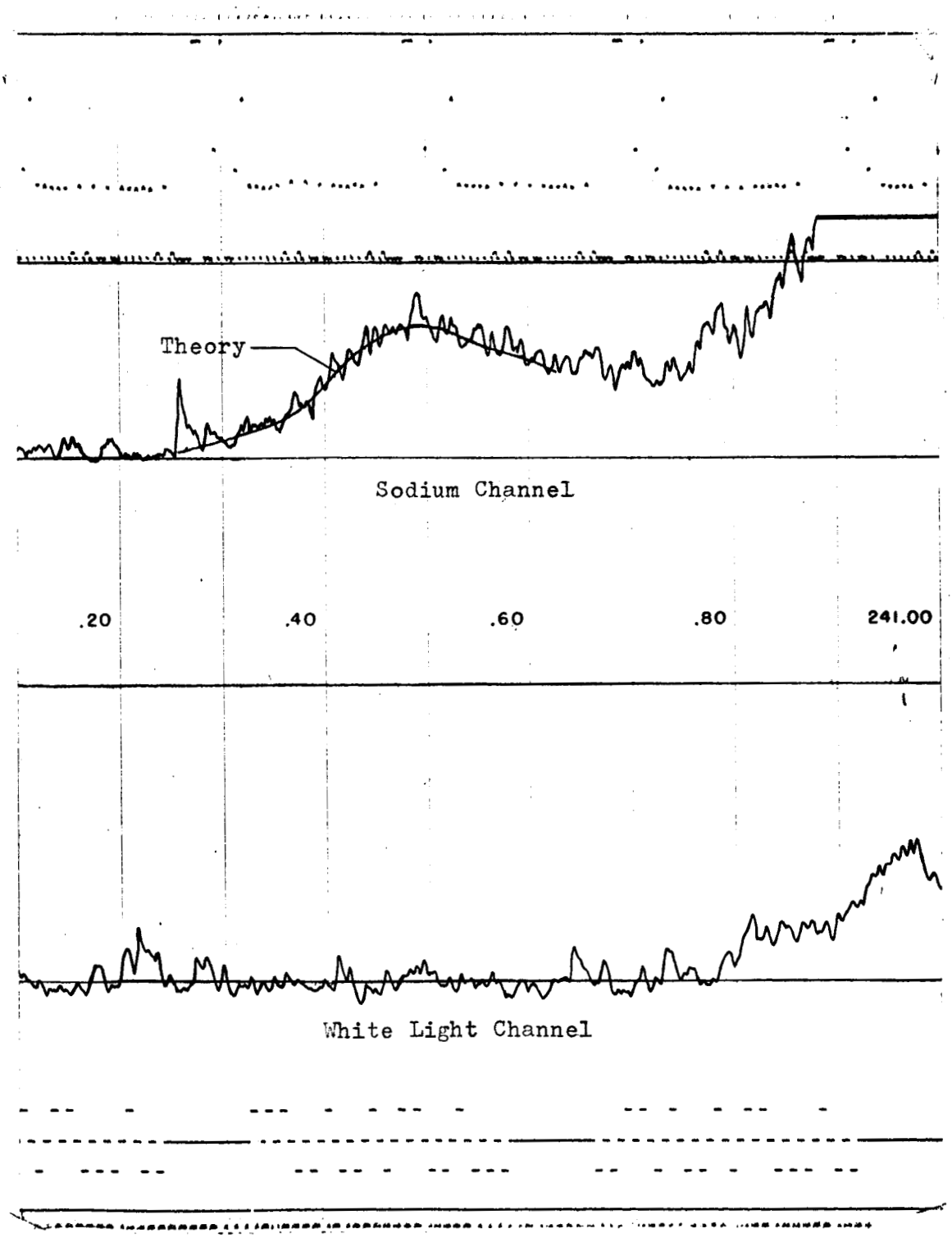

Figure 29. Oscillograph trace showing theoretical match to Scan 5a. The abscissa is elapsed time.

data reduced the error to less than 10% for the intensity measurements.

In the first few scans, the deviation of z_o from the mean altitude was greater than for the later scans. This may have been due to the fact that the attitude information was worse in this region. Also the experimental data were more difficult to interpret due to the slower rocket rotation.

The "middle" sweeps (3a to 5b) were easily matched to the theoretical models. The effect of Rayleigh scattering was evident at lower impact parameters because the instrumental solid angle enabled detection of intensities below the line of sight when the distance from the rocket was large. Some patchiness was evident, possibly due to inhomogeneities in different parts of the layer. In particular, 4a showed a sharp decrease in intensity below 75 km. An effect like this was not explainable by a "smooth layer" distribution because at lower altitudes, contributions came from two different sections of the layer. 3b may have been slightly wider than the theoretical model. Other than these discrepancies, the fits of the theoretical models in this region were quite good.

As the vehicle approached the layer, the data gave evidence of diverging from the exponential shape. In particular 6a showed a very large concentration of sodium near the peak. If the theoretical density were increased to fit the observed intensity at that point, it would have been impossible to match the data at lower impact parameters. Therefore, the curve given in Figure 25 represents a compromise. In 6b there was a much

better fit. Scan 7a had the worst agreement of all. This was not surprising since the photometer was very near the layer peak. The accuracy needed to determine the rocket orientation in this case was simply not available.

In the previous analysis, the comparison of the experimental data to theory was dependent upon the attitude determination. There was a special case in which attitude information was not required. This case occurred in each of the scans when the photometer recorded the maximum sodium emission. At those points, only the intensity and the rocket altitude were required to obtain a layer profile. The direction of observation for these points is indicated on the right side of Figure 30. As the rocket scanned the sodium, the direction of maximum intensity was tangent to the layer. A plot of these points gave a measure of the sodium distribution. This plot is shown in Figure 31 for the eight scans and the point when the rocket traversed the layer on ascent. The theoretical curve for the average distribution is also given. The decrease in intensity at higher altitudes was caused by the finite field of view of the instrument. The dashed curve shows the constant intensity for an infinitely small solid angle.

Thus agreement of experiment with the theoretical model was n o t b a d for the case when the rocket orientation was not necessary for interpretation of the data.

Another case, which was relatively independent of rocket attitude, was readily available from the data. This case occurred between scans when the photometer was looking away from the earth. The signal at that time was dependent only on the approximate

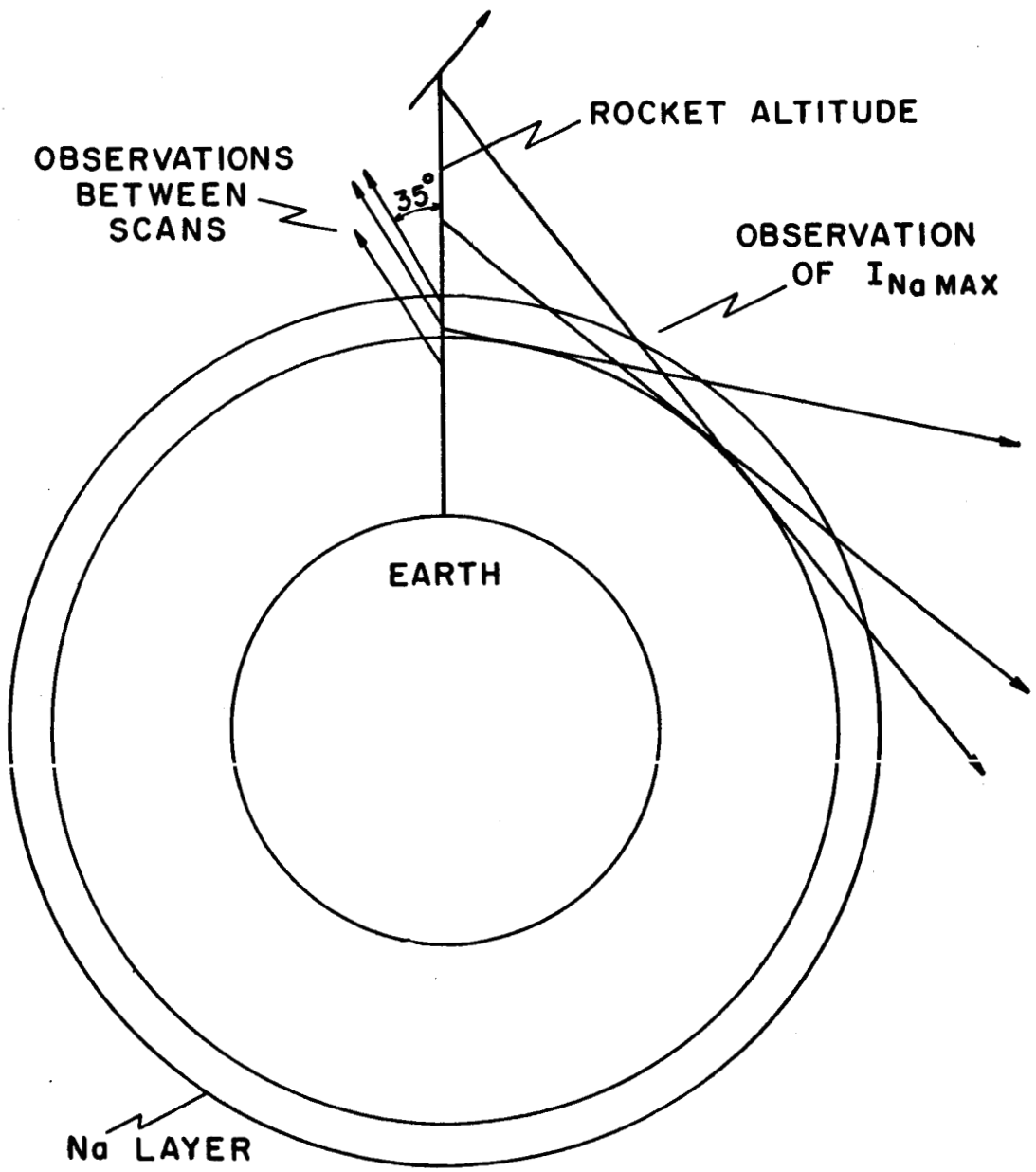

Figure 30. Direction of observation for $I_{Na\ max}$ (on right) and I_{Na} (35° zenith angle).

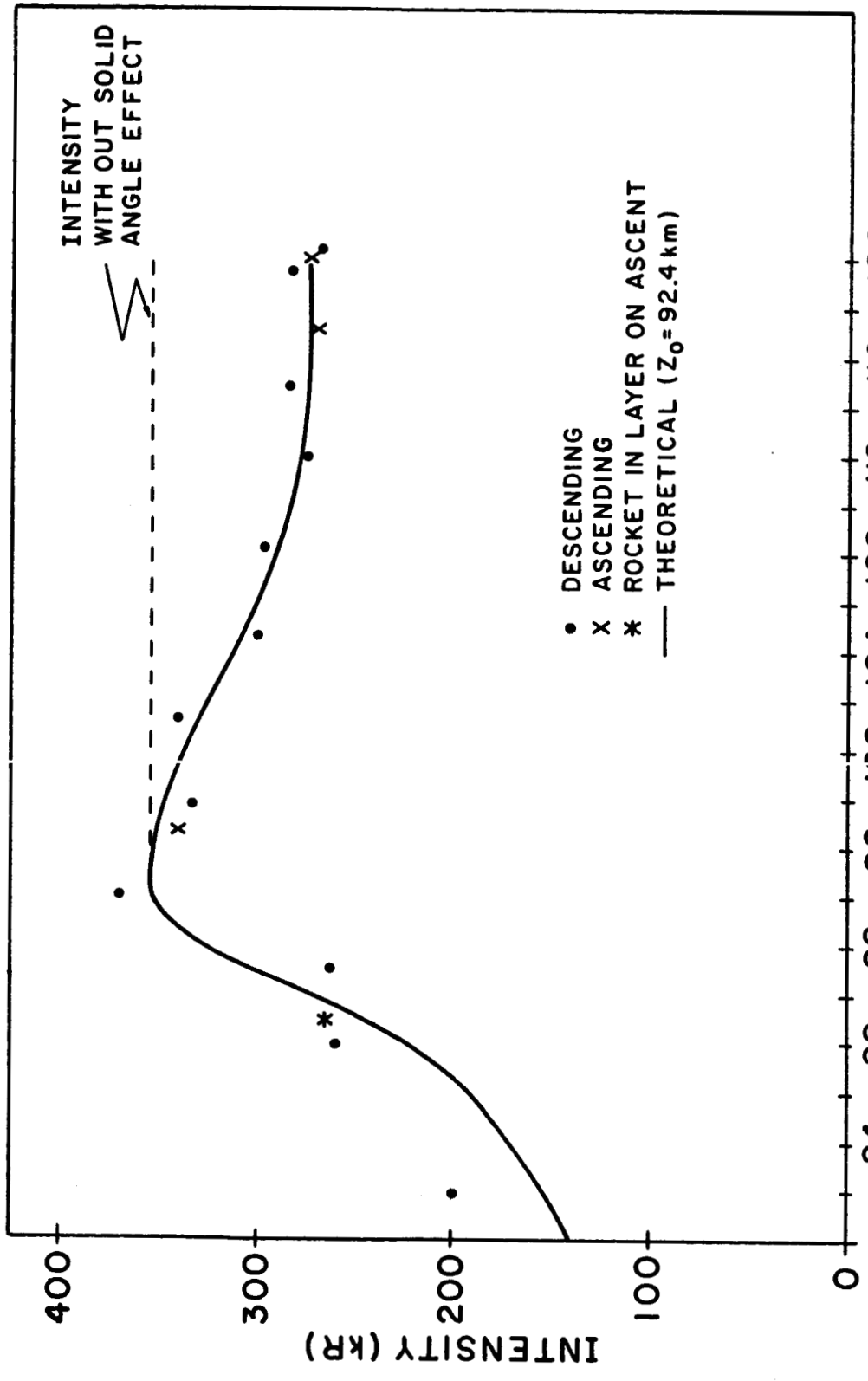

Figure 31. Maximum sodium emission for each scan.

value of the rocket zenith angle (within 5^{o}) because the emission was from sodium above the rocket. The observations are depicted on the left of Figure 30. As the rocket descended through the layer, only three scans yielded information. The other scans occurred at higher altitudes where there was much less sodium. The theoretical case for the average model is seen in Figure 32 along with the experimental points. For these low intensities the signal was somewhat marginal with respect to the amplifier noise so that error bars were included. The fit was acceptable within the observational error. Thus there was another piece of information which supported the experimental analysis.

The question which remains unanswered so far is whether or not the deviations from the average model were real. Of particular concern are the altitudes of maximum density. Since each of the scans looked at a different place in the sky, it should be possible to determine whether or not the altitude of the layer was different for each place.

To get an idea of the scope of the variations in the direction of observation, consider Figure 33. Shown is the projection of z_o on the surface of the earth for each sweep. Also included is the place where the rocket traversed the layer. Rays are drawn from the points of observation on the trajectory to the corresponding z_o. There was apparently no significant trend or correlation of altitude with direction of observation, even though the "a" scans gave an average impact parameter of 92.0 km. while the average of the "b"'s was 93.0 km. In order

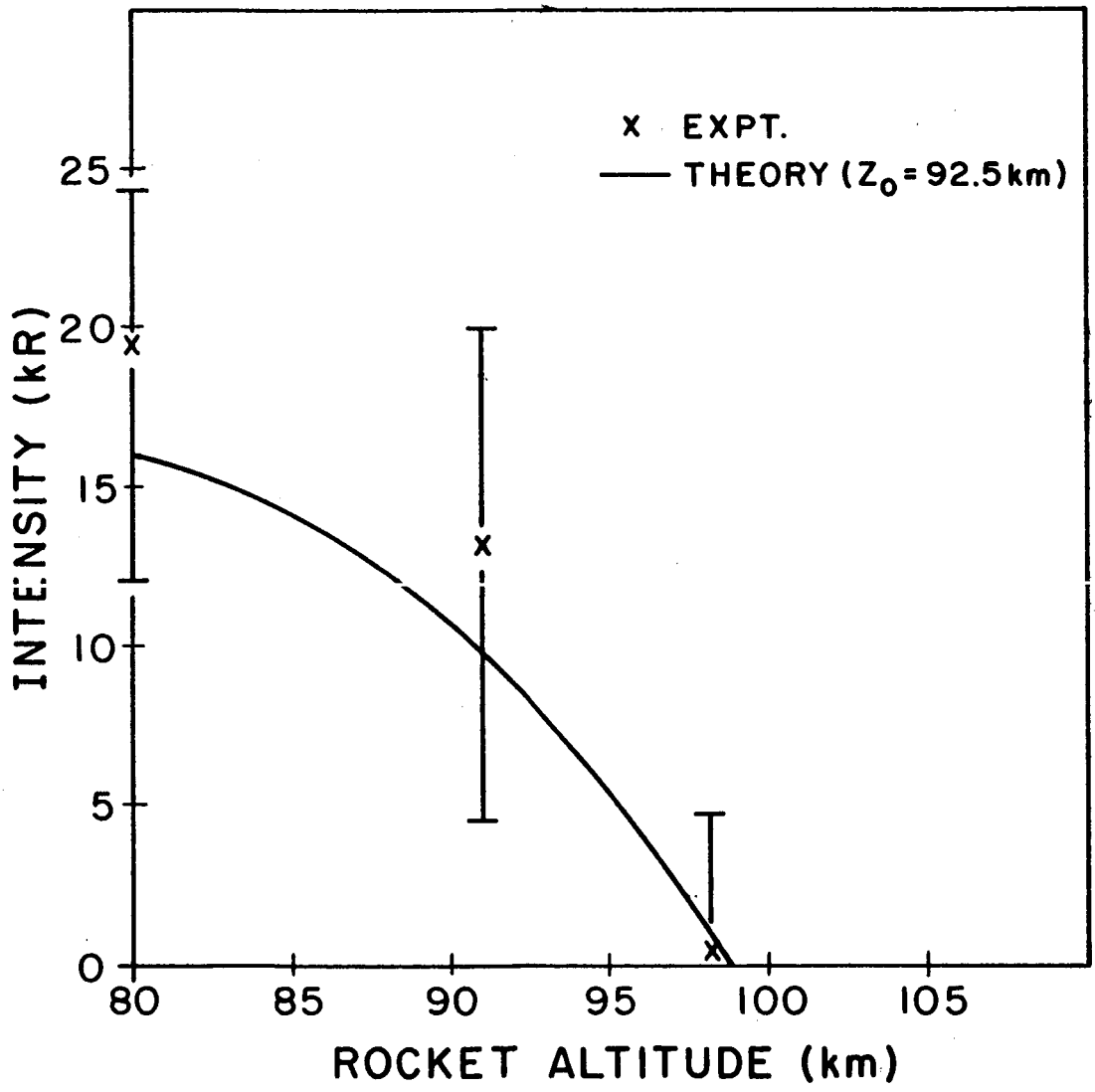

Figure 32. Sodium emission during descent for 35° zenith angle of observation.

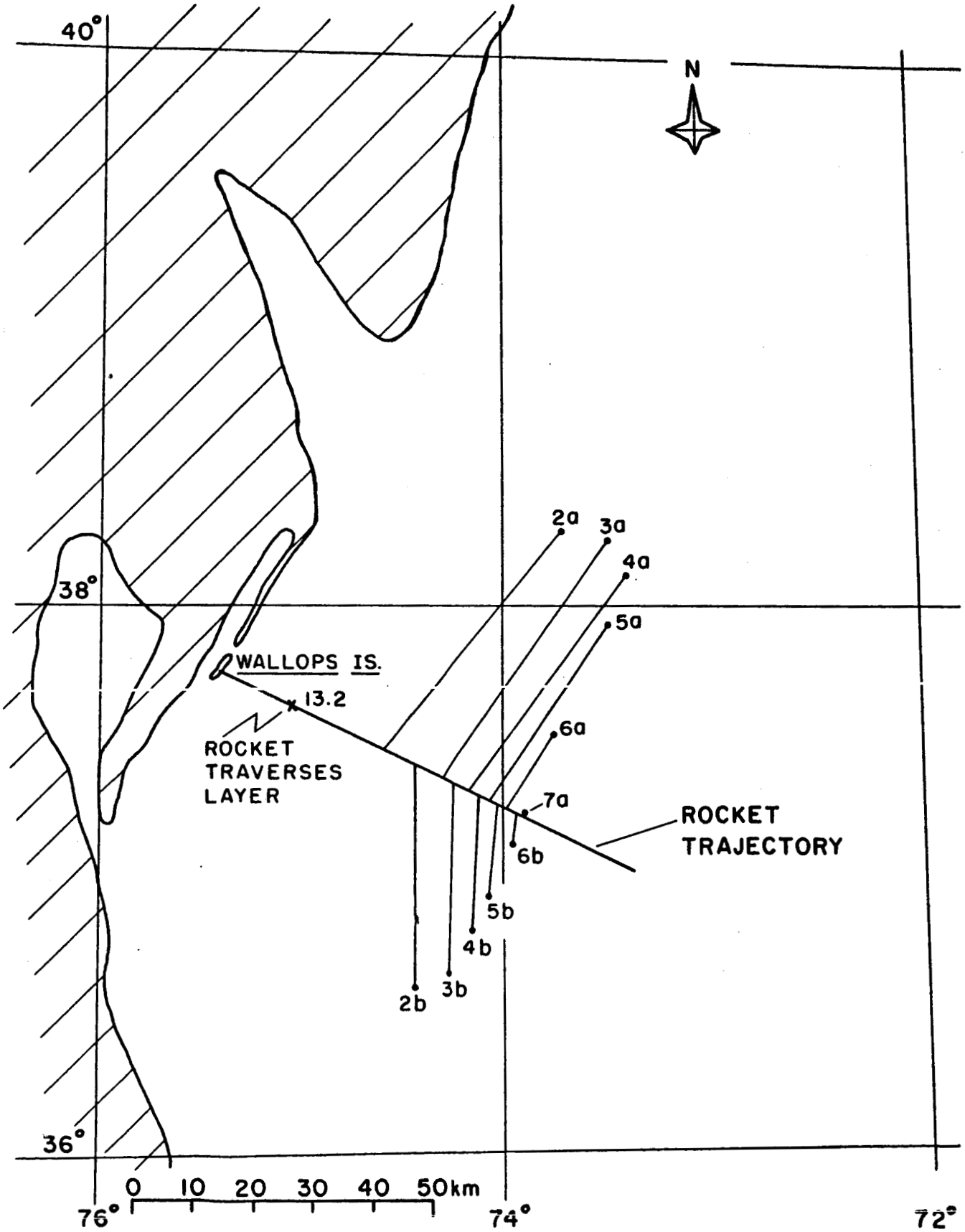

Figure 33. Projection of z_o for each scan on the surface of the earth.

to have seen a consistent variation with direction, if there was any, much better attitude resolution was necessary. It appears that the problem of altitude dependence of the layer on direction of observation will not be resolved until more information is obtained from future flights.

3.0 THEORY

Using a photochemical and eddy diffusion model based on the assumption of a non-local source for the sodium, a daytime density distribution is obtained which is about 30% wider than the twilight layer[5]. The observed daytime layer was much too narrow to be supported against the effects of diffusion using a photochemical source. To produce such a layer, it is necessary to have an even more narrow source for the sodium. Then the removal mechanism must act in a time which is less than or equal to the diffusion time in order to have a thin density distribution.

The classical theory for the production of free sodium is to invoke oxidation at lower altitudes through

$$Na + O_2 + M \rightarrow NaO_2 + M \qquad k_1 \qquad (15)$$

$$Na + O + M \rightarrow NaO + M \qquad k_2 \qquad (16)$$

$$Na + O_3 \rightarrow Na + O_2 \qquad k_3 \qquad (17)$$

and reduction at higher altitudes by

$$NaO_2 + O \rightarrow NaO + O_2 \qquad k_4 \qquad (18)$$

$$NaO + O \rightarrow Na + O_2 \qquad k_5 \qquad (19)$$

The possibility of a reaction with hydrogen is neglected since O is probably more than two orders of magnitude greater than H at 90 km.

Recently the reaction of sodium and potassium with oxygen has been investigated by Kaskan[11]. He found that the rate constant for the three body reaction involving O_2 is about $2 \times 10^{-33} cm^6/sec.$ this certainly eliminates (15) as a possible removal mechanism. The ozone reaction is then the most likely candidate since (16)

is undoubtedly much slower.

Another possible source of removal was suggested by Jones[12] after the discovery of Mg^+ in the atmosphere by Istomin[13]. It is charge exchange by the following process:

$$Na + Mg^+ \rightarrow Na^+ + Mg \qquad (20)$$

However as Jones points out, with a gas kinetic cross section, a density of 10^4 /cm^3 leads to a removal mechanism which is about one third of the photo-ionization rate. Although this may be important in the production of Na^+, it is not efficient for Na removal.

Narcisi and Bailey[14] have measured ion densities in the D region. Their data indicatethat sodium ions are about a factor of 30 less abundant than neutral sodium, thus eliminating the ions as a source for the layer. The interesting feature of their results is that the ions have a profile remarkably similar to the neutral distribution below 100 km. A comparison of the two distributions is given in Figure 34. This comparision will be discussed later.

Coupling the above information to the fact that the daytime layer was found to be higher than or equal to the twilight layer suggests that the sodium has a local, non-photochemical source. To satisfy these requirements, a model is proposed where charged dust particles containing sodium are concentrated in a vary small altitude interval by a wind shear mechanism. During the daytime, solar radiation liberates sodium atoms from the dust and they diffuse away until they are either oxidized by ozone or ionized. The attractive feature of the model is the ability to

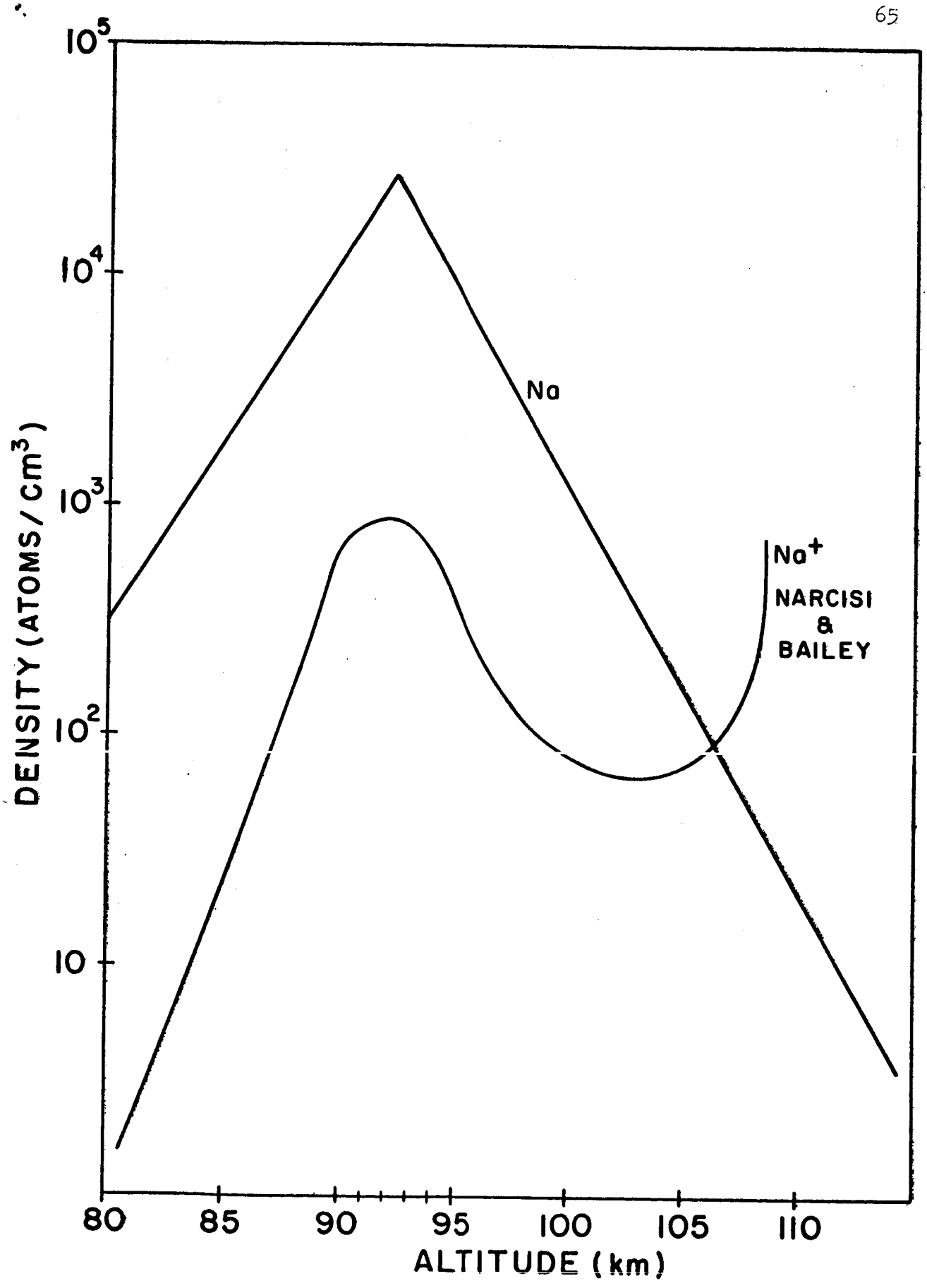

Figure 34. Comparison of sodium atom and ion densities.

form extremely thin layers of dust at the zero-velocity points of the horizontal winds despite the effects of eddy diffusion.

This process involving ions rather than aerosols has been proposed as an explanation of the Sporadic E phenomena[15,16,17]. There is definite experimental evidence showing a correlation between Sporadic E and ionospheric winds[18,19], even though discrepancies exist in some of the details. In particular, the ionized layers occasionally occur when the horizontal wind gradient is in the wrong direction. This suggests that negative particles may be forming at these nodes and producing the observed ionization. However, there are not enough negative ions to produce anywhere near this effect. Since dust particles may become negatively charged through frictional forces and accumulate at the "negative" nodes, they may be the cause of this second layer. It is also interesting that in nearly all of the observed cases, the wind gradients are such that the "positive" layer forms in the region of 110 to 120 km., whereas the second ionization peak is 15 to 20 km. lower, near where the sodium density is maximum.

Due to the above reasons and to the fact that meteoric ions, which have a small recombination coefficient, are likely to play a major role in the process (Axford and Cunnold[18], Donahue[15]), an interrelationship between Sporadic E, meteor activity, and the sodium airglow would be expected. A close correlation between Sporadic E and meteor influxes has been established experimentally by Singh[21] and by Fiocco[22]. The similarities are remarkable, showing a strong linkage between the two phenomena. Also the seasonal variation in frequency

of Sporadic E at temperate latitudes[23] follows the variation in radar meteor rates very well[24], even though the data were not taken at the same place. To compare the meteor rates and the sodium abundances, the airglow data of Blamont and Donahue[5] are considered. It has been found that polarization of the Rayleigh scattered continuum caused a systematic error in the reduction of the data from the Zeeman photometer[9]. After correcting for this effect the large seasonal variation in the daytime sodium abundance is removed.

In Figure 35 the corrected seasonal variation is shown for 15 day averages over the 5 year period from 1961 to 1965. The solid lines indicate the maximum and minimum values of the sodium abundance. The meteor rates of Millman and McIntosh[24] are included for comparison.

There are several observations which can be made. The February maximum in the sodium abundance occurs almost exactly at a time when an annual dust shower is thought to take place[25]. The same thing happens in November where the dust shower is considered to be associated with the Leonid shower. Some of the other fluctuations in the abundance occur near times of shower activity. That there is not an extremely close relationship between the two is not surprising for the following reasons. First, the data were taken at two different places (Ottawa and Haute Provence), and second, other factors such as wind and ozone variations may affect the sodium abundance. Also the sodium content of the dust showers may be a highly variable quantity. This is suggested by the fact that in some years

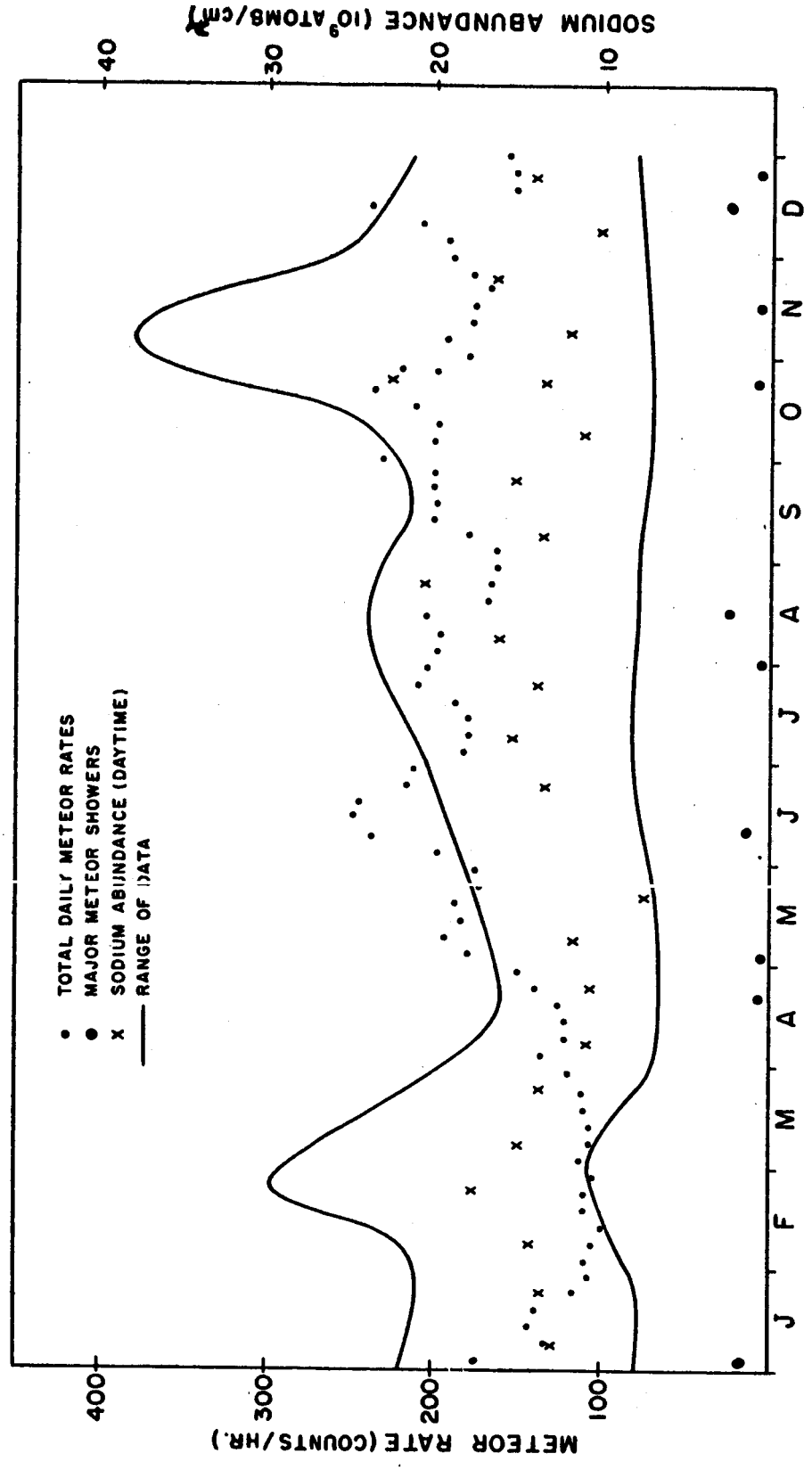

Figure 35. Seasonal variation of sodium abundance and meteor rates.

enhancements do not occur.

Another effect was very apparent in the re-evaluation of the sodium dayglow data. Afternoon abundance were systematically higher than morning abundances. In 80 cases where data were available on the same day, (three hours before noon and three hours after noon), the average ratio of afternoon sodium to that in the morning was 1.31. In only 15% of the cases was the afternoon abundance less than the morning value. It is not yet clear what effects cause this, although the abundance increase may be related to the meteoric influx.

3.1 Formation of the Sodium Layer

To obtain the observed density distribution, three processes are assumed to be acting on the free sodium atoms: eddy diffusion, production by a dust layer source, and removal by ozone. In the steady state, where there is no net change in density with time, conservation of particles gives

$$D\frac{d^2 Na(z)}{dz^2} - \frac{Na(z)}{\tau_0} + Q(z) = 0 \qquad (21)$$

where D is the eddy diffusion coefficient, τ_0 is the lifetime against removal by ozone, and $Q(z)$ is a term representing production. For brevity's sake the notation N(Na) = Na = free sodium atom density has been adapted. Photoionization and charge exchange are neglected, compared to oxidation.

In solving the radiative transfer problem, an excellent fit to the experimental data was obtained by use of a model

consisting of two exponentially varying functions for the sodium density. This requires an extremely narrow source function since the scale heights were found to be 2.5 km. As a first approximation to the problem, a delta function source is tried. The steady state equation then becomes

$$D\frac{d^2 N_a(z)}{dz^2} - \frac{N_a(z)}{\tau_0} - \frac{N}{\tau_c}\delta(z-z_0) = 0 \qquad (22)$$

where N is the number of sodium "compounds" (or total amount of sodium contained in the meteors) per cm^2 in the layer defined by the delta function, τ_c is the lifetime of the compounds (time interval in which they can participate in the process), and z_o is the altitude of maximum sodium density. Whenever $z \neq z_o$, the solution is

$$N_a(z) = N_a(z_o)\exp\left(\pm\frac{z-z_o}{H}\right) \qquad (23)$$

where + is used when $z \leq z_o$, - when $z \geq z_o$ and H is $\sqrt{D\tau_o}$. Of course this has assumed constant values of D and τ_o over the region of interest and the same scale height for both the top and bottom of the layer. Near $z = z_o$ we can integrate (22) from $z_o - \epsilon$ to $z_o + \epsilon$, and then let ϵ go to zero. This gives the following requirement for the sodium compound density,

$$N = \frac{2 D \tau_c N_a(z_o)}{H} \qquad (24)$$

An appropriate value for D was found to be 2-6 x $10^6 cm^2/sec$[24]. H and Na(z_o) were found experimentally to be 2.5 km. and 2.8 x $10^4 atoms/cm^3$, respectively. Therefore if $\tau_c \approx$ 1 day, then N is about 3.9 x $10^{10}/cm^2$.

The condition that the ozone process removes sodium in a time which is of the order of the diffusion time is

$$\tau_o = \frac{H^2}{D} \tag{25}$$

or

$$k_3 O_3 = \frac{D}{H^2} \tag{26}$$

If the ozone density at 92 km. is 5.0 x $10^7/cm^3$ and D is 4 x 10^6 $cm^2/sec.$ then k_3 is about 1.3 x $10^{-12} cm^3/sec.$, certainly not an unreasonable value.

The relative merits of a δ - function source will be discussed in the next section.

3.2 Formation of Aerosol Layer

To demonstrate the ability of charged dust particles to produce a thin source function for the sodium, a number of assumptions are made. They are the following:

(a) a steady state exists so that any net change in momentum of the particles can be neglected. This is reasonable since the gyro-

periods and collision times are short compared with inertial effects.

(b) $\underline{U}$ is the neutral wind velocity with components only in the horizontal directions. Experimental evidence of meteor trails[27,28], and sodium vapor releases[29] show negligible vertical winds.

(c) the earth's magnetic field $\underline{B}$ is of constant magnitude and direction over the region of interest.

(d) electrical neutrality is maintained, i.e., the positive particle and ion densities are equal to the electron, negative ion, and negative particle densities.

(e) an infinite layer is assumed so that $\partial/\partial x = \partial/\partial y = 0$ and $\partial/\partial z = d/dz$, where x is taken to be the direction of the horizontal component of $\underline{B}$ in a right hand coordinate system, and z is altitude. Note that the y direction is magnetic east.

(f) the particles are assumed to be uniform spheres. This is not very realistic since they can have practically any shape[30]. This assumption may appreciably affect the drag force.

(g) the effects of gravity will be small compared to the other forces for the small particles in this discussion.

With these assumptions, the equation of motion for a charged particle in the steady state is

$$q(\underline{E} + \underline{V} \times \underline{B}) + \underline{F}_d = 0 \tag{27}$$

where q and $\underline{V}$ are the charge and velocity of the dust particle, $\underline{F}_d$ is the drag force acting on it, and $\underline{E}$ is the polarization electric field. The drag force is given by

$$\underline{F}_d = \pm \rho_a A C_d |\underline{U} - \underline{V}| (\underline{U} - \underline{V}) \tag{28}$$

where $|\underline{U}-\underline{V}|$ is given by $\sqrt{(U_x-V_x)^2+(U_y-V_y)^2+(-V_z)^2}$, ρ_a is the mass density of air, A is the particle cross section, and C_d is the appropriate drag coefficient.

With the following definitions,

$$\omega = \frac{B q}{m} \qquad \text{and} \qquad \nu = \tfrac{1}{2}\rho_a \frac{A C_d |\underline{U}-\underline{V}|}{m} \tag{29}$$

where ω is the gyro frequency, ν is analogous to collision frequency, and m is the particle mass, the equation of motion can be separated into its cartesian components and solved for V_x, V_y, and V_z. Assuming that ω/ν is small, and in the steady state the polarization electric fields are zero, the following equations result:

$$\begin{aligned} V_x &= U_x + U_y \frac{\omega}{\nu} \sin\theta_B \\ V_y &= U_y - U_x \frac{\omega}{\nu} \sin\theta_B \\ V_z &= - U_y \frac{\omega}{\nu} \cos\theta_B \end{aligned} \tag{30}$$

where θ_B is the magnetic dip angle. These equations are derived in Appendix B.

Using the above equations, it is easily shown that

$$|\underline{U}-\underline{V}| = \left[\frac{2 B q}{\rho_a A C_d}\sqrt{U_x^2 \sin^2\theta_B + U_y^2}\right]^{\frac{1}{2}} \tag{31}$$

$$\frac{\omega}{\nu} = \pm\left[\frac{2 B q}{\rho_a A C_d \sqrt{U_x^2 \sin^2\theta_B + U_y^2}}\right]^{\frac{1}{2}} \tag{32}$$

and, therefore,

$$V_z = \mp\left[\frac{2BQ}{\rho_a A C_d \sqrt{U_x^2 \sin^2\theta_B + U_y^2}}\right]^{\frac{1}{2}} U_y \cos\theta_B \,. \qquad (33)$$

q is now defined as the absolute value of the charge, so that the upper sign is used for a positive charge, and the lower sign, for a negative charge. It is shown in Appendix B that the above equations hold under ordinary circumstances.

Appropriate values for the quantities in (33) are: B(92 km) is 0.5 gauss, ρ(92 km.) is 10^{-9}gm/cm^3, $A=\pi a^2$, where a is the particle radius, $U_x \approx U_y = 10^4$cm/sec, $\theta_B = 45^\circ$. Since C_d is proportional to $|\underline{U} - \underline{V}| / \bar{v}$, where $\bar{v}$ is the mean molecular speed, the value of C_d is about 2.5. Substituting these values into (33), $V_z = 7 \times 10^6 \, q^{1/2}/a$. With q = 1 e, and a = 10^{-7}cm., V_z is about 8.9×10^3cm/sec.

Thus there is an altitude variation in vertical velocity which tends to concentrate negatively charged particles at the zero velocity point in the regions where there is a positive gradient in the east-west neutral wind and positive particles at the node of a negative gradient.

Due to the dependence of V_z on θ_B, a latitude variation in the sodium abundance should be expected. However, this effect may be masked by a dependence of horizontal winds, ozone, and dust influx on latitude.

3.3 Density Distribution of Sodium Source

Due to the lack of knowledge of many of the spatial

parameters and time constants of meteoric dust and especially of their physical properties, a quantitative theory is attempted by making a number of assumptions, many of which are certainly not very realistic.

In formulating the distribution problem, it is assumed, following Whitehead[15], that the east-west component of the neutral wind varies sinusoidally with altitude, and, therefore the vertical velocity of the charged particles can be represented by

$$V_z = - V_0 \sin\left(\frac{2\pi(z-z_0)}{\lambda}\right) \tag{34}$$

where λ is the vertical "wavelength" of the movement, and V_0 is given by V_z (max). Then if the rate of increase in density of dust particles is zero in the steady state, the dust density, M,is given by

$$D\frac{d^2M}{dz^2} + \frac{d}{dz}\left[M V_0 \sin\left(\frac{2\pi(z-z_0)}{\lambda}\right)\right] - \frac{M}{\tau_M} + S_M = 0 \tag{35}$$

where D is the eddy diffusion coefficient, τ_M is the lifetime of the dust species, and S_M is a term representing production of dust. Since sodium is probably imbedded in the dust particles, the lifetime of the sodium compound is defined as the lifetime of the dust or the time interval in which the dust particle can take part in production, and, therefore $\tau_m = \tau_i$. Recombination of positive particles, electron detachment from negative particles and vaporization are possible loss mechanisms for the dust.

Introducing a new vertical scale χ, defined by

$$\chi = \frac{2\pi (z - z_0)}{\lambda} \tag{36}$$

we have M given as

$$\frac{d^2M}{d\chi^2} + \frac{R}{L}\frac{d}{d\chi}(M \sin\chi) - \frac{M}{L} + \frac{\tau_c S_M}{L} = 0 \tag{37}$$

where

$$R = \frac{2\pi V_0 \tau_c}{\lambda} \tag{38}$$

$$L = \frac{4\pi^2 D \tau'}{\lambda^2} \tag{39}$$

and

$$\frac{R}{L} = \frac{V_0 \lambda}{2\pi D} \tag{40}$$

To solve this equation for $M(\chi)$, the values of τ_c and S_M must be known. Since S_M represents direct population of sodium-containing dust particles, it can only be estimated at the present time. Assuming that the source is meteoric, an enhanced contribution from S_M during times of high activity would be expected unless τ is small. Because of the large diurnal vairation in meteor rates,[24] which may be evident in the daytime sodium abundance as suggested by the morning-afternoon ratio of 1.31, τ_c is probably of the order of a day. S_M could not be much greater than M/τ , or any enhancement effects would be completely damped out. Now the ratio of the transport rate to the removal rate is given by

$$\frac{R/L}{1/L} = R \tag{41}$$

If V_o were about 10^3 cm/sec and λ were 10 km. then R would be given by

$$R = 6.28 \times 10^{-3} \tau_c \,. \tag{42}$$

With τ_c about one day, we can certainly neglect the loss term, and very likely, the direct population term. However, V_o is a highly variable quantity, depending upon many parameters, as has been shown. In any case, lacking any other information about these quantities, it will be assumed that S and M/τ_c are small compared with the effects of wind shear and diffusion. This corresponds to the case where there is no production and loss and the particles are rearranged in space by diffusion and Lorentz forces.

Thus the particle equation becomes

$$\frac{\partial^2 M}{\partial \chi^2} + \frac{R}{L} \frac{\partial}{\partial \chi} (M \sin \chi) = 0 \tag{43}$$

Integration yields

$$\frac{\partial M}{\partial \chi} + \frac{R}{L} (M \sin \chi) = C \tag{44}$$

where C must vanish for a solution which has a maximum at $\chi = 0$. The solution of this first order equation is

$$M(\chi) = M(0) \exp\left(-\frac{R}{L}(1-\cos\chi)\right) \tag{45}$$

As long as R/L is large, (45) is a near-delta function distribution (at least compared to the sodium distribution).

The point of half maximum density occurs when

$$\chi = \cos^{-1}\left(1 - \frac{L}{R}\right) \tag{46}$$

With $V_o = 10^3$ cm/sec, λ = 10 km, and $D = 2.0 \times 10^6 \text{cm}^2/\text{sec}$, $z - z_o$ is about 250 m. If V_o is 10^4 cm/sec, $z - z_o$ is about 80 m.

Whenever R/L is not large, there are two other methods of solution. First, as many delta function sources as are necessary to represent the source function can be used in (22). Each equation can be solved separately and the solutions added to obtain the total density function for sodium. Secondly, the source function (45) may be substituted directly for q (z). The boundary condition

$$\int_{z_o - \frac{\lambda}{2}}^{z_o + \frac{\lambda}{2}} M(z)\, dz \propto N \tag{47}$$

can be used and the problem solved numerically. In any case, at the present time these tedious methods of solution are not warrented due to the meager knowledge of so many parameters.

The effect of a finite source width is to widen the sodium density distribution a proportional amount. As long as the width of the source is less than 0.5 km., the experimental uncertainty in the sodium distribution half width, the delta function approximation is not bad.

To obtain quantative information, f is defined as the

average number of sodium compounds per meteor. Then M(0) can be determined by using the delta function condition for the source and the value of f. That is,

$$f \int_0^{2\pi} M(\chi)\, d\chi = \frac{2\pi}{\lambda} N \tag{48}$$

or upon integrating,

$$M(0) = \frac{N}{f\lambda} \frac{e^{\frac{R}{L}}}{J_0(-i\frac{R}{L})} \tag{49}$$

where J_0 is the zeroth order Bessel function. This has assumed that all of the sodium compounds in a dust particle can participate in production, that f is a constant for all particles, and that the region over which the averaging has been done is large enough so that the average number of sodium compounds can be linearly related to the dust particle density.

For large values of R/L, J_0 (-i R/L) may be given by its asymtotic form:

$$J_0(-i\frac{R}{L}) \longrightarrow \frac{e^{\frac{R}{L}}}{(2\pi R/L)^{\frac{1}{2}}} \tag{50}$$

and then

$$M(0) = \frac{N}{\lambda f}\sqrt{\frac{2\pi R}{L}} \tag{51}$$

To get an approximate value for f, the following form is assumed,

$$f = p \frac{m}{m_N} \tag{52}$$

where p is the fractional part of the meteor which is sodium, m is the meteor mass, and m_N is the mass of the sodium compound. For spherical particles of radius a, f can be written as

$$f = p \frac{\frac{4}{3} \pi a^3 \rho_M}{m_N} \tag{53}$$

The best available information concerning p is from chemical analysis of chondrites[31]. These analyses assign to p a value of about 0.9% for the compound Na_2O. However observations of Hunten and Sullivan[32] indicate that the percentage of sodium may be much higher in meteors, providing that the other metallic atoms have the same source. The percentage is probably a function of the type of meteor.

There is also considerable uncertainty in the density of meteors. Values have been theorized ranging from 0.05 gm/cm^3 [25] to about 5.0 gm/cm^3 [33]. The latter is a typical value for meteorites. Likely densities seem to be in the region of 0.2 to 0.5 gm/cm^3 [34,35] although there is undoubtedly a spectrum present. There is also a spectrum of particle sizes present as shown by the data of Soberman and Hemenway[30]. The particle size is heavily weighted in the direction of decreasing radius, with most of the particle radii less than 10^{-6} cm. The data were collected over an altitude range of 75 km. to 95 km. and represent an average over that interval. Their results agree with the calculations of

Rosinski and Snow[36] who show that secondary particulate matter produced by meteoric disintegration is in this size range.

With V_o proportional to $q^{1/2}/a$, τ_c = 1 day, $Na(z_o)$, τ_o as found experimentally, λ = 10 km., D = 2 x $10^6 cm^2/sec$, f as given in (53), and z_o = 92.4 km., the meteoric dust density is as shown in Figures 36 and 37 for two values of ρ_M (0.44 and 3.0 gm/cm^3) and two values of p (2.5% and 5.0%). The meteoric charge has been assumed to be 1 e . per particle. The parameter is the particle radius. In Figures 38 and 39, the same values of the various quantities are used except that the charge is arbitrarily assumed to vary as the radius, with q proportional to a^2 for $a > 10^{-7}$ cm. and q = 1 e for $a = 10^{-7}$ cm. τ_c is also assumed to be proportional to a^2 in order to take into account the longer lifetime of a multi-charged particle. The widths at half maximum density are indicated for the wider distributions. V_o is also given for each distribution.

Obviously the case where $M(z) \gg 10^4/cm^3$ cannot participate in the process since the dust particles are charged. If their densities were normally greater than the electron densities, the dust layer would have been observed as a prominant feature of the D region of the ionosphere. However enhancement during a dust shower may cause a violation of this boundary condition, and a lower Sporadic E phenomena may take place.

Because of the many unknowns, these density distributions cannot be taken too seriously. For example, there must be a large dependence of sodium percentage, or charge, or both on meteor size in order to prevent the very small particles from completely

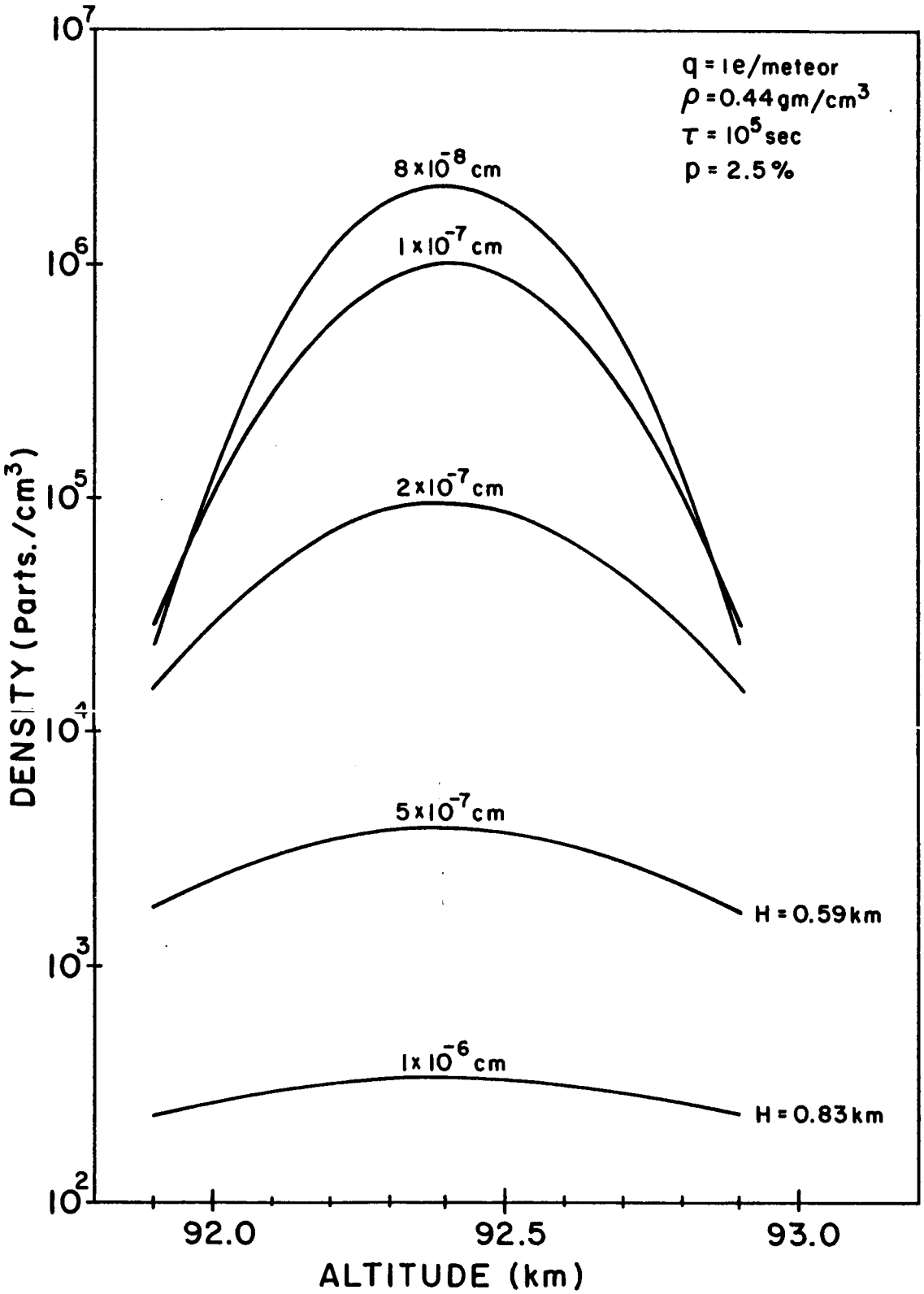
q = 1e/meteor
ρ = 0.44 gm/cm³
τ = 10⁵ sec
p = 2.5%
8 x 10⁻⁸ cm
1 x 10⁻⁷ cm
2 x 10⁻⁷ cm
5 x 10⁻⁷ cm
1 x 10⁻⁶ cm
H = 0.59 km
H = 0.83 km
DENSITY (Parts./cm³)
10⁷
10⁶
10⁵
10⁴
10³
10²
92.0
92.5
93.0
ALTITUDE (km)

Figure 36.

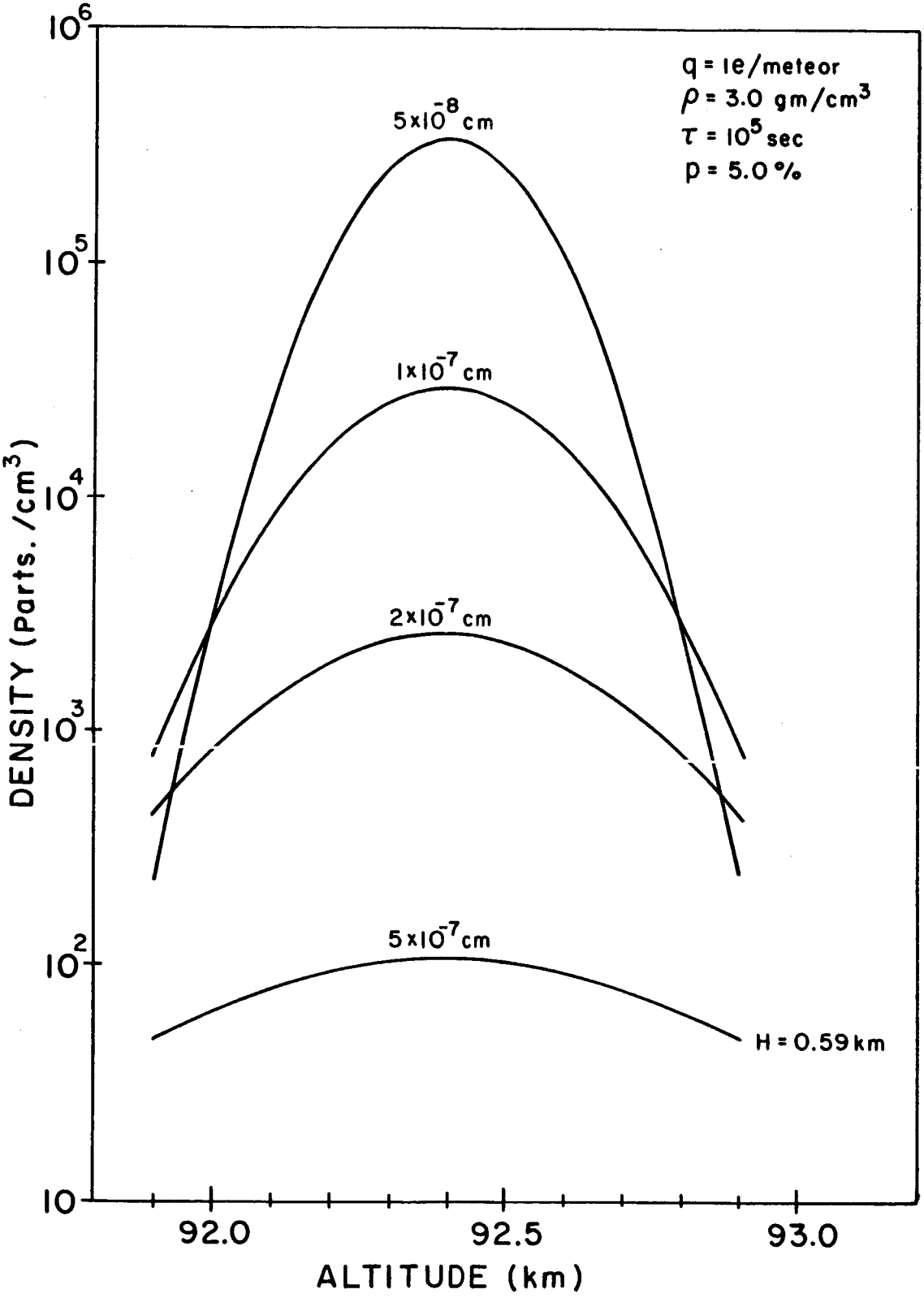
q = 1e/meteor
ρ = 3.0 gm/cm³
τ = 10⁵ sec
p = 5.0 %
5x10⁻⁸ cm
1x10⁻⁷ cm
2x10⁻⁷ cm
5x10⁻⁷ cm
H = 0.59 km
DENSITY (Parts. /cm³)
10⁶
10⁵
10⁴
10³
10²
10
92.0
92.5
93.0
ALTITUDE (km)

Figure 37.

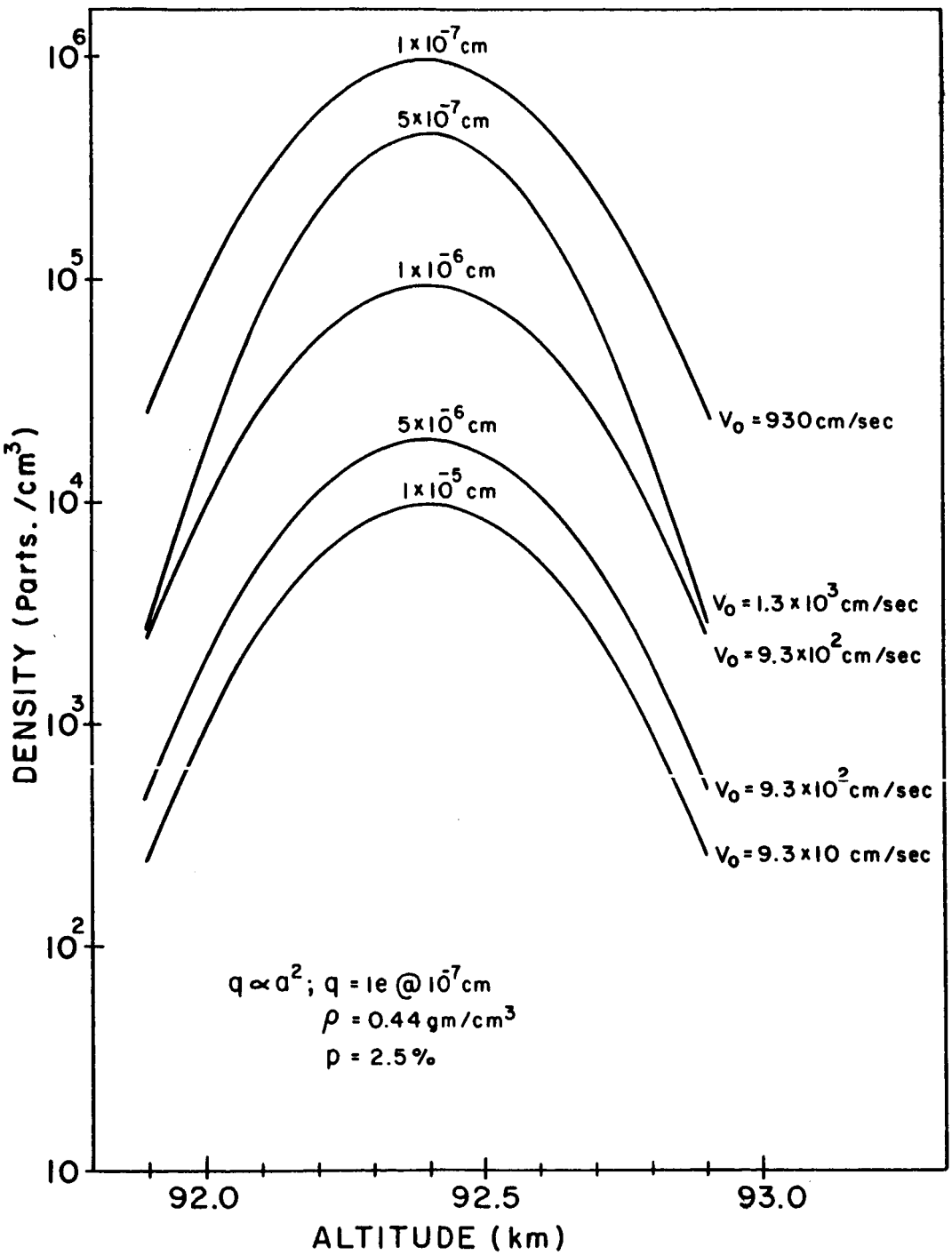
10^6
10^5
10^4
10^3
10^2
10
DENSITY (Parts./cm^3)
1×10^{-7}cm
5×10^{-7}cm
1×10^{-6}cm
5×10^{-6}cm
1×10^{-5}cm
V_0 = 930 cm/sec
V_0 = 1.3×10^3 cm/sec
V_0 = 9.3×10^2 cm/sec
V_0 = 9.3×10^{-2} cm/sec
V_0 = 9.3 x 10 cm/sec
$q \propto a^2$; q = 1e @ 10^{-7}cm
ρ = 0.44 gm/cm^3
p = 2.5%
92.0
92.5
93.0
ALTITUDE (km)

Figure 38.

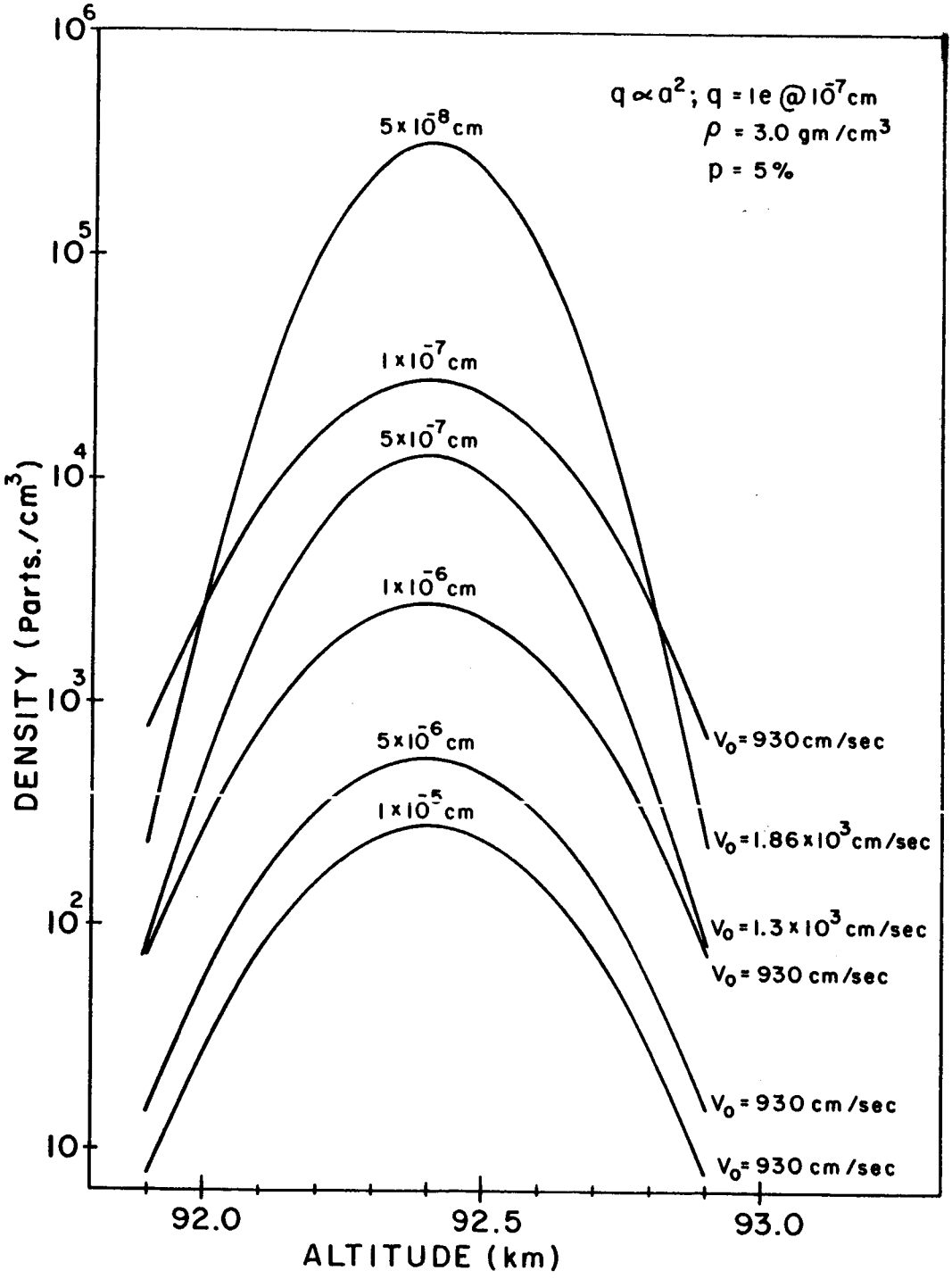
10^6
10^5
10^4
10^3
10^2
10
DENSITY (Parts./cm^3)
$q \propto a^2$; q = 1e @ 10^{-7}cm
ρ = 3.0 gm/cm^3
p = 5%
5×10^{-8}cm
1×10^{-7}cm
5×10^{-7}cm
1×10^{-6}cm
5×10^{-6}cm
1×10^{-5}cm
V_0 = 930 cm/sec
$V_0 = 1.86\times10^3$ cm/sec
$V_0 = 1.3\times10^3$ cm/sec
V_0 = 930 cm/sec
V_0 = 930 cm/sec
V_0 = 930 cm/sec
92.0
92.5
93.0
ALTITUDE (km)

Figure 39.

overwhelming the process. If the time constant for depositing dust into the source region were defined as

$$\tau_o = \frac{\lambda}{V_o} \tag{54}$$

then this, too, requires a greater weight to be placed on the heavier particles because of the small values of τ_o for the smaller ones.

There seems to be little problem in supplying the necessary amount of meteoric material. Mass influxes for meteors are estimated to be from 2×10^{-15} gm/cm^2-sec [37] to 2×10^{-14} gm/cm^2-sec [38]. This can be compared to

$$\frac{M_M N / 5}{\tau_c} \tag{55}$$

which is the mass influx for a particle of mass M_M. This may be written as

$$\frac{N M(Na_2O)}{p \tau_c} \tag{56}$$

Taking τ_c to be about 1 day, p= 2.5%, together with the previously given value of N, the mass influx required is about 10^{-15} gm/cm^{2}sec. Thus anywhere from 5% to 50% of the incoming material must participate in the process for this model. This requirement stems from the small value of f. Since f is probably a function of the meteor type, the influx should be integrated over all distributions. In any case, this model has not violated the influx requirement.

So far the effect of neutral dust particles has been neglected. If the charged particles are removed by disintegration, there is no effect by the neutrals. However, if neutralization is the removal process, the neutral particles will remain in this altitude region for a time of the order of the diffusion time. If the lifetime of the charged dust against recombination is about a day, then the neutrals will not have much effect at the density peak. In general, the neutrals will tend to widen the sodium layer because they produce a wider source. This reduces the density requirement on the source but increases the sodium removal condition. If the particles are charged many times, the neutrals will have negligible effect. Until experimental evidence is obtained, it will be assumed that the role of non-charged dust is relatively minor.

It is to be noted that the possibility of telluric sources of dust (such as volcanos) cannot be ruled out since the theorized processes could act equally well on them. However, it is much more plausable that at these heights the dust is extra-terrestrial in origin.

Sea water has previously been suggested as a possible source of sodium in the upper atmosphere. It is not clear, under the present circumstances, how it could produce a model consistent with the experimental observations, although Chapman and Kendall[43] have suggested a process involving water vapor and dust which can produce a narrow aerosol layer in the noctilucent cloud problem. However, their calculations indicate a layer formation at about 80 km. which is too low for sodium production.

3.4 Sodium Ions

The physical processes acting on sodium ions are diffusion, photochemistry, and wind effects. Since the ions have been observed to be about 30 times less abundant than free atoms, (Figure 34) the removal rate must be at least 30 times faster. The rate must be even greater if the dust is also a source of ions. However, below 105 km. the ions have a profile very close to that of the neutral distribution. Therefore, in this region a steady state solution will be sought to satisfy the observed ratio. Caution must be exercised in satisfying the ion-atom density ratio since the observations were made at different times and places. In view of the fact that these observations are the only ones so far, they will tenatively be used for comparison.

Photochemically, production of Na^+ will be by

$$Na + h\nu \longrightarrow Na^+ + e \qquad j_1 \qquad (57)$$

and

$$Na + X^+ \longrightarrow Na^+ + X \qquad k_6 . \qquad (58)$$

Removal can be accomplished by

$$Na^+ + e \longrightarrow Na + h\nu \qquad \alpha \qquad (59)$$

$$Na^+ + X + M \longrightarrow NaX^+ + M \qquad k_7 \qquad (60)$$

$$Na^+ + XY \longrightarrow NaX^+ + Y \qquad k_8 \qquad (61)$$

$$Na^+ + X^- \longrightarrow Na + X \qquad k_9 . \qquad (62)$$

The production rate at 95 km. is about 2.3×10^{-5}/sec, if j_1 is about 2.0×10^{-5}/sec, k_6 is 3.0×10^{-10} cm^3/sec and X^+ is Mg^+, having a density of 10^4 atoms /cm^3. Thus the removal rate must be about 6.9×10^{-4}/sec. (59) can certainly be ignored. If X were

O in (60), then with an oxygen density of $5.0 \times 10^{11}/cm^3$ at 95 km, and an M density of $10^{13}/cm^3$, k_9 would have to be about $1.4 \times 10^{-28} cm^6/sec$ which is unlikely. Molecular oxygen is not a probable prospect either because it requires a rate of $1.4 \times 10^{-29} cm^6/sec$ for an O_2 density of $5.0 \times 10^{12}/cm^3$. For the mutual neutralization reaction, an upper limit of 10^{-6} cm^6/sec for k_9 requires a negative ion density of $690/cm^3$ which is fairly high. Thus a good condidate for removal is (61) with ozone as the reagent. For an O_3 density of $5.0 \times 10^7/cm^3$ at 95 km, k_8 would have to be $1.4 \times 10^{-11} cm^3/sec$. This certainly is not an unreasonable value for an ion-molecule rate. The problem here is that Na^+, having a closed electronic shell, is not likely to form an ion of either NaO or NaO_2. This objection also applies to the three body reactions. However, recently Mann[39] has experimentally found NaO^+ to be a stable molecular ion so that polarization effects probably play an important role. The above values of the oxidation rates for Na^+ may then be possible.

One other possibility for Na^+ loss would be collisions with dust particles. However, neutralization by negative dust particles would occur only near the center of the layer where there is a large concentration. Even with a very large cross section for this process, there remains the difficulty of getting rid of the ions at higher altitudes, where the dust is considerably less abundant than at the peak.

The experimental results of Narcisi and Bailey[14] showed a large increase in ion density above 105 km. Unfortunately,

their rocket did not reach an altitude high enough to give the complete ion distribution. The rise in density could be caused by the fact that at these heights, reduction of NaO, and in turn, ionization of Na predominate so that most of the sodium is in the ionized state. More likely is the effect of wind shear and diffusion, which can quickly transport Na^+ to the higher regions. Supporting evidence for wind shear concentration of these ions was given by Pharo et.al.[40] Their results followed Narcisi and Bailey's except that their rocket traversed the ion maximum at 113 km. The concentration of Mg^+ was so narrow (less than 1 km. wide) that it is difficult to see how anything other than a wind shear could produce the distribution. Unfortunately, their spectrometer sensitivity was too low to detect Na^+.

The transport rate for this mechanism may be defined as

$$J_{ws} = \frac{V_{zi}}{\lambda} \tag{63}$$

where V_{zi} is the vertical ion velocity, and λ is the scale of the process. V_{zi} is given by

$$V_{zi} = -\frac{\omega_i}{\nu_i} U_y \cos\theta_B = \frac{\omega_i}{\nu_i} U_{EW} \cos\theta_B \tag{64}$$

where ωi and νi are the gyro and collision frequencies for ions[15]. This has assumed that ω_i/ν_i is small compared to $(\omega_i/\nu_i)^2$. If ν_i is 7.0×10^2/sec, and ω_i is 2.2×10^2/sec. for Na^+ , then with $\theta_B = 45^\circ$ and $\lambda = 10$ km,

$$J_{ws} = 2.2 \times 10^{-7} U_{EW} \tag{65}$$

With $U_{EW} = 10^2$ cm/sec near the density peak, J_{WS} is 2.2×10^{-5}/sec, somewhat smaller than required by production. Thus in the region of the peak, the ozone process will be more effective in removing the ions. Na^+ decreases much faster with altitude than O_3, which varies very little near 95 km. However vertical transport becomes increasingly important with height reaching a maximum at U_{EWmax}. This should occur near 105 km. where Na^+ has a minimum. The production and removal processes become equal when U_{EW} is about 3.0×10^3 cm/sec. The ions are then transported to the opposite node at about 112 km. where they will have a maximum density. The condition for this rearrangement to take place is that the vertical gradient in the horizontal wind be in the proper direction. This condition is consistent with the requirement for concentrating negative dust particles at the sodium peak.

The problem with the foregoing discussion is that the loss mechanism at higher altitudes must be very fast in order to prevent a large build-up of ions. Again a likely candidate is oxidation by ozone. The ozone density must be

$$O_3(112\ km.) = \frac{\bar{J}_{WS}}{k_8} \tag{66}$$

where $\bar{J}_{WS}$ is the wind shear rate averaged over one wavelength. Assuming k_8 is 1.4×10^{-11} cm^3/sec, then if $\bar{J}_{WS}$ is 10^{-5}/sec, the ozone density would have to be 7.1×10^5/cm^3 at 112 km. $\bar{J}_{WS}$ is probably larger than this, so that the amount of ozone must be very large.

Even more stringent is the removal requirement for the

other ions, notably Mg^+, which has a density of about $10^4/cm^3$ at 112 km. Due to the fact that NaO^+ has been found experimentally to be stable, the three body reaction (60) with O may be important at higher altitudes.

In any case, until more information about the reactions involving alkalai ions is obtained, the removal problem is far from being closed.

3.5 Twilight and Night Sodium

On the day of the flight, the Zeeman photometer gave a twilight abundance of 4.7×10^9 atoms/cm^2 while the daytime value was about three times larger. The twilight layer was about 3.8 km. wider (full width) than that during the day and had lower altitude than the average daytime height by 3.2 km.

It still seems likely that the increase in the O_3 to O ratio suggested by Blamont and Donahue[45] can account for the day to twilight abundance change. However, it is not clear why the spatial distribution should vary in this way. Perhaps the effect is due to changes in the neutral wind characteristics. Rosenberg et.al.[18] found a slight decrease in the altitude of the east-west wind shear node after sunset. Also the magnitude of the gradient tended to decrease toward twilight. Both of these effects are in the right direction to explain the observations.

Before formulating a quantitative comparison of day and twilight results, however, it is necessary to check the validity of the twilight profile by means of a rocket photometer, backed

up by a ground based photometer. This is because the twilight technique really gives the difference in altitude between the sodium and a screening layer which is located by calculations of attenuation of sunlight traversing air and ozone.

To explain the existence of nighttime sodium is also somewhat difficult. The increase in ozone at night may be between one and two orders of magnitude so that even if Na is being produced at the same rate at night as it is during the day, it would suffer a large decrease in density. Since the effects of solar radiation are no longer present, another source of sodium must be found. A likely candidate is reaction (19) involving NaO and O. In fact this may produce the night glow if the free sodium thus produced were excited. So far its reaction rate has not been measured. If (19) is fast, then it is probable that the photochemical-diffusion theory of Blamont and Donahue is a valid description of the night processes.

Support for this possibility is rendered by the NRL rocket observations[41,42] which indicated an emission region near 90 km. which was very broad compared to the dayglow layer. This would be expected from photochemical considerations.

4.0 CONCLUSIONS

The sodium dayglow was measured on September 26, 1964, by means of a rocket experiment. The radiation was found to come from an extremely thin layer of free sodium atoms centered at about 92.4 km. The sodium density was about 2.8×10^4 atoms/cm^3 at the center and decreased in altitude with a scale height of 2.5 km. A comparison with the twilight layer on the same day yielded a 3 to 1 diurnal variation in the sodium abundance. The twilight layer was found to be slightly lower than that during the day. These results are inconsistent with a photochemical explanation of the source of sodium. Therefore, a new model is proposed to account for the observed distribution in terms of a very thin layer of charged, sodium-containing dust particles which can liberate meteoric atoms through the action of solar radiation. In the steady state, the free atoms are confined to a small region about the source layer because ozone oxidizes them before they can diffuse very far.

A quantitative calculation has been performed to see if the dust particles can act as the origin of the sodium. Under simplified conditions it was found that such a source is possible. However, the results were hindered by a lack of knowledge of many parameters. In particular, the influx, residence time, and physical characteristics of meteoric debris need to be determined. Also laboratory measurements of the chemical reaction rates are needed to justify or exclude the proposed processes.

Experimental investigations of the present theory can be made in several forms. Ground based experiments such as ionosondes, sodium photometers, and meteor radar equipment operated at the same place could supply information concerning the correlation of Sporadic E, sodium dayglow, and meteor rates. In addition, rockets carrying sodium photometers, ion mass spectrometers, and aerosol detectors with high altitude resolution and sensitivity would provide direct information about the D region processes.

Future plans include the flight of two more sodium experiments, one to be launched at twilight to obtain information about the layer at that time. The second is to be flown later during the same day to observe the corresponding dayglow. This program will yield direct information about the diurnal variations of sodium.

APPENDIX A

A method has been developed to determine the direction of observation of a laterally mounted rocket experiment. It is applicable only under specialized conditions. These conditions are the following: very little or no rocket precession and at least two reference points, such as the horizon or the sun, must be obtainable from the photometer output. The altitude of the rocket is given by radar. For the present experiment, both horizons and the sun vector were obvious from the white light data (see Figure 13). The period of rocket rotation can be extracted from these points by averaging the various time intervals between them. Agreement of the spin rate thus determined with that given by the solar sensors was excellent. The period of rotation is given in Figure 40.

The geometry of the situation is shown in Figure 41. θ is the rocket zenith, and h is the rocket altitude. Y_1 indicates the direction where the photometer is looking at the lowest point on the lateral or spin plane. Y_2 is the direction where the photometer is looking with an impact parameter z above the surface of the earth and ψ is the angle between Y_1 and Y_2. C is the circle which defines the intersection of the lateral plane and the sphere defined by the radius $R_o + z$. The following equations are evident from the figure:

$$Y_1 = (R_o + h) \sin\theta \tag{67}$$

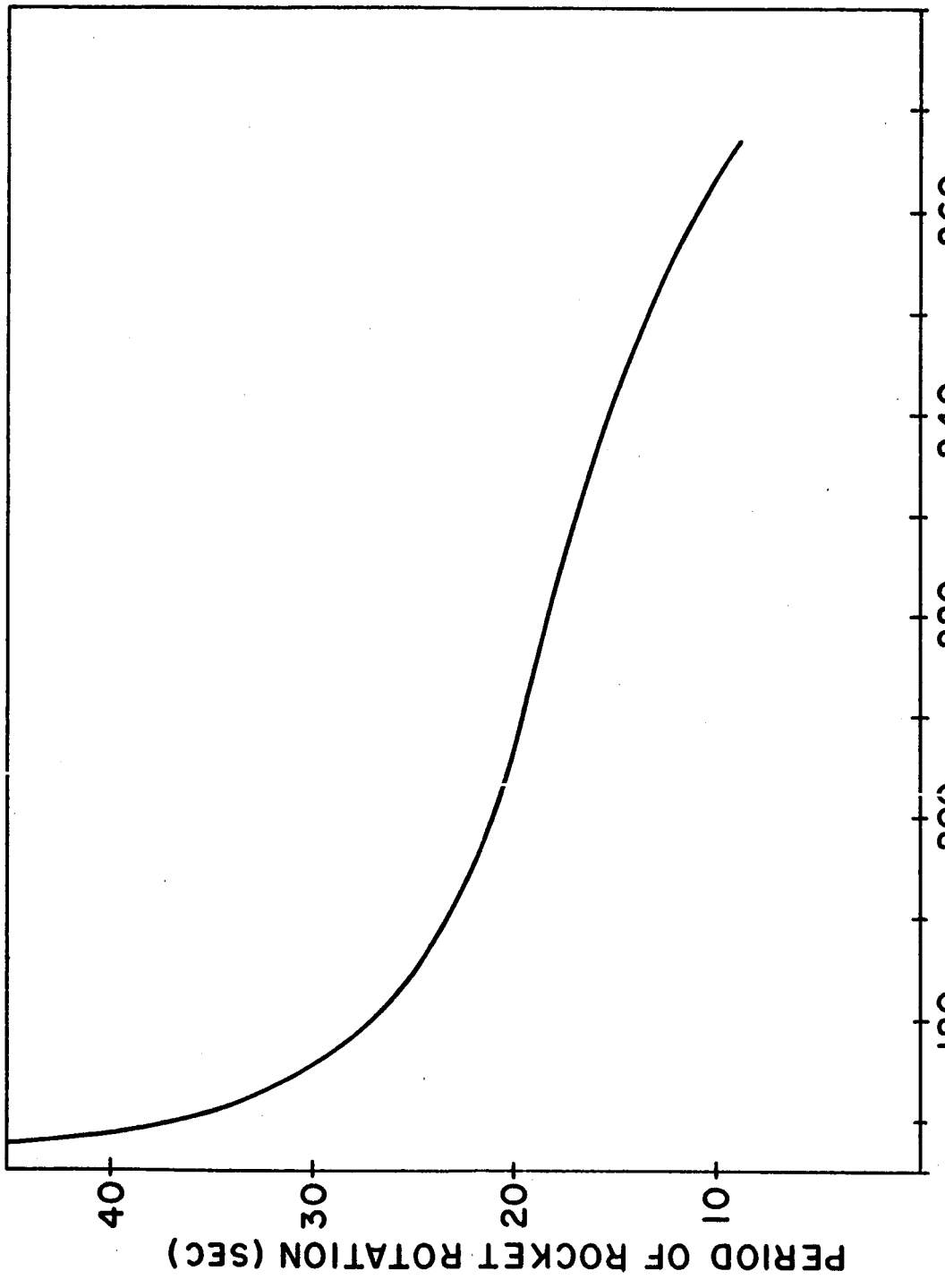

Figure 40. Period of rocket rotation determined from white light data.

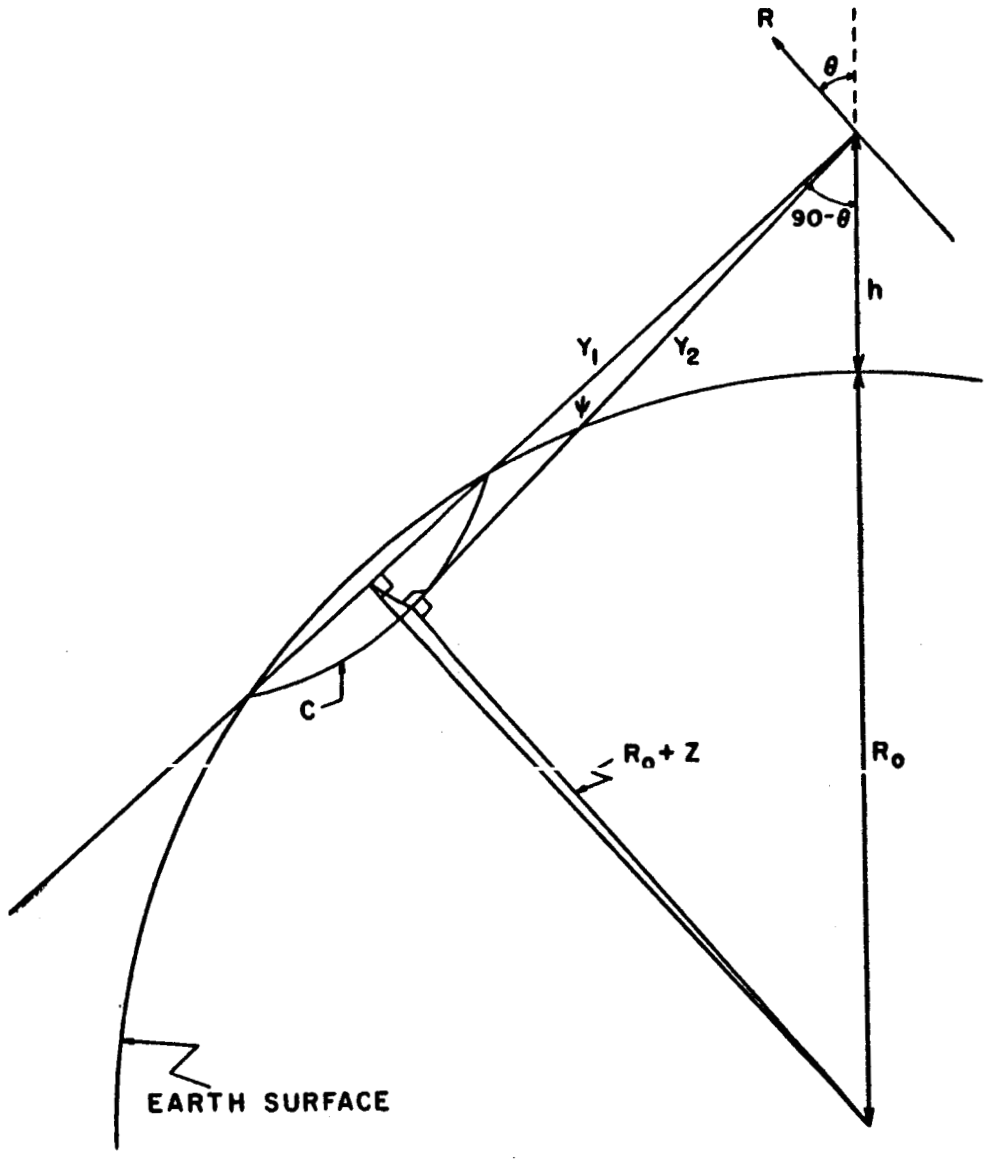

Figure 41. Geometry for attitude reduction method using white light data.

$$Y_2 = \sqrt{(R_0+h)^2-(R_0+Z)^2} \approx \sqrt{2R_0(h-Z)} \qquad (68)$$

$$Y_3 = Y_2 \sec\psi . \qquad (69)$$

It is clear from these relationships that the zenith angle of the rocket is given by

$$SIN\,\theta = \frac{\sqrt{2R_0(h-Z)}}{(R_0+h)\cos\psi} . \qquad (70)$$

At the horizon, z=0 and $\psi = \psi_H$ so that

$$\frac{\sqrt{2R_0(h-Z)}}{(R_0+h)\cos\psi} = \frac{\sqrt{2R_0h}}{(R_0+h)\cos\psi_H} \qquad (71)$$

or

$$z = h\left(1-\frac{\cos^2\psi}{\cos^2\psi_H}\right) \qquad (72)$$

Thus the impact parameter of the direction of observation is obtainable if the horizon point can be located, along with the minimum of the lateral plane.

For the present flight, ψ was zero when the photometer observed the reflection of the sun in the ocean. Then if the rocket had a constant period of rotation, T, ψ would have been given by

$$\psi = 360^\circ \frac{\Delta t}{T} \qquad (73)$$

where Δt is the time interval in going from $\psi = 0$ to ψ. Since T was a function of t, ψ must be given as

$$\psi = 360^{\circ} \int \frac{dt}{T(t)} \tag{74}$$

Unfortunately the horizon points could not be determined with sufficient accuracy since the solid angle effect integrated out the intensity distribution. Thus this method could not be used to find z. However, ψ could still be found. It was determined and used in conjunction with the azimuth and zenith angles of the vehicle obtained by the magnetometer and sun sensor data.

If precession is present, it cannot be taken into account by this method. However, the analysis was still performed and the limiting errors were calculated. They were found to be much smaller than those involved in the solar sensor-magnetometer spin evaluation.

APPENDIX B

The equation of motion for a charged dust particle is

$$q(\underline{E} + \underline{V}\times\underline{B}) + \tfrac{1}{2}\rho_a S C_d |\underline{U}-\underline{V}|(\underline{U}-\underline{V}) = 0 \qquad (75)$$

With the definition of ω and ν given in (29), and noting that $B_y=0$, we separate the above equation into cartesian components:

$$\nu(U_x - V_x) + \frac{\omega}{B} E_x + V_y \omega \sin\theta = 0 \qquad (76)$$

$$\nu(U_y - V_y) + \frac{\omega}{B} E_y + V_z \omega \cos\theta - V_x \omega \sin\theta = 0 \qquad (77)$$

$$\nu(-V_z) + \frac{\omega}{B} E_z - V_y \omega \cos\theta = 0 \qquad (78)$$

Solving these for V_x, V_y, and V_z, the following equations result,

$$V_x = (U_x + \frac{E_x}{B}\frac{\omega}{\nu})(\frac{\nu^2+\omega^2\cos^2\theta}{\omega^2+\nu^2}) + (U_y\nu + \frac{E_x}{B}\omega)(\frac{\omega\sin\theta}{\omega^2+\nu^2}) - \frac{E_z}{B}\frac{\omega}{\nu}(\frac{\omega^2\sin\theta\cos\theta}{\omega^2+\nu^2}) \qquad (79)$$

$$V_y = -(U_x\nu + \frac{E_x}{B}\omega)(\frac{\omega\sin\theta}{\omega^2+\nu^2}) + (U_y\nu + \frac{E_y\omega}{B})(\frac{\nu}{\omega^2+\nu^2}) + \frac{E_z}{B}(\frac{\omega^2\cos\theta}{\omega^2+\nu^2}) \qquad (80)$$

$$V_z = (U_x + \frac{E_x}{B}\frac{\omega}{\nu})(\frac{\omega^2\sin\theta\cos\theta}{\omega^2+\nu^2}) - (U_y\nu + \frac{E_y\omega}{B})(\frac{\omega\cos\theta}{\omega^2+\nu^2}) + \frac{E_z}{B}\frac{\omega}{\nu}(\frac{\omega^2\sin^2\theta}{\omega^2+\nu^2}) \qquad (81)$$

If ω/ν is small and the polarization electric fields are zero (or at least $\frac{E_i}{B}\frac{\omega}{\nu} \ll u_i$), then

$$V_x = u_x + u_y \frac{\omega}{\nu} \sin\theta \tag{82}$$

$$V_y = u_y - u_x \frac{\omega}{\nu} \sin\theta \tag{83}$$

$$V_z = -u_y \frac{\omega}{\nu} \cos\theta - u_x \frac{\omega^2}{\nu^2} \sin\theta \cos\theta \tag{84}$$

The second assumption is justifiable on the grounds that in a conducting medium in a steady state, the fields are zero. The second term in V_z may be neglected compared to the first as long as ω/ν is small. In general ω/ν is small enough that V_z is negligible when $\bar{u}_y = 0$.

There is one other case of interest. That is when both positive and negative particles are present. The wind shear would tend to separate them until a vertical electric field is set up. If the field were strong enough, there would be no concentration of particles at the nodes. This is because the field would prevent a large separation. However, calculations showed that the smallest possible electric field caused by the shear mechanism is many orders of magnitude greater than the polarization field. In the case of positive and negative ions, polarization is important because $(\omega/\nu)_{ion}$ can exceed unity.

To see the conditions under which ω/ν is small, it

is noted that

$$\left(\frac{w}{\nu}\right)_{MAX} = \frac{2 B q}{\rho_a S C_d |\underline{U}-\underline{V}|_{MIN}} \tag{85}$$

and that $|\underline{U}-\underline{V}|_{min}$ occurs when $V_y \approx U_y$. Then from (78)

$$|V_z|^2 = \left|\frac{w}{\nu} V_x \cos\theta\right|^2 \approx \left|\frac{w}{\nu} U_y \cos\theta\right|^2 = |V_{z\,MAX}|^2 \tag{86}$$

Under extreme conditions, which in general do not occur, the minimum value of $|\underline{U}-\underline{V}|$ demands that $V_x \approx U_x$ and thus,

$$|\underline{U}-\underline{V}|_{MIN} = |V_z|_{MAX} \quad . \tag{87}$$

Under these circumstances, with q= 1 e.s.u., a = 10^{-7} cm. and values of the other factors as given after (33), $(w/\nu)_{max}$ is found to be about 0.1. If q becomes large, and $V_x = U_x$ simultaneously with $V_y = U_y$, then the smallness assumption does not hold. However this is extremely unlikely.

REFERENCES

1. J. W. Chamberlain, Physics of the Aurora and Airglow, Academic Press, New York, 1961.

2. D. M. Hunten, Science, 145, 26, 1964.

3. T. M. Donahue, International Dictionary of Geophysics, (ed. S. Runcorn). Pergamon Press, (in press).

4. D. M. Hunten, J. Atmos. Terr. Phys., 5, 44, 1954.

5. J. E. Blamont and T. M. Donahue, J. Geophys. Res., 69, 4093, 1964.

6. T. M. Donahue, J. Geophys. Res., 61, 663, 1956.

7. J. C. Brandt and J. W. Chamberlain, J. Atm. Terr. Phys., 13, 90, 1958.

8. J.E. Blamont and T. M. Donahue, J. Geophys. Res., 66, 1407, 1961

9. M. Gadsden, J. E. Blamont, and T. M. Donahue, to be published.

10. L. M. Biberman, J. Exptl. Theoret. Phys. USSR, 17, 416, 1947; 19, 584, 1949.

11. W. E. Kaskan, Tenth Symposium (International) on Combustion, 41, The Combustion Institute, 1965.

12. A. V. Jones, Ann. Geophys., 14, 179, 1958.

13. V. G. Istomin, Space Research III, North Holland Publishing Co., Amsterdam, 1963.

14. R. S. Narcisi and A. D. Bailey, J. Geophys. Res., 70, 3687, 1965.

15. J. D. Whitehead, Ionospheric Sporadic-E, Pergamon Press, New York, 1962.

16. W. I. Axford, J. Geophys. Res., 69, 5093, 1964.

17. T. M. Donahue, S.R.C.C. Report No. 27, University of Pittsburgh, Pittsburgh, 1966.

18. N. W. Rosenberg, H. D. Edwards and J. W. Wright, Space Research IV, North Holland Publishing Co., Amsterdam, 1964.

19. P. J. Bowen, K. Norman, A. P. Willmore, J. M. Baguette, F. Murtin, and L. R. O. Storey, Planet. Space Sci., 12, 1173, 1964.

20. W. I. Axford and D. M. Gunnold, GSUAC Report No. 14, Cornell University, Ithica, 1965.

21. R. N. Singh, J. Atmos. Terr. Phys., 25, 589, 1963.

22. G. Flocco, J. Geophys. Res., 70, 2213, 1965.

23. E. K. Smith, Ionospheric Sporadic-E, Pergamon Press, New York, 1962.

24. P. M. Millman and B. A. McIntosh, Can. J. of Phys., 42, 1730, 1964.

25. W. M. Alexander, C. W. McCracken, L. Secretan and O. E. Berg, Space Research III, North Holland Publishing Co., Amsterdam, 1963.

26. F. D. Colegrove, W. B. Hanson and F. S. Johnson, J. Geophys. Res., 71, 2227, 1966.

27. P. M. Millman, J. Geophys. Res., 64, 2122, 1959.

28. J. S. Greenhow and E. L. Neufeld, J. Geophys. Res., 64, 2129, 1959.

29. J. E. Blamont, Planet. Space Sci., 10, 89, 1963.

30. R. K. Soberman and C. L. Hemenway, J. Geophys. Res., 70, 4943, 1965.

31. J. A. Wood, The Moon, Meteorites and Comets, University of Chicago Press, Chicago, 1963.

32. H. M. Sullivan and D. M. Hunten, Can. J. Phys., 40, 1964.

33. C. W. Allen, Astrophysical Quantities, The Athlone Press, London, 1964.

34. F. L. Whipple, J. Geophys. Res., 68, 4929, 1963.

35. F. Verniani, Nuovo Cimento, Serie X, 33, 1173, 1964.

36. J. Rosinski and R. H. Snow, J. Meteor., 18, 736, 1961.

37. G. Newkirk and J. A. Eddy, J. Atm. Sci., 21, 35, 1964.

38. M. Dubin and C. W. McCracken, Astron. J., 67, 248, 1962.

39. D. Mann, private communication.

40. M. W. Pharo, C. R. Smith, H. A. Taylor, H. C. Brinton, Paper presented at 47th A. G. U. Meeting, Washington, 1966.

41. J. P. Heppner and L. H. Meredith, J. Geophys. Res., 63, 51, 1958.

42. D. M. Packer, Ann. Geophys., 17, 67, 1961.

43. S. Chapman and P. C. Kendall, J. Roy. Meteor. Soc., 91, 115, 1965.